NAME OF AUTHOR/*NOM DE L'AUTEUR* Elsayed Aly Orady

TITLE OF THESIS/*TITRE DE LA THÈSE* "The Study of the Effect of Thermal Cycling on the Tool Life in Intermittent Cutting Processes Using the Finite Element Technique"

UNIVERSITY/*UNIVERSITÉ* McMaster

DEGREE FOR WHICH THESIS WAS PRESENTED/ *GRADE POUR LEQUEL CETTE THÈSE FUT PRÉSENTÉE* Ph.D.

YEAR THIS DEGREE CONFERRED/*ANNÉE D'OBTENTION DE CE DEGRÉ* 1982

NAME OF SUPERVISOR/*NOM DU DIRECTEUR DE THÈSE* Dr. J. Tlusty

DATED/*DATÉ* September 8, 1982. SIGNED/*SIGNÉ* Elsayed Orady

PERMANENT ADDRESS/*RÉSIDENCE FIXÉ* 17E Deerfield Dr., Nepean K2G 3R7 in Canada

~~5 Balsam St., El matteria~~

Cairo, Egypt (If out of country)

THE STUDY OF THE EFFECT OF THERMAL CYCLING ON THE TOOL LIFE IN INTERMITTENT CUTTING PROCESSES USING THE FINITE ELEMENT TECHNIQUE

by

© ELSAYED A. ORADY, B.Sc., M.Sc., M.Eng.

A Thesis

Submitted to the School of Graduate Studies

in Partial Fulfilment of the Requirements

for the Degree

Doctor of Philosophy

McMaster University

April 1982

THERMAL CYCLING IN INTERMITTENT CUTTING

DOCTOR OF PHILOSOPHY (1982)
Mechanical and Manufacturing Engineering

McMASTER UNIVERSITY
Hamilton, Ontario

TITLE: THE STUDY OF THE EFFECT OF THERMAL CYCLING ON THE TOOL LIFE IN INTERMITTENT CUTTING PROCESSES USING THE FINITE ELEMENT TECHNIQUE

AUTHOR: Elsayed Aly Orady, B.Sc. (Cairo University)
M.Sc. (Cairo University)
M.Eng. (McMaster University)

SUPERVISOR: Dr. J. Tlusty

NUMBER OF PAGES: xviii, 174, A12, B7, C9

ABSTRACT

The objective of this thesis is to investigate the influence of thermal cycling on tool life in intermittent cutting processes. Particular emphasis is given to the peripheral milling process.

In intermittent cutting processes, it has been established that the thermal cycling is the most significant factor which controls the type of failure and the life of cutting tools. The previous theoretical studies of the thermal cycling were based on strongly simplified models. The experimental studies were based on the measurement of the tool/chip interface temperature in the cutting period. Consequently, any implications for tool wear or breakage could only be indirectly estimated.

In this work, the thermal cycling is studied by means of finite element computation of the transient temperatures and stresses in the tool wedge. The finite element formulation of the energy equations and the associated boundary conditions, which govern the heat transfer mechanism, is developed for the intermittent cutting processes. A two-dimensional tool/chip model is developed which reflects the interaction between the heat sources, and provides the capability of computing a complete temperature field. The computed temperature field is then used to determine the thermal stresses.

The computation of a complete temperature field and the associated thermal stresses is necessary to explain experimentally determined characteristics of tool wear, cracking and breakage. The transient

temperature field in both the chip and tool, and the corresponding thermal and mechanical stresses, are computed for the peripheral milling process with different cutting conditions. The theoretical results are correlated with experimental data. The experimental data are taken, mostly, from the tests of Barrow and Yellowley[12] and from similar tests conducted by the author. The experimental work concentrates on the flank wear of both high speed steel and sintered carbide milling cutter. It is found that the cutting time ratio has significant effect on tool life. The correlation shows that the number of thermal cycles is the most important parameter which affects the tool life in peripheral milling.

The thesis starts with a statement of the problem and the scope of this work in Chapter 1. Chapter 2 provides a summary of the state of knowledge in the area of tool damage in intermittent cutting processes. The temperature problems in continuous and intermittent cutting process are discussed in Chapter 3. The mathematical modelling and the finite element formulation of the heat transfer problem are developed in Chapter 4. The modelling of the cutting process and the computation of the transient temperature distribution are presented in Chapter 5. Chapter 6 is devoted to the presentation and discussion of the computed thermal stresses. The important parameters which may affect the tool flank wear in milling are established and correlated to the experimental data in Chapter 7. Finally, Chapter 8 provides conclusions and recommendations for further research.

Specifically, this thesis provides the following contributions:

1. The mathematical modelling and the finite element formulation of the

transient heat transfer problem in intermittent cutting (Chapter 4).

2. Derivation of an automatic time step control algorithm for two-point recurrence schemes for the first order ordinary differential equations (Chapter 4).

3. Development of a two-dimensional tool/chip model for the cutting process (Chapter 5).

4. Implementation of a software system, based on the developed models, to compute the temperature and stress fields (Chapters 5 and 6).

5. The study of the influence of thermal cycling on tool flank wear in peripheral milling based on correlating the computed results with experimental data (Chapter 7).

ACKNOWLEDGEMENTS

I wish to express my deepest gratitude and indebtedness to Professor J. Tlusty for his excellent supervision and guidance throughout the course of this work.

I am thankful to Dr. I. Yellowley for his valuable suggestions and constructive comments. I, also, appreciate his permission to use his experimental data. My sincere thanks to Professor M. Dokainish for his active role in the supervising committee and his support. I, also, appreciate the encouragement and advice of Professor W.R. Newcombe and Professor G.W. Torrance while serving in the supervisory committee.

I would like to express my appreciation to Dr. F. Mirza for his assistance and for allowing me to use his basic finite element programs for heat transfer and stress evaluation. I have built my software on these basic programs.

I cannot find words to adequately express my appreciation to my wife Soraya for her support, encouragement and assistance. Special thank you's are due to my little twins, Aly and Mona, for the joy they offered during the difficult times of preparing this thesis.

The typing of this thesis by Diane Vallieres with the help of Helen Cuccaro is highly appreciated.

The financial assistance from McMaster University is gratefully acknowledged.

TABLE OF CONTENTS

LIST OF FIGURES

LIST OF TABLES

LIST OF PRINCIPAL SYMBOLS

Below is a list of principal symbols used in this thesis presented for easy reference, although all are defined in the text as they occur. On many occasions, additional ones have to be used in a minor context and a non-uniqueness arises.

A_c	Chip cross sectional area
A_{ct}	Tool/chip contact area
[B]	Strain shape
[C]	Heat capacitance matrix
C	Specific heat
[D]	Elasticity matrix
D_c	Distance from cutting edge
D_r	Distance from rake face
E	Modulus of elasticity
E_p	Plastic strain
E_r	Strain range
E_T	Truncation error
{F}	Load vector
F	Tangential cutting force
F_f	Friction force
F_s	Shear force
[H]	Characteristic matrix
K_s	Specific cutting force

$[K]$	Stiffness matrix
N	Number of cycles
N_i	Interpolation function
P_f	Friction power
P_s	Shear power
Q	Internal energy
R	Rotational speed or thermal number
T	Temperature
T_m	Mean temperature °K
T_r	Room temperature °K
T_s	Shear plane temperature °K
T_t	Tooth life
V_B	Flank land wear
Z	Fatigue parameter
$\{a\}$	Field variables
a_r	Radial depth of cut
b	Width of cut
d	Cutter diameter
h	Chip thickness
$\bar{h}$	Coefficient of heat transfer
k	Thermal conductivity
k_x, k_y	Thermal conductivity in x and y directions
ℓ_c	Contact length
n_x, n_y	Vectors normal to boundary
q_f	Friction heat flux
r	Chip ratio

s_t	Feed/tooth
t	Time
t_h	Heating time
t_c	Cooling time
u,v	Velocity or displacement components in x and y direction
v_c	Chip velocity
v_s	Shearing velocity
Γ	Domain boundary
Γ_1	Specified temperature boundary
Γ_2	Conduction or convection boundary
Ω	Space domain of the problem
ϕ	Shear angle
α	Coefficient of thermal expansion
θ_o	Room temperature °C
$\bar{\theta}_s$	Shear plane temperature °C
λ_i	Eigenvalue
λ_s	Proportional of shear plane heat energy conducted back to the workpiece
μ	Coefficient of friction
ν	Poisson's ratio
ρ	Density
$\sigma_1,\sigma_2,\sigma_3$	Principal stresses $\sigma_1 > \sigma_2 > \sigma_3$
T_{max}	Maximum shear stress
ψ	Rotational angle

CHAPTER 1

INTRODUCTION

Cutting processes such as milling, planing, sawing, etc. are known as intermittent cutting processes. These processes are far more complex than continuous turning. The most significant differences between intermittent cutting and turning processes are, firstly, the repeated interrupted nature of cutting, and secondly, the varying undeformed chip thickness. These characteristics lead to increasing the number of variables which must be considered when assessing the tool life in intermittent cutting processes as compared to turning. The common variables in both turning and intermittent cutting processes include tool material, work material, cutting speed, feed, depth of cut and tool geometry. Other significant variables, which must be considered in intermittent cutting processes, are time-in-cut (cutting time) and time-out-of-cut (non-cutting time), and entry and exit conditions.

The repeated interruption of cutting results in frequent heating and cooling of the cutting tool. When the tool starts cutting, a high temperature develops very rapidly due to contact and friction with the hot chip, which has been heated as a result of the conversion of cutting energy into sensible heat. Also, the tool flank heats up due to friction between the machined surface and the tool. Subsequently, as a part of the heat conducted away through the tool wedge, the temperature inside the tool increases too. During the cooling period after the tool leaves a

cut, the tool surface is cooled first by the ambient air or by cutting fluid while the cooling of the interior follows later.

During the heating period, the surface of the tool expands more than the inside, and high compressive stresses are induced on the tool wedge. During the cooling period, the outside layers contract more than the interior, and tensile stresses are developed on the tool faces. Hence, the repeated heating and cooling of the tool is associated with cyclic thermal stresses in the tool wedge.

The thermal stress cycling is considered as the decisive factor which controls the type of failure and the life of cutting tools in intermittent cutting[1-12]. The thermal cycling was found to be responsible for the development of the cracks on carbide and ceramic tools[1-9]. Also, it is concluded that the number of thermal cycles and the range of thermal strain have a significant influence on the wear rate of carbide and high speed steel tools in peripheral milling[10-12].

1.1 STATEMENT OF THE PROBLEM

Hitherto, there have been conclusive experimental or theoretical studies of the thermal conditions in intermittent cutting processes which answer the questions concerning the influence of the thermal cycling on tool wear, cracking and breakage.

The experimental studies have concentrated on the measurement of the tool/chip interface temperature in the cutting period[19,21,44,45]. Obviously, the results of these experiments can only have indirect implication for tool wear or breakage.

On the other hand, the theoretical studies of the thermal cycling have been based on rather strong simplifications in the models used to compute the temperature distribution and associated thermal stresses[9,20]. The computations were based either on a single dimensional tool model[20] or a two-dimensional tool model with a square-wave pulsing heat source[9]. Such modelling approaches neglect the thermal interaction between tool, chip and workpiece, which is of paramount importance.

1.2 SCOPE OF THE THESIS

The main objective of this thesis is the study of the influence of the thermal cycling on the tool life in intermittent cutting processes.

The study requires the computation of the transient temperature distribution and the associated thermal stresses using appropriate modelling techniques. The model should introduce the interaction between the heat sources in the cutting processes. The nature of the problem boundary and the complexity of the distribution of heat source preclude any accurate solution using analytical or finite difference method. However, the finite element method can cater for such complexities with relative ease. Therefore, the finite element technique is employed to solve this problem.

The computed results can be used to try to explain various experimentally determined characteristics of tool wear, cracking and breakage.

In Chapter 2, we started by presenting a summary of the state of knowledge in the area of tool damage in intermittent cutting processes. The influence of the thermal cycling on tool wear and the formation of cracks is discussed. This is followed by a review of the investigations

which have concentrated on the study of the mechanical influence on tool chipping and breakage.

In Chapter 3, the temperature problems in both the continuous and intermittent cutting processes are identified. The solution techniques which were previously used in assessing the temperature problem are reviewed.

In Chapter 4, the energy equation, which governs the heat transfer mechanism, is derived together with the associated boundary equations. This is followed by the finite element formulation of the above equation which yields a system of ordinary differential equations (ODEs) in time. The two-point recurrence schemes which can be used to solve the system of ODEs are presented together with a discussion of their numerical stability. An automatic steplength control algorithm is developed for the two-point recurrence schemes.

In Chapter 5, the model for the cutting process is presented. A summary of the transient temperature distribution in peripheral milling is given for up- and down-milling cuts. This is followed by a discussion and conclusion.

Chapter 6 is devoted to the study of the stress cycling in peripheral milling. The stress computation is based on a two-dimensional finite element model for the tool. The thermal stresses are computed using the transient temperature results in the previous chapter and are combined with the stresses due to the cutting forces. A summary of the computed results are provided and the stress parameters which may affect the tool wear in milling are presented.

In Chapter 7, the computed results are correlated with experimental data which indicates that the number of cycles is the most significant parameter which influences the flank wear rate in peripheral milling.

Finally, Chapter 8 provides the conclusion and recommendation for further studies.

CHAPTER 2

FACTORS INFLUENCING THE MODES OF FAILURE AND TOOL LIFE IN INTERMITTENT CUTTING PROCESSES

In metal cutting, various modes of tool failure have been used to define the tool life. The common modes are diagrammatically summarized in Fig. 2.1. The most important forms of tool wear are the flank wear and crater wear. Tool life is usually defined by specified values of these forms of wear. The wear land (V_B) arises on the flank and displaces the cutting edge and, therefore, affects the finishing of the workpiece. The crater is formed on the rake face by the chip. As cutting proceeds, the crater becomes deeper resulting in the weakening of the cutting edge, which can lead to breakage.

Other modes of failure include the chipping of the cutting edge, cracks and breakage. These phenomena are irregular and their development is difficult to predict. Chipping and breakage are usually caused by brittle fracture and are related to the cracking phenomenon.

In intermittent cutting processes, the repeated interruptions result in mechanical and thermal stress cycling, and each plays a significant role in the tool damage. While chipping and breakage are usually related to the mechanical influences, the tool wear and cracking are due to the thermal cycling..

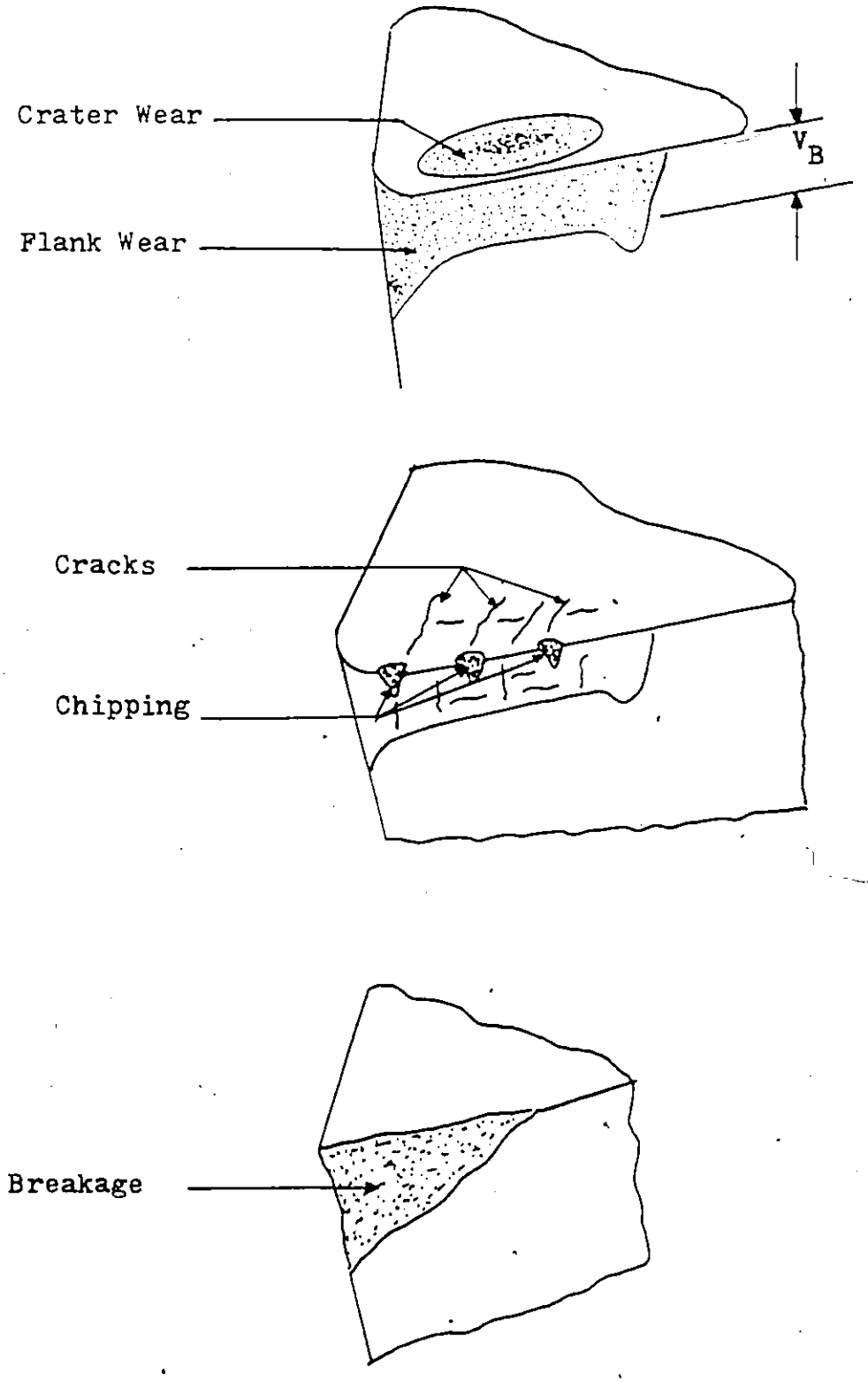

Fig. 2.1 Modes of tool failure.

This chapter is a summary of the present state of knowledge in the area of tool damage in intermittent cutting processes. The influence of the thermal and mechanical cycles on the modes of failure and tool life in intermittent cutting processes are presented.

2.1 THERMAL INFLUENCES ON TOOL DAMAGE IN INTERMITTENT CUTTING

2.1.1 Factors Governing the Thermal Performance of the Tool

When a cutting tool, operating in intermittent cutting condition, enters the cutting, the rake face heats up very quickly and high compressive stresses are induced on the surface layers of the rake face. When the tool emerges from the cut, the rake face cools off rapidly while the tool body is still hot, producing tensile stresses in the rake face. The magnitudes of the stresses developed generally depend on the number of cutting/cooling cycles undergone by the tool, and on the cutting/non-cutting time ratio.

The tool must, therefore, withstand the compressive load due to the thermal stresses during cutting, together with the stresses imposed by the mechanical loads of the cutting process. During the non-cutting period the mechanical stresses are absent, and the tool must endure any tensile thermal stresses which might develop. The performance of relatively ductile tool steel in intermittent cutting may therefore be governed by those variables which determine the mechanical and thermal stresses during the cutting period. Tungsten carbide and ceramic materials, however, are much stronger in compression than in tension. The average ratio of tensile to compressive

strength is about 0.3 for carbide and 0.2 for ceramics[22]. This may give an indication that the tensile stresses, developed in the cooling part of the cycle, are more damaging to these materials than the compressive stresses of the cutting period.

Thus the factors which may govern the performance of a tool in an intermittent cutting operation may be summarized as:

1. The cutting condition which governs the amount of heat generated.
2. The cutting/non-cutting time ratio which governs the amount of heat supplied to/withdrawn from the tool.
3. The properties of tool material such as Young's modulus, thermal conductivity and coefficient of thermal expansion.

2.1.2 Influence of Thermal Cycling on Crack Formation

Boston and Gilbert[17] noticed the formation of thermal cracks on carbide tools when face milling high strength cast iron. The cracks were formed perpendicular to the cutting edge and caused chipping of the cutting edge.

Optiz and Frohlich[18] appear to be the first to suggest a thermal mechanism of crack formation for tools used in intermittent cutting. They tested the wear properties of several carbide tools in milling constructional steels, measuring tool/chip interface temperature, using the tool-work thermocouple technique, and tool forces.

Whilst studying crater and flank wear, Optiz and Frohlich observed cracks on the rake face of the tool, and postulated that

these were developed by a thermal stress system. They proved their hypothesis by performing a number of simulative experiments using a high frequency generator to heat carbide rods in which cracks appeared after several heating and cooling cycles. They did not, however, attempt any calculation of the thermal stress magnitude during cutting.

Pekelharing[3] studied the formation of cracks on ceramic tools when used in interrupted cutting. He found that there was a limiting value of speed/feed combination, below which no cracks appeared. Therefore, the cracks were thought to be due to thermal effect as in carbides. The cracks were only found after several cutting/cooling cycles, but Pekelharing suggested that the cracks were developed after only one cycle in an invisible form. He was able to show that they are, in fact, present after one cycle by detecting them using a special dying technique.

The results of the experiments led Pekelharing to reject any theory which suggests that cracks are formed by fatigue effect due to repeated elastic stresses, although such effect may enlarge the cracks. Pekelharing suggested that the formation of the cracks in the first cycle is due to plastic deformation resulting from compressive stresses at high temperatures in the first heating cycle. Cracks develop on subsequent cooling, since the plastically deformed area can not maintain a strain compatibility with the surrounding material. This theory explains the fact that the cracks first form someway back from the cutting edge, in the region where the crater wear will be later formed.

The cracks which were developed in the ceramic tool form a series of fine parallel lines on the tool rake face. They are called "comb cracks". This kind of cracks were found to be innocuous to tool life. Thus the tool would continue to cut satisfactorily with such cracks present.

This work of Pekelharing may be considered the most significant report on the formation of cracks in intermittent cutting. However, he has not measured the tool temperature and has not calculated any stresses.

Zorev[4] in U.S.S.R. had conducted experiments to study the influence of intermittent cutting on tool life. The experiments' results showed no difference in the tool life of H.S.S. tools when making continuous or intermittent cuts, and a considerable difference in the life of the carbide tools under these conditions. The actual cutting life of TT7K12 (equivalent to P40) carbide tipped cutting tools, when planing steel at speed v = 35 m/min (116 sfpm) and feed f = 2 mm/rev. (.08 in/rev.), is four times shorter than with turning. The mode of failure and how the tool life had been determined is not clear in this paper[4]. Zorev, also, compared the lives of carbide tools in a series of experiments, turning bars of various rectangular cross sections, hence obtaining intermittent cuts with a series of cutting time ratios. He found that the tool lives depend not only upon the tool material but also upon the blank shape, i.e. cutting time ratio.

To clarify the role of impacts as the tool enters the cut, he conducted two experiments on planing steel. In the first one the cut

starts with the full depth of cut at entry which decreases to zero at the end of the stroke, while in the second the depth of cut starts at zero and gradually increases to a maximum at the exit. In both cases the results showed that there is no significant difference in tool life. This led Zorev to conclude that the initial entry does not play an effective role on tool life.

Further planing tests with different cooling periods enabled Zorev to show that the length of the cooling period had an effect on the life of carbide tools. Also, in studying the face milling cutters, tests showed that all the factors which increase the cooling rate of the cutting edge during the cooling period aid the formation and extension of cracks, and the reduction of tool life. At the same time, the heating of the milling cutter by a gas flame during the non-cutting period increased the tool life. Based on these experiments, Zorev concluded that the basic cause for the formation of cracks and the reduction in tool life of a carbide tipped cutting tool in intermittent cutting lies in the cyclic cooling of cutting edge. He attributed this to the development of tensile stresses during the cooling-off period.

Furthermore, Zorev pointed out that the tool life of carbide tools in intermittent cutting is determined not only by the amplitude of the change of stress in the surface layer, but also by the number of these changes.

Whilst Zorev was working in Russia, Okushima and Hoshi in Japan, were studying the performance of carbide tools in intermittent cutting[1,2,5]. They investigated the cracks produced in a variety of

carbide tools, when face milling carbon steels, and were able to classify the tool damage into three categories:

(i) Tool chipping at low cutting speeds.

(ii) Tool chipping of a large size without preceding crack.

(iii) Damage occurring after many cycles, broadly classified as "fatigue damage".

The authors found that failure of type (i), and type (ii) occurred at low cutting speeds, and suggested that the reason for these failures is the impact at tool entry in the cut. Further, failures of category (ii) were found to be fairly random in occurrence. These failures, also, were found to be independent of the duration of a cut, occurring both at the commencement of cutting and after a long cutting time.

Category (iii) is the most important one and it consists of several types of breakage which occur due to preceding cracks in either the rake or the flank faces. The authors classified them into the following modes of failure (Fig. 2.2):

(i) chipping on the rake face initiated by a crack running on the rake face parallel to the cutting edge (Fig. 2.2-I),

(ii) chipping on the flank face, caused by a crack running along the flank face parallel to the cutting edge (Fig. 2.2-IIA and IIB),

(iii) a fracture starting on both the rake face and the flank, and caused by combined propagation of the above two cracks (Fig. 2.2-IIIA, B, C and D), and

(iv,v) fracture, and pitting (Fig. 2.2-IV).

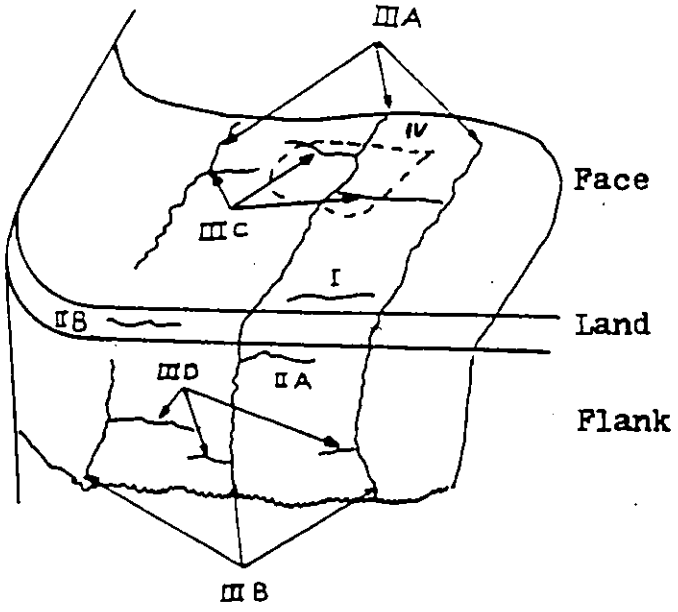

Fig. 2.2 Typical locations and appearances of various types of fatigue cracks.

The first three modes of failure are all taken to be fatigue failures. The last two modes of failure are associated with a crack running along the rake face perpendicular to the cutting edge. These have been observed by several workers[3,6,7,8], and are popularly called "thermal cracks".

Okushima and Hoshi discussed the formation of the above cracks as fatigue phenomena[1,2]. They suggested that the tool undergoes plastic deformation during the cutting period due to the compressive stress present, and hinted that this may aid the formation of cracks in the tool. They demonstrated the plastic deformation by carrying out an experiment, in which carbide specimens were heated intermittently in a spot welding machine. The test specimen ruptured suddenly after many thermal shocks. The ruptures were due to radial and submerged cracks which are similar to the cracks obtained with intermittent cutting. The localized plastic deformation and cracking can occur in carbide, if the temperature gradient is made high by rapid heating and cooling. However, this does not prove that the cracks which form in tungsten carbide cutting tools are preceded by plastic deformation.

In order to find a better explanation for the cracking phenomenon, Okushima and Hoshi measured the tool/chip interface temperature in milling when cutting steel with face milling carbide tools[19]. Then, they used the measurement to compute the cyclic temperature inside the tool using single dimensional analysis[20]. The measurement and computation results showed that the tool tip temperature builds up very rapidly in the heating period and the surface layers of the tool/

chip interface area cool faster than the inside layers in the cooling period. Consequently, in the heating period the tool expands and high compressive stress occurs on the tool surface. Then, the thermal stress turns to tension during the non-cutting period, because the surface temperature becomes lower than the internal one. Thus, a maximum range of thermal stress arises on the surface, where fatigue damage due to the repetition of the maximum stress range accumulates to initiate thermal cracks. Although Okushima and Hoshi measured and computed the temperature, they did not compute any stresses to verify their postulates.

Braiden and Dugdale[6,21] investigated the formation of cracks on carbide tools when used in intermittent turning operation. Their tests showed that cracks perpendicular to the cutting edge developed on the tool rake face someway back from the cutting edge, in the area where crater wear occurs. The cracks developed after almost two minutes of cutting. The tool materials were three grades of carbide and the workpiece was steel plate of 2 × 10 inches (50.8×254 mm). The typical cutting conditions were: speed v = 112.5 m/min (375 sfpm), feed f = 2.54 mm/rev. (.01 in/rev.) and depth of cut d = 6.25 mm (.25 inch).

To analyze the crack formation, they measured the tool-chip interface temperature using the tool-work thermocouple technique, and thermistors scattered on the carbide tip faces to measure the temperature at identified spots in both heating and cooling. Assuming the tool will reach a steady condition after several cycles, they computed the steady state temperature distribution. Hence, they solved the

Laplace heat transfer equation and the applicable boundary conditions using the relaxation method. Then, they used the computed temperature fields to determine the thermal stresses assuming perfectly elastic behaviour. The computed thermal stresses did not reveal any tensile stresses in the direction of the cutting edge during the cooling part of the cycle. Therefore, they suggested that during the heating part of a cutting cycle compressive thermal stress may cause plastic yielding along a strip of the tool face just behind the cutting edge. As the strip subsequently cools under the constraint of the surrounding elastic material, tensile stress is set up, which may become high enough to produce the cracks.

2.1.3 Influence of Thermal Cycling on Tool Wear

The aforementioned work showed the influence of thermal cycling on the cracking of the sintered carbide tools when used in intermittent cutting. Other work done by Yellowley and Barrow[10,11,12] showed the influence of thermal cycling on the tool wear rate in peripheral milling. Yellowley and Barrow conducted tool life tests in which they concentrated on the flank wear of H.S.S. and sintered carbide tools. They found a strong effect of the cutting/non-cutting time ratio. The most significant feature of the test results is the large increase in the active tool life (actual cutting time) which occurs in going from a half immersion cut (up and down) to full immersion cut (slotting); tool life is more than doubled. This phenomenon could be attributed either to mechanical or to thermal influence. In order to distinguish

between these influences, the authors repeated the slotting test with a prearranged thin gap in the middle to include the mechanical influence of both up- and down-milling. The test results showed that the presence of the gap did not change the tool life. Hence, they concluded that the difference in heating and cooling times influences the tooth life and the mechanical influence could be excluded.

In order to explain the thermal influence, it was shown that cutting time ratio has considerable effect on the range of thermal strain developed in the cutter teeth. The range of thermal strain, and also the number of cycles of thermal strain are shown to have considerable influence on tooth life. To characterize the influence of thermal cycling on tooth wear, the authors developed the strain range parameter (E_r), which is a function of the heating time (t_h) and the cooling time (t_c). The relation is:

$$E_r = 39 \log t_c - 23 \log t_h + 37.5$$

The use of this parameter (E_r) is intended to characterize the relative influence of heating and cooling time at constant peripheral speed, constant equivalent feed and constant depth of cut for one mode of milling (i.e. up cut or down cut). The authors conducted a series of tests to show the validity of (E_r) as an important factor determining tool life, see Fig. 2.3. The form of the relationship between these parameters is then used to develop an expression for a thermal fatigue parameter which takes into account both the range of strain and the number of cycles of thermal strain per unit time.

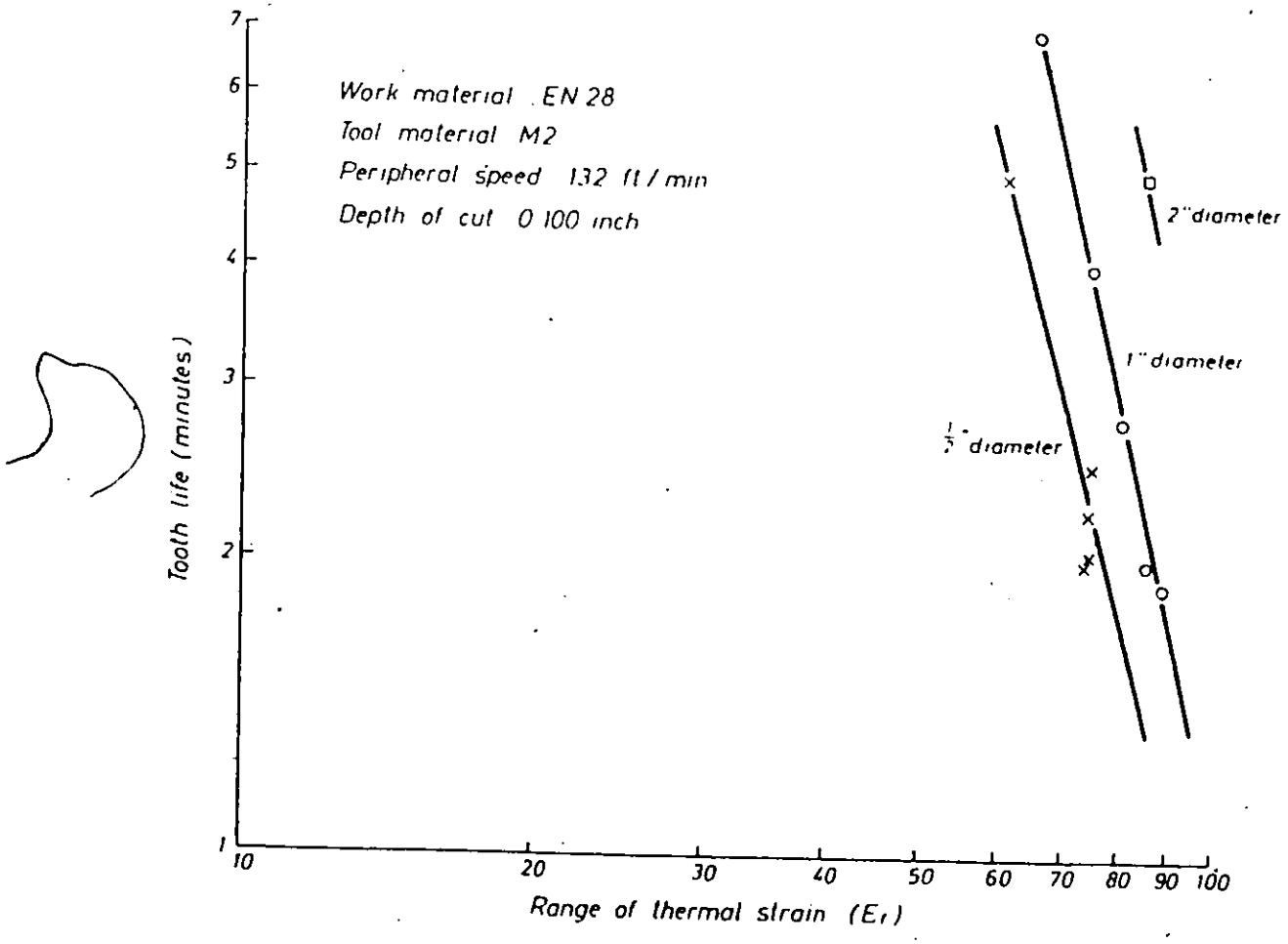

Fig. 2.3 Influence of the range of thermal strain on tooth life.

To develop the thermal fatigue parameter, the authors assumed that the tool undergoes plastic strain cycling and the relation between the range of plastic strain (E_p) and the number of cycle (N) is valid. The relation is

$$N = C\ E_p^{-2}$$

where C is constant.

The following assumptions are then made:

(i) In the absence of thermal cycling (i.e. in turning process) the relation between wear rate and time is in the form:

$$\frac{dV_B}{dt} = A.t^m$$

where A and m are constants, and V_B is the land wear.

(ii) The wear resistance of the tool in milling is inversely proportional to the product

$$E_r^n\ N^{n/2}$$

where N is the number of thermal cycling, and n is a constant.

Based on the above assumptions, the authors derived a simple power relation between the tooth life (T_t) and the thermal fatigue parameter (Z); which is

$$T_t\ Z^y = C$$

where

$$Z = E_r\ (R.X)^{\frac{1}{2}}$$

R = rotational speed,

X = ratio of the total cycle to the cutting time (t/t_h), and

y and c are constants.

Figure 2.4 shows the resulting relationships when Z is plotted against T_t for three different diameter end mills (same data in Fig. 2.3). The relationship would appear to indicate that the thermal straining and the number of cycles are by far the most important of any other factors such as cutter diameter and number of teeth.

2.2 MECHANICAL INFLUENCES ON TOOL FAILURE IN INTERMITTENT CUTTING

The reviewed work, so far, showed the importance of the thermal cycling on the tool life when used in intermittent cutting processes. This section is a review of the work in which special consideration was given to the mechanical influences on the tool damage in intermittent cutting. Generally, the investigators laid the emphasis on the mechanical effects of the entry and exit of the tool to/from the work piece which lead mainly to premature failure of the cutting tools.

2.2.1 Effect of Entry Condition on Tool Life

In face milling operations different points of the tool rake face may prove to be points of initial contact of tool and workpiece. Figure 2.5 shows the various points of contact where the parallelogram STUV represents the region of tool contact on entry. The initial contact could be either at points S, T, U, V or along the lines VU, UT, TS, and SV. Initial contact is of crucial importance on the tool life of the carbide tools, and even H.S.S., particularly when machining high strength materials[14,15]. Beckhaus[14] concluded that machining with unfavourable

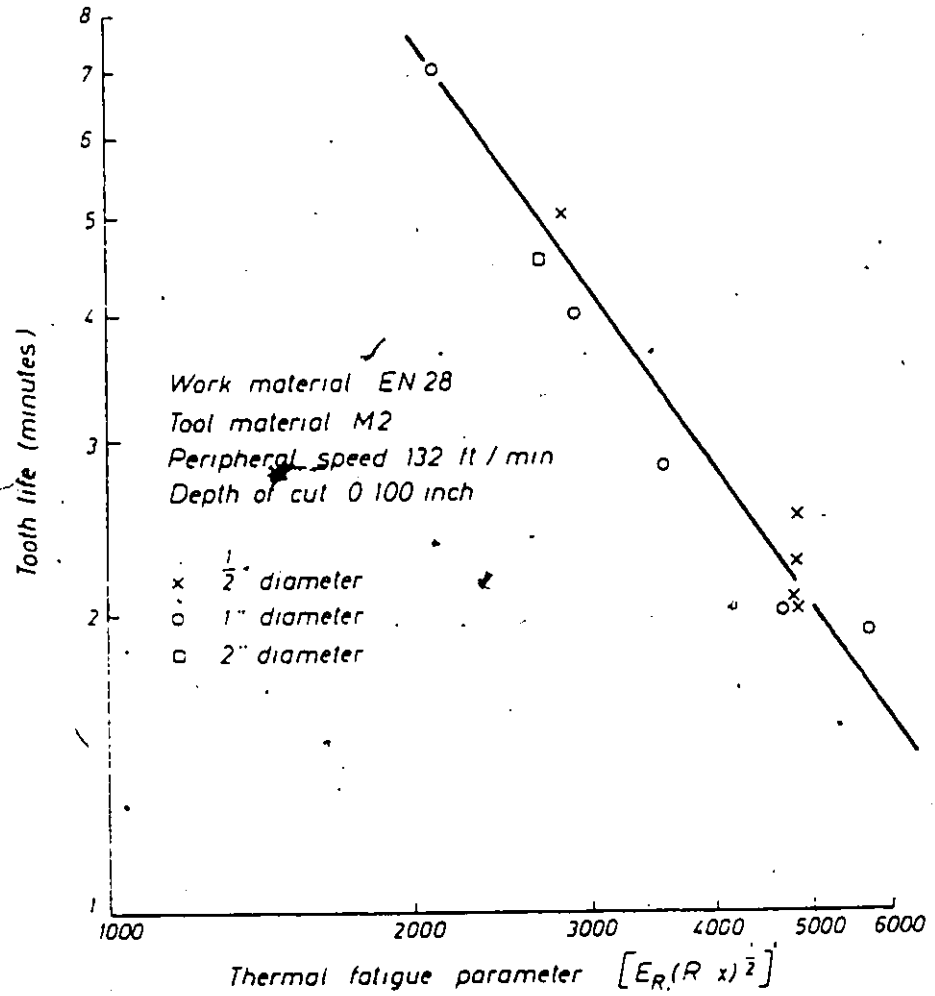

Fig. 2.4 Influence of the thermal fatigue parameter on tooth life.

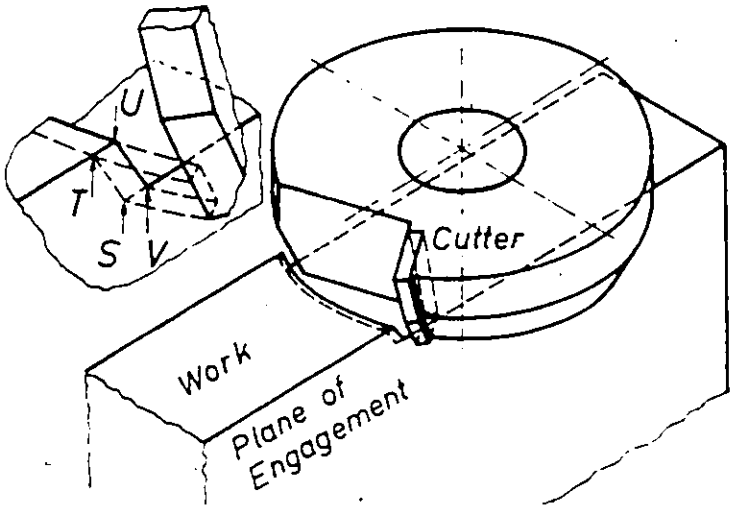

Fig. 2.5(a)
Face milling cutter and workpiece shortly before initial contact.

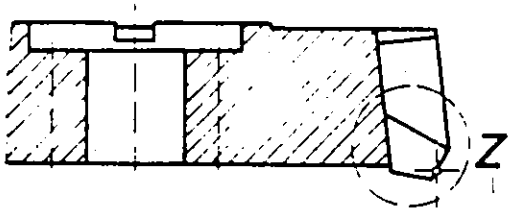

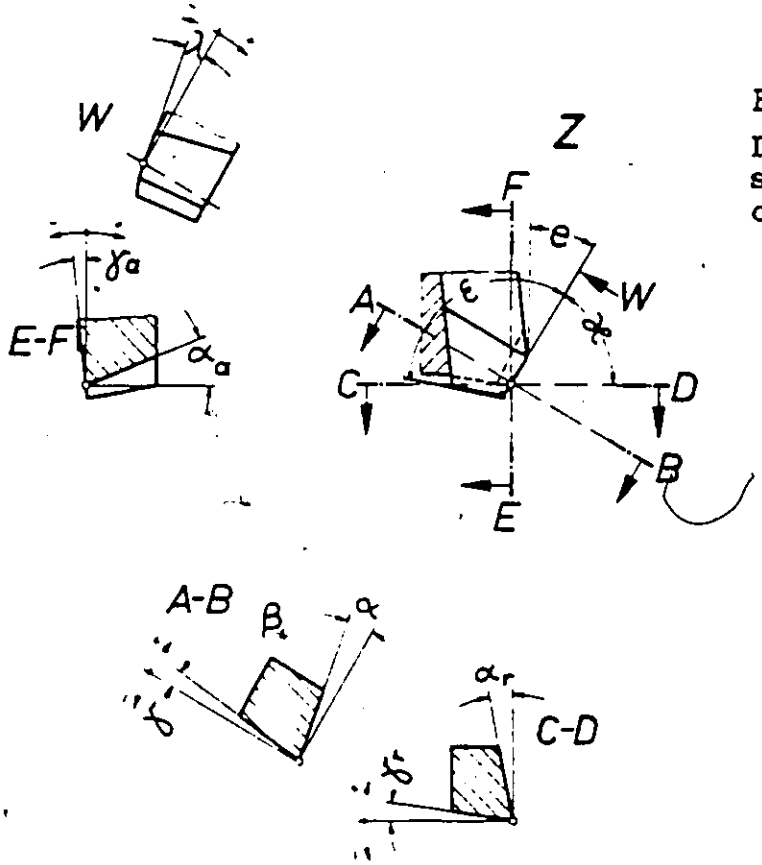

Fig. 2.5(b)
Definition and specification of tool geometry.

contact condition leads to premature tool failure. In order to relieve the weakest spot of the cutting edge (the cutting edge Point S), Beckhaus[14] and Kronenberg[15] recommended using a particular tool geometry leading the impact further back on the rake face. In order to construct a mathematical model, Kronenberg introduced the concept of "partial time of penetration" (that proved insignificant) and "partial area of engagement". Beckhaus believes that the "partial area of engagement" and the line of initial contact with the workpiece (see Figs. 2.6 and 2.7) have direct influence on the relief of the impact and consequently on the tool life. However, increasing the "partial area of engagement", in order to decrease stresses in the tool, inevitably involves large plastic deformation of the material during the formation of the chip. Also, the particular tool geometry required for partial area of engagement would lead to a negative rake angle. This is one of the conditions for very high crater wear, and, therefore, the reason of premature failure of the cutter, particularly in the case of machining high strength steel[14].

The type of contact and the "partial area of engagement" depend on the tool geometry and on the relative positions of tool and workpiece in terms of the angle of engagement which is shown in Fig. 2.8. It can be seen from Figs. 2.9 and 2.10 that there is an abrupt decrease of tool life within a certain interval of the angle of engagement (ε_E). The function curves of the partial area of engagement (Fig. 2.7) agree well with the results shown in Figs. 2.9 and 2.10. Therefore, Beckhaus concluded that the partial area of engagement is a useful parameter to

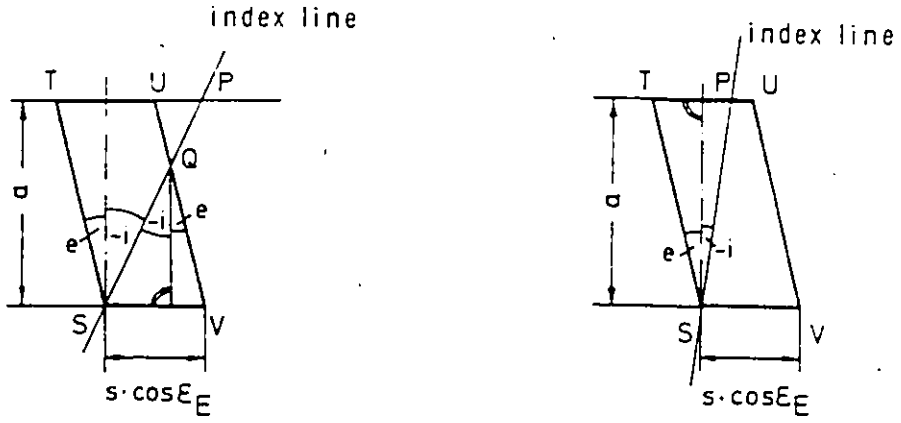

Fig. 2.6 Calculation of "partial area of engagement" F_s

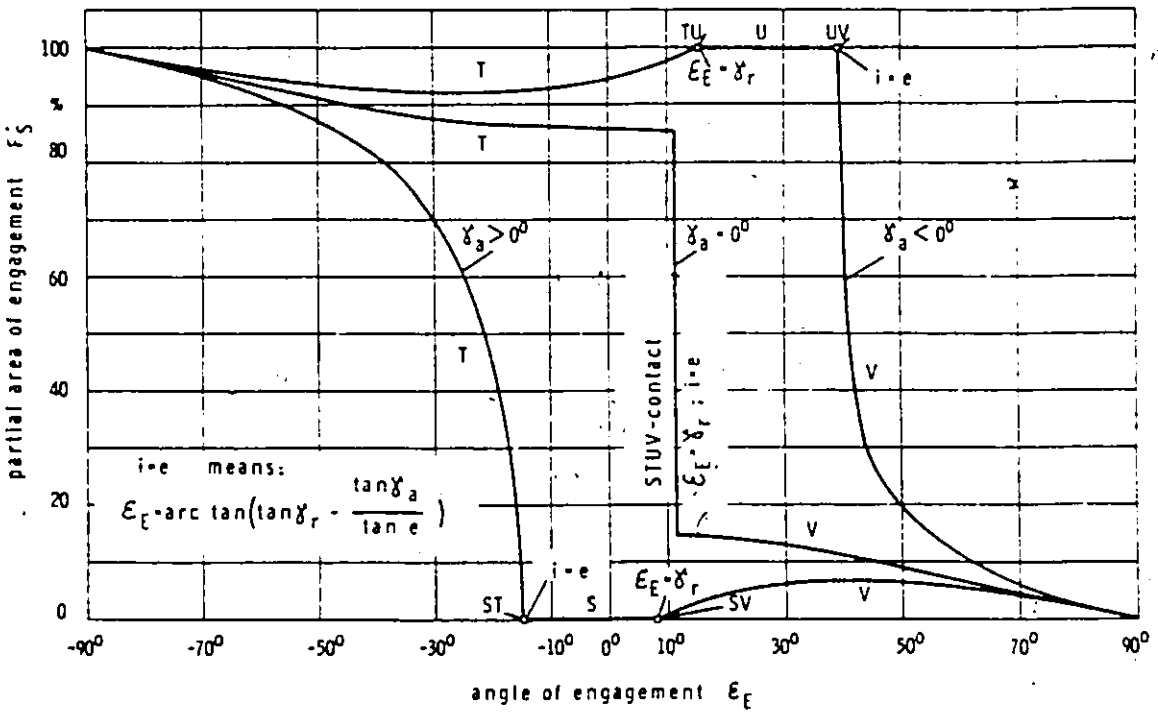

Fig. 2.7 Partial area of engagement F_s as a function of the angle of engagement ε_E.

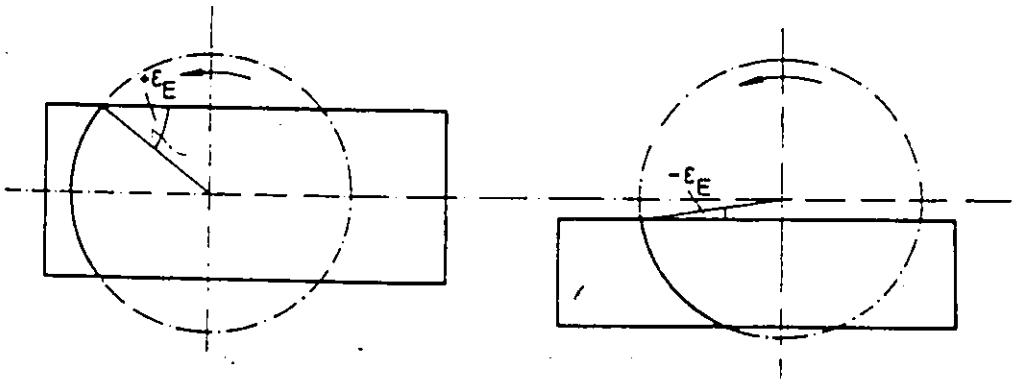

Fig. 2.8 Definition of the angle of engagement.

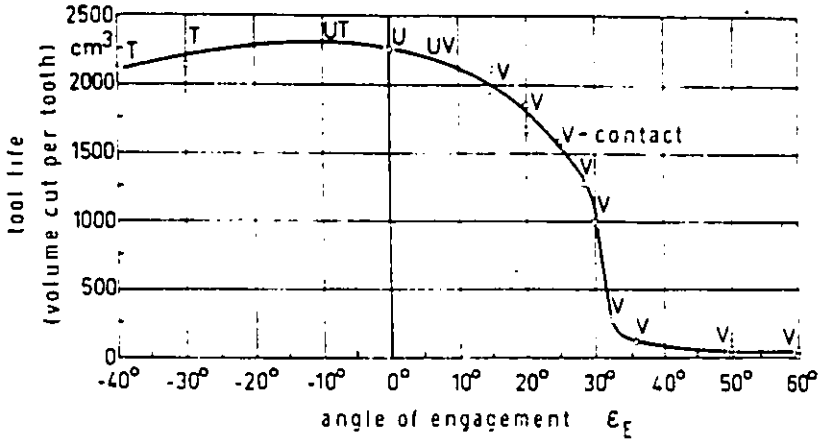

Fig. 2.9 Tool life as a function of angle of engagement. The initial contact on the rake face is 'U' contact.

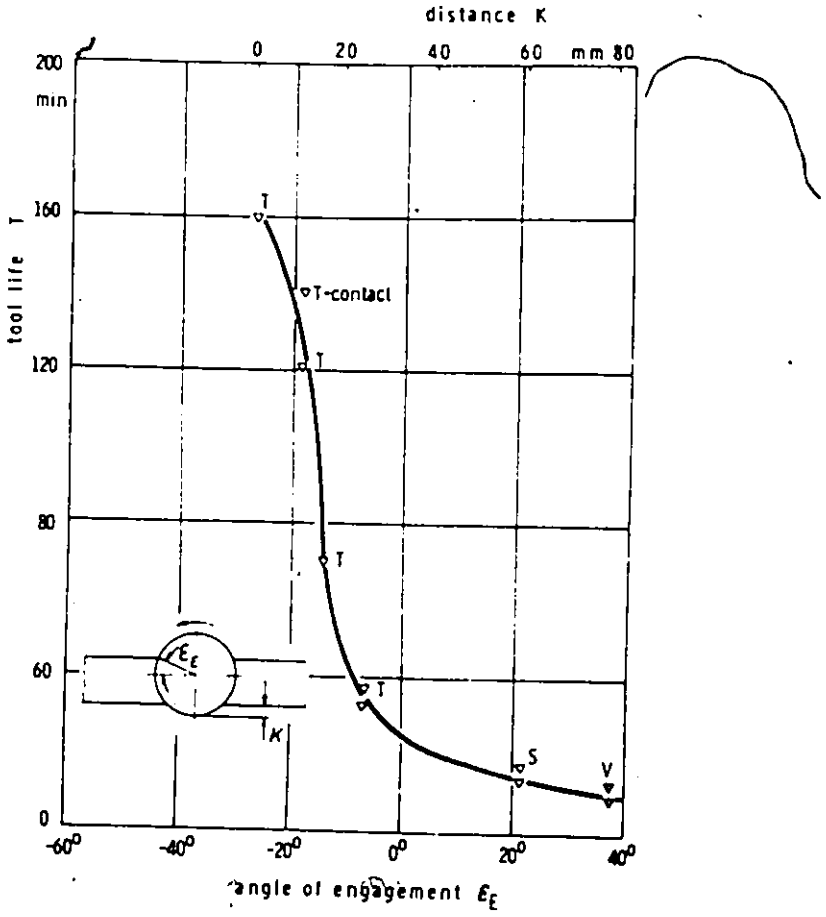

Fig. 2.10 Tool life as a function of angle of engagement. The initial contact of the rake face is 'S' contact.

optimize the contact conditions in order to obtain maximum tool life. Hence, he computed the relation between the tool geometry and the "partial area of engagement". It is found that the face milling with a low cutting edge angle "χ" (Fig. 2.5 b)) should be advantageous. He carried out tool life tests which proved that this assumption is true.

2.2.2 Effect of Exit Condition

In one of his revealing research projects, Pekelharing[16] explained the mechanism of tool breakage at its exit from a cut. He carried out orthogonal cutting tests in which the workpiece was pre-arranged to eliminate the influence of the entry. The tests were carried out using sharp carbide tools (two different grades), cutting steel on a lathe with practical cutting conditions (speed range 30-300 m/min (100-1000 sfpm), and thickness of cut range .1-.5 mm (.004-.02 inches)). The results showed that none of the sharp tools did survive the first cut. Hence, Pekelharing attributed this immediate destruction of the cutting tools to the mechanism of chip formation at the end of a cut. The mechanism is illustrated in Fig. 2.11. A chip "foot" is formed at the end of a cut which is curved and separates the workpeice, not by brittle fracture but by plastic shearing, requiring a high shear force until separation. The developed "negative shear" close to the end of cut, causes a negative friction force and possibly a negative chip speed which may cause high tensile stress on the rake face. These hypotheses were tested by finite element analysis based on a tool-chip model representing the mechanism of chip formation.

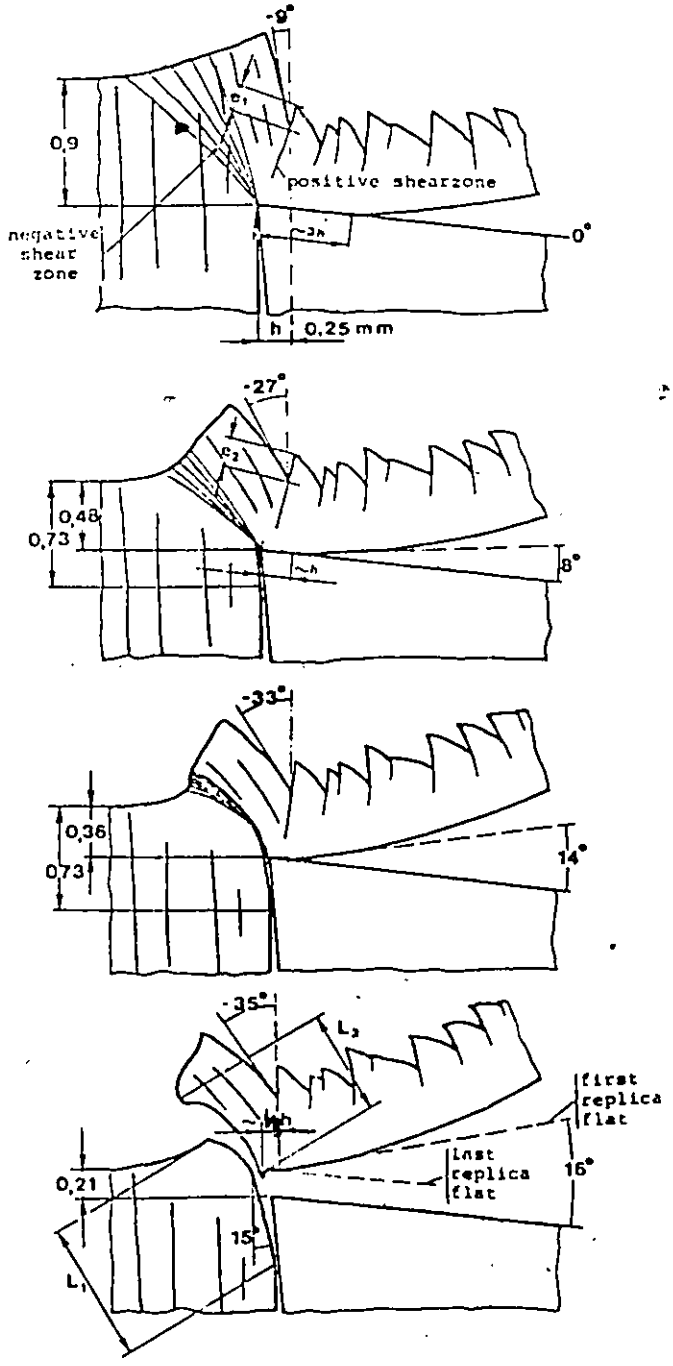

a) Negative shear has started but positive shear continues.

b) Negative shear zone concentrates and chip has rotated 8°.

c) Narrow negative zone and crack grows.

d) Chip and foot are free before tool reaches end face of workpiece.

Fig. 2.11 Mechanism of chip formation at the end of a cut - after Pekelharing (16).

The analysis revealed the formation of negative shear and the increase of the tensile stresses on the tool wedge when applying a negative friction force.

It should be noticed that the difference between the above tests and practice is threefold; (a) the tool is chamfered or round, (b) the cutting edge works under an inclination angle, and (c) a radius or minor cutting edge is active. Pekelharing conducted tests to investigate the influence of chamfering and rounding of the cutting edge in the foot formation and chip rotation at the end of cut. He concluded that the rounding or chamfering of the cutting edge does not prevent the dangerous chip rotation during the exit. Nevertheless rounding or chamfering gives tool life instead of the immediate failure of sharp carbide tools. Regarding the influence of the inclination angle, he maintained that an inclination angle of up to 20° does not suppress the negative shear and foot forming. Thus, the exit condition could be harmful even for practical milling tools.

2.2.3 Effect of Mechanical Stresses

Tlusty and Masood[13] studied the effect of the mechanical stresses on the chipping and breakage of carbide tools. Their investigation was carried out through cutting tests, fractography and stress analysis.

The cutting tests were conducted by turning three grades of steel (1040, 4340/217BHN, 4340/380) in both continuous and intermittent cutting. The intermittent turning experiments were carried out on workpieces with very short interruptions so as to induce cyclic thermal

stresses. The test results showed, for continuous cutting, that chipping occurs at medium feeds of 0.3 to 0.6 mm/rev. (.012 to .024 in/rev.) and breakage occurs at heavy feeds of 0.7 to 1.1 mm/rev. (.028-.044 in/rev.). Breakage occurred either after some accumulation of chipping (and consequent increase of cutting force), or outright after a very short time. In interrupted cutting, breakage occurred at a lower feed of about 0.5 mm/rev., after a very short time. Therefore, the authors excluded fatigue as an explanation, and related the occurrence of breakage to the change of loading mode either at the exit or at the entry (shockwave at exit out of cut or chip interference at entrance into tool). The nature of this change was not investigated.

The types of fracture were inspected under an electroscanning microscope. The chipping appeared to have been accompanied with plastic deformation, while the breakage was due to brittle fracture.

Stress analysis simplified to a two-dimensional analysis plane strain problem confirmed the above observation. A local maximum of tensile stress was indicated on the rake face at a distance between 2 and 4 mm, which coincides with the origin of the observed brittle fracture. The level of stress roughly corresponds to the Transverse Rupture Strength (TRS) of the sintered carbide. Shear stress maxima were found close to the cutting edge at levels corresponding to the shear flow strength of the sintered carbide.

The investigation of Tlusty and Masood could be considered the first comprehensive work to assess the occurrence of chipping and breakage in carbide tools. However, in the analysis, they neglected many

aspects such as thermally induced stress, anisotropy and non-homogeneity of sintered carbide, and three-dimensional analysis.

2.3 SUMMARY AND DISCUSSION

In this chapter, several of the most recent and significant investigations on tool life in intermittent cutting have been discussed. While many investigators agreed on the importance of thermal cycling, others laid the emphasis on the role of mechanical stresses in tool damage. The former group agreed that thermal cycling has a great influence on tool wear and tool cracking. Okushima and Hoshi[1,2,5], and Zorev[4] concluded that the formation of cracks on the sintered carbide is due to the resulting tensile stresses on the cooling part of the thermal cycle. Pekelharing[3], and then Braiden and Dugdale[6,21], postulated that the crack formation on ceramic or carbide tool tips is due to plastic deformation in the heating period, which reverses to tensile stresses in the cooling period. Yellowley and Barrow[10,11,12], by contrast with the former authors, maintain that the range of thermal plastic strain developed in the cutter teeth due to thermal cycling, and also the number of cycles of thermal strain have considerable influence on flank wear of the tool.

The mechanical role in tool damage in intermittent cutting has been studied by many investigators. Bechaus[14] and Kronenberg[15] laid great emphasis on the influence of the initial contact of tool and workpiece, and pointed out that this influence becomes extremely significant when machining high strength materials. Pekelharing[16] showed that the

exit condition has a great influence on tool chipping and breakage. Thus, they concentrated on mechanical rather than thermal shock.

In the previously discussed work, the analysis of thermal cycling was based on strongly simplified models. Okushima and Hoshi[20] based their analysis on a computed single dimensional temperature distribution. Braiden and Dugdale[6] based their analysis on a postulated temperature field. Hitherto, there has been no comprehensive study of thermal cycling in intermittent cutting which can answer the questions of:

(i) Thermal stresses developed during heating and cooling periods.

(ii) Plastic deformation and plastic strain cycling.

(iii) The relation between the above stresses and the formation of cracks and tool wear.

The study of the thermal cycling necessitates the computation of a complete temperature field during the cutting cycle. Therefore, the next chapter is devoted to a review of the state of knowledge of the temperature problem in metal cutting.

CHAPTER 3

TEMPERATURE IN METAL CUTTING

The knowledge of cutting temperature is essential when studying most metal cutting operations. In addition to the temperature influence on the various tool wear mechanisms, it is also important when determining the behaviour of material in chip formation. Therefore, considerable attention has been devoted to the study of the temperature problem in metal cutting operations in the last three decades.

Whilst temperature is obviously of importance in all metal cutting operations, a considerable effort was made to study the temperature problem in turning as compared to the intermittent cutting operations such as milling, grinding, etc. This may be because of the transient nature of the intermittent cutting processes which makes the problem more difficult. However, the fundamentals of the temperature problem in turning are also applicable to both continuous and intermittent cutting operations.

This Chapter is a review of the techniques used in assessing the temperature problem in both continuous and intermittent cutting operations.

3.1 TEMPERATURE PROBLEMS IN METAL CUTTING WITH PARTICULAR REFERENCE TO CONTINUOUS ORTHOGONAL MACHINING PROCESSES

The machining of metals is invariably accompanied with heat generation. The energy expended in cutting is converted into heat

which is distributed in the tool, chip and workpiece. The energy is liberated essentially in two distinct regions (see Fig. 3.1): (i) the shear zone (AB), where the heat is generated due to plastic deformation associated with the chip formation, and (ii) the tool/chip interface zone (BC), where the heat is generated due to a combination of plastic deformation and frictional resistance between the chip and the tool. A third heat source (BD) may be generated when the tool flank is worn out. Heat is generated due to the friction between the workpiece and the tool flank. The heat generated in this zone is comparably very small.

The pattern of heat generation as depicted in Fig. 3.1, leads to a temperature gradient in the chip, tool and workpiece. The shear zone thermal energy raises the temperature of the shear plane, and flows partly into the chip and partly into the workpiece. Also, the generated thermal energy on the tool/chip interface region is divided between the chip and the tool. Thus, the research has been directed towards two problems in attempt to analyze the temperature problems in metal cutting. These are:

1) The division of energy between chip and workpiece, and the determination of the average temperature and temperature distribution in the shear zone.

2) The division of the rake face thermal energy between the chip and the tool, and the determination of the mean temperature along the tool face, and the temperature distribution at tool/chip interface.

The solution of these problems determines only the temperature in the shear and tool/chip interface zones. The knowledge of the

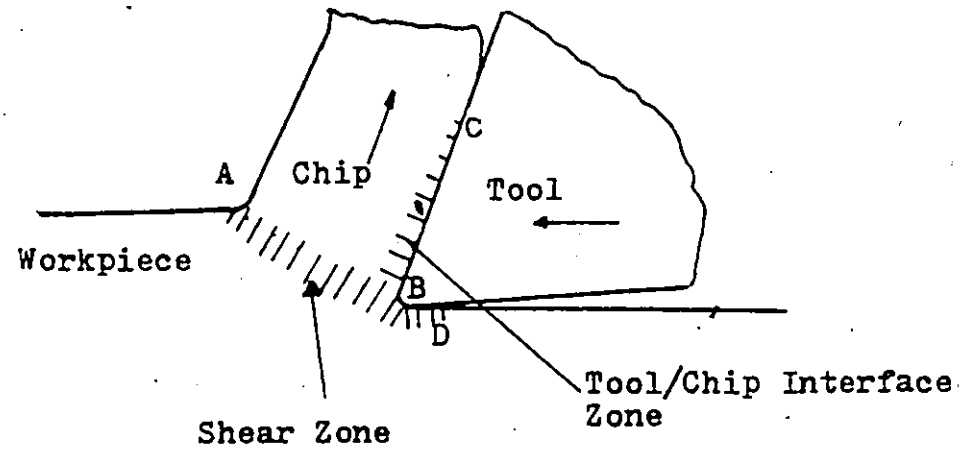

Fig. 3.1 Generation of heat in orthogonal cutting.

temperature distribution in the tool, chip and workpiece is advantageous when studying such phenomena as basic tool wear mechanisms. However, less effort has been directed towards the assessment of the temperature distribution in the tool, chip and workpiece.

3.1.1 Temperature Distribution Due to Shear Plane Heat Source

Several theoretical analyses for the temperature distribution in the workpiece and the shear plane have been carried out using two general methods of solution. These are discussed next.

i) The shear plane is considered to be an oblique band source of heat moving through the workpiece in the direction, and with the magnitude, of the cutting velocity vector. The solution of this problem involves the heat transfer calculation for a moving heat source.

The problem of a plane source of heat, moving either parallel, or perpendicular to the plane of infinite, or semi-finite solid has been investigated by Blok[24], Jeager[25], and Rosenthal[26]. The results of their investigation have been applied to the shear plane solution by several workers[28-33].

ii) The solution due to Weiner[34] who showed clearly that, with practical cutting speeds, conduction in the workpiece in the direction of motion of workpiece and chip could be neglected. This permits the relevant heat transfer equation to be simplified. Weiner, thus, was able to find an analytical solution for the simplified equation for given boundary conditions. Rapier[35] used the relaxation method without using Weiner's assumption, to compute the temperature distribution on the chip, tool and workpiece. Both solutions, by Weiner and Rapier,

agree on the magnitude of the average temperature along the shear plane. Nakayama[40] employed a thermocouple technique to measure the heat carried away by the workpiece and his results agree with the work of Weiner and Rapier over the range of the cutting conditions examined.

3.1.2 Division of Shear Plane Thermal Energy

The shear plane thermal energy is partly carried away by the chip and partly conducted back to the workpiece. The amount of heat conducted back in a cutting operation depends on a number of factors, such as cutting speed, feed, chip size compared to the size of workpiece, etc. An exact treatment including these factors is very difficult. Trigger and Chao[30] assumed a constant value of 10% of the total heat is conducted back to the workpiece. This assumption is based on the work of Schmidt and Roubik[27] in drilling. Weiner[34], in his analytical solution for the shear plane temperature, derived a formula expressing the proportion (λ_s) of the total heat generated on the shear plane, which flows into the workpiece. The proportion λ_s is a unique function of R tanϕ, where R is the thermal number and ϕ is the shear angle. The formula is:

$$\lambda_s = \frac{1}{4Y} \operatorname{erf} \sqrt{Y} + (1+Y) \operatorname{erfc} \sqrt{Y} - \frac{e^{-Y}}{\sqrt{\pi}} \left(\frac{1}{2\sqrt{Y}} + \sqrt{Y}\right) \qquad (3.1)$$

where

$$Y = \frac{1}{4} R \tan \phi$$

erf(x) = error function; $\frac{2}{\sqrt{\pi}} \int_0^x e^{-u^2} du$, and

erfc(x) = complementary error function; 1-erf(x).

The experimental results after Nakayama and Boothroyd[36], together with the theoretical equation are shown in Fig. 3.2. It can be seen from the figure that at high values of R tan ϕ the theoretical prediction of Weiner leads to a lower value of λ_s. But as pointed out by Boothroyd, the percentage error in the mean shear plane temperature will be small, and under practical cutting condition, negligible.

3.1.3 Tool-Chip Interface Temperature and Distribution of Friction Heat Energy

At the tool-chip interface, the heated chip is moving with high speed, and it is in intimate contact with the tool under high friction forces. The thermal effect of this situation is comparable to the theoretical case of a perfectly insulated slider moving across a conducting surface. The solution of this problem involves the heat transfer calculation for stationary and moving heat sources. The solution is due to Kelvin[23] and has been further developed by Blok[24] and Jeager[25].

Chao and Trigger[30] applied this work to the particular case of the tool/chip interface temperature problem. They solved the problem to determine the average tool/chip interface temperature and the division of heat between chip and tool. In their work, two assumptions were unrealistic and are considered weaknesses. The first concerns the amount of energy stored in the deformed chip, and the second concerns the heat conducted back to the workpiece. These points were modified by Loewen and Shaw[31], whose method is otherwise similar to that of Chao and Trigger.

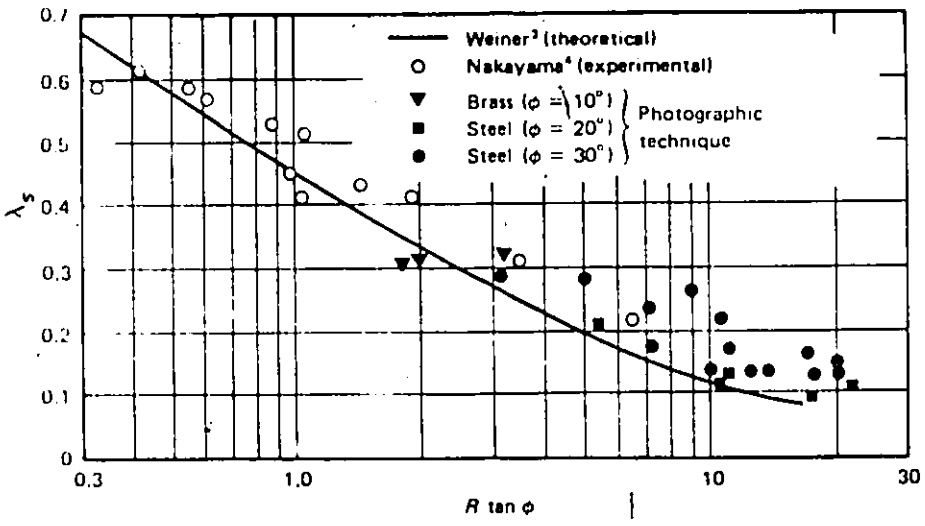

Fig. 3.2 Effect of R tanϕ on division of shear-zone heat between chip and workpiece.

Chao and Trigger[33], in 1955, published their second paper on this subject, making use of Loewen and Shaw's modification concerning the shear plane heat distribution. In addition to this modification, they assumed that the heat flux distribution along the tool/chip interface is non-uniform. The temperature was obtained by a method of successive approximation. This method ultimately allows not only the temperature distribution but also the heat flux at the tool/chip interface to be found.

Rapier[35] also studied this problem, and assumed a plane heat source of uniform strength covering the whole contact area and neglected the heat flow into the tool. Thus, he was able to calculate the temperature distribution along the tool/chip interface area. His computation predicts that the maximum temperature on the rake face occurs at the end of the contact between chip and tool. This result disagrees with Chao and Trigger's latest solution which showed that the maximum temperature occurs within the tool/chip contact area. Moreover, Rapier's solution contradicts the experimental results for the temperature distribution on the tool/chip interface, which indicate that the maximum temperature occurs within the tool/chip contact length[36,41,42]. This contradiction would indicate that the assumptions made by Rapier are inaccurate.

Boothroyd[36,43] measured the temperature distribution in the tool, chip and workpiece using a photographic technique. The maximum temperature rise data obtained experimentally are compared with the theoretical solution by Rapier. A poor agreement was observed. Thus, Boothroyd suggested that the discrepancy was due to the assumption of plane heat source along the tool/chip contact area. He proposed alternative forms

of heat sources in which the friction heat is distributed over either a triangular or rectangular area in the chip. Comparing the theoretical solution using these heat sources, he found that the triangular heat source distribution compares more favourably with the experimental and with the theoretical prediction of Chao and Trigger.

3.1.4 Solution for a Complete Temperature Distribution

In the aforementioned work, the studies were directed towards the determination of the mean temperature and the temperature distribution on the shear and tool chip interface zones. The first successful attempt for the determination of a complete temperature distribution in orthogonal machining was the Infra-Red Photography used by Boothroyd[36,43]. The advantage of this technique was the ability to give a detailed picture of the thermal fields which are developed at high cutting speeds. The disadvantage was the limited sensitivity of the photographic plates in a high temperature range only. This necessitated preheating of the workpiece.

Tay et al.[37] applied the finite element method to compute the temperature distribution field generated in the workpiece, chip and tool during orthogonal machining. In their analysis, the shear and tool/chip heat sources were considered to be distributed over a wide range. The distribution of the heat sources was calculated using experimentally obtained flow fields from a quick-stop experiment, together with measured cutting forces. This numerical solution takes into account the actual chip and tool geometries, and the variation of thermal properties of the materials with temperature.

The maximum tool/chip interface temperature obtained with the above solution is higher than that obtained with Boothroyd's method. This contradiction indicates that the assumptions made concerning velocity and strain rate distribution in the tool/chip interface zones, are inaccurate. Other important results, such as location of the maximum temperature and percentage of heat conducted back to workpiece, agreed with the previous analytical and experimental results[33,36,42].

The above method gives relatively accurate results, but the preparation of the input data from the flow field is laborious. It also requires substantial computation time. To overcome these difficulties, Tay et al.[38], in their second paper, employed an analytical method to compute the velocity and strain in both the shear and tool/chip interface zones, instead of the flow field. This method allowed the complete temperature distribution to be obtained given only experimental values of cutting forces, chip thickness and thermal properties of tool and workpiece materials. The results obtained with this method agreed fairly well with Boothroyd's method.

3.2 TEMPERATURE PROBLEM IN INTERMITTENT CUTTING

In intermittent cutting processes, high temperature develops very rapidly in the vicinity of the cutting edge when cutting starts. This is due to the transformation of the cutting energy into heat. Similar to continuous cutting, the heat generation occurs in two major regions, namely the shear zone and the tool/chip interface zone. The heat continues liberation until the end of the cutting period, where the tool leaves the workpiece and passes into the cooling media. In the

cooling period, the tool loses heat to surroundings by conduction, convection or radiation. As the machining continues, the tool undergoes repeated heating and cooling cycles.

In milling, the variation of the undeformed chip thickness causes corresponding variations in the intensity and temperature of heat sources. Hence, the transient nature is not only due to the interruptions of cutting, but also due to the variations in heat sources. This transient nature further complicates the solution of the temperature problem in intermittent cutting as compared to turning.

McFeron and Chao[44] determined the transient tool/chip interface temperature in peripheral milling using experimental and analytical techniques. They measured the temperature using the tool-workpiece thermocouple. The tool-work thermocouple does not work in the cooling period, and, therefore, they did not analyze the temperature problem in the cooling period.

In the analytical solution, the transient nature in the cutting period was considered in the model. The shear plane temperature and the tool/chip interface temperature were computed over equal time intervals during the cutting period. The shear plane heat source was represented by a plain slider moving at the shear velocity on the surface of the workpiece, which was regarded as semi-infinite in extent. Using Jeager's solution for a similar case, it was determined that, for practical cutting conditions, the instantaneous shear plane temperature can be evaluated to a good approximation by using a simple expression derived for steady state condition (continuous orthogonal machining).

The average tool/chip interface temperature in each interval was determined using the heat transfer solutions for stationary and moving heat sources. The instantaneous rise of the tool/chip interface temperature was determined from two points of view; the tool and the chip. For the tool, the stationary heat source of varying intensity was acting over a variable area of contact. The mean temperature in a time interval, in this case, was determined by applying Kelvin's integration for the Fourier heat conduction equation. The chip, however, "sees" the heat source as a moving-plane slider and Blok's solution was used to determine the temperature. Equating the average temperature obtained from the two viewpoints, the division of the heat between the two elements and the average temperature were determined.

McFeron and Chao compared the analytical and experimental solutions for typical cutting conditions (see Fig. 3.3), and concluded that the agreement is fairly good. The change in the measured maximum interface temperature on successive cuts is shown in Fig. 3.4. It can be seen that a slight change in temperature occurs between successive cycles.

The work of McFeron and Chao may be considered the first comprehensive solution for the tool/chip interface temperature in milling. However, the temperature distribution inside the tool and the tool temperature in the non-cutting period were not investigated.

Okushima and Hoshi[19] used the tool-work thermocouple to measure the tool tip temperature of a face milling fly cutter during the cutting period, in machining medium carbon steel. In a cycle of temperature change, three important characteristic temperatures were observed; first, the maximum temperature (the highest of tool/chip interface temperature

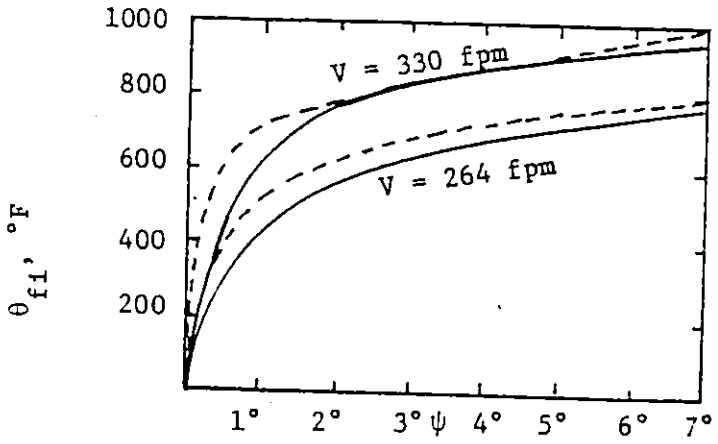

Fig. 3.3 Comparison of calculated and measured tool/chip interface temperature in milling

—— measured ---- calculated

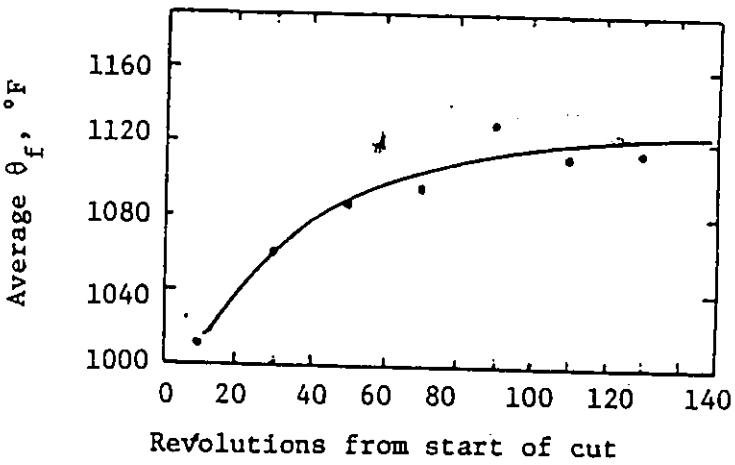

Fig. 3.4 Measured change in maximum tool/chip interface temperature during milling

Work material: 4140, 270 BHN

Tool material: K3H

v: 330 fpm

s_t: .0043 cpr

in the cycle), second, the minimum temperature (at the start of a cut), and finally, the finish temperature (at the end of a cut). The effect of several cutting parameters such as cutting speed, feed, cutting fluid, etc. on the three temperatures were investigated. The test results showed that for every rotation of the tool, the tool tip temperature builds up abruptly in a few milliseconds to a definite value which is determined by the operating condition. The tool and chip temperatures depend mainly upon the carbide grade, the cutting speed and the feed. The minimum temperature was also affected by those three factors as well as by the cutting fluids, the cutter diameter and the work width.

Okushima and Hoshi[20], in their second paper, made use of the results obtained from the measurements to calculate the internal temperature distribution inside the tool. A prediction of the cooling temperature on the rake face was also attempted. This investigation assumed a one-dimensional heat flow within the tool. The heat generated at the rake face was assumed to flow perpendicular to the tool/chip interface. The temperature at any depth is uniform over an adequately wide area. The problem, thus, is reduced to the solution of the Fourier heat conduction equation in one dimension. The Fourier equation was numerically solved, using the applicable boundary conditions, by implementing the finite difference method. The computation was performed by means of a digital computer. The temperature distribution during the cutting cycle was obtained by successive iterations. The value of the heat transfer coefficient on the tool surface was assumed and then adjusted iteratively until the calculated temperature at the end of the cooling period matched those obtained in the experimental work.

In the above investigation, Okushima and Hoshi studied the temperature cycling. However, no attempt was made to compute the thermal stresses.

Wang, Wu and Iwata[45] studied the temperature response for multi-tooth milling cutters. They measured the temperature by using a multi-signal grater spring pickup and standard thermocouple positioned at the back of the inserts. Consequently, a knowledge of the temperature distribution was necessary in order to obtain the tool/chip interface temperature. A series of experiments was performed to grind off the insert gradually to various thicknesses so that temperature gradients could be obtained for the purpose of extrapolation. Figure 3.5 shows four extrapolated temperature distributions.

Wang, Wu and Iwata[46], in their second paper, presented simulation techniques for further studying the temperature distribution curves reported in the above investigation. The first technique was experimental in which an oxyacetylene torch, in conjunction with a pulse control, was used to simulate the heat source and the intermittent nature of the cutting process. The second technique was a numerical solution for the heat transfer equation in three dimensions. The heat source at the tool/chip interface was represented by a square wave function with respect to time.

The temperature distribution curves obtained from the metal cutting experiments, from the experimental simulation, and from the numerical solution are shown in Fig. 3.6. The results obtained from the experimental simulation yield lower temperature response than the actual cutting. On the other hand, the results obtained from the numerical solution yield higher values.

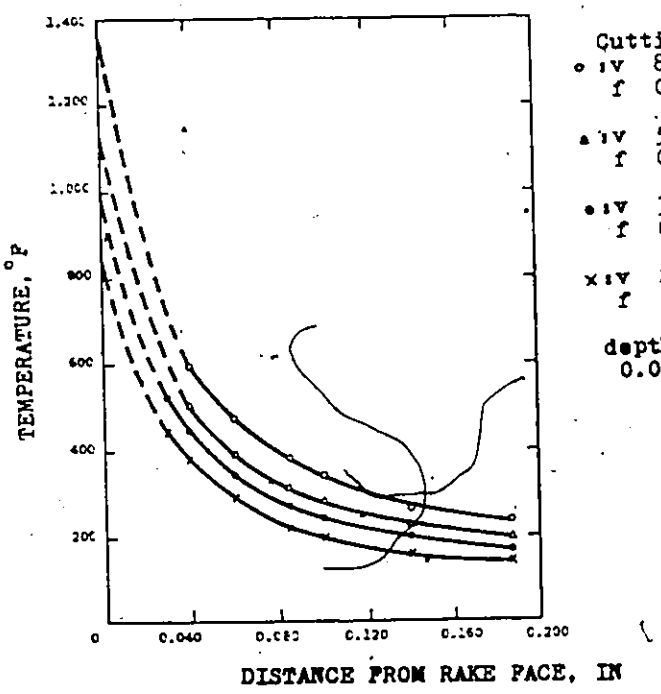

Fig. 3.5 Temperature distribution in the tool.(45)

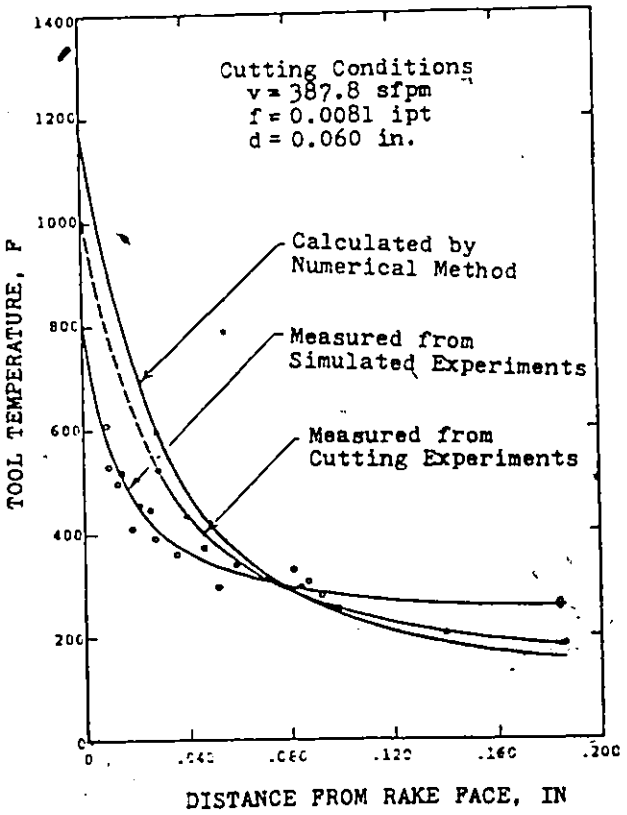

Fig. 3.6 Comparison of results.(46)

Wu and Mayer[9] investigated the problem of thermal cracking of carbide tools during intermittent cutting. They computed the transient temperature field and the associated thermal stresses in the tool using the finite element method. The tool was represented by a two-dimensional rectangular plate. A square wave type of heat source was assumed to simulate the thermal loading of the tool during cutting and non-cutting periods. The transient temperature field was obtained on the tool wedge by solving the two-dimensional Fourier equation using the applicable boundary conditions.

Modelling the thermal load by a square wave type of heat flux lacks the representation of the interaction between the heat sources and the presence of the chip and the workpiece. The experimental measurement of the tool/chip interface reported abrupt build up of the tool/chip interface temperature to a definite value, which is determined by the cutting condition. This abrupt change is due to the tool and chip coming in intimate contact once the cut starts. This action cannot be modelled by a square wave heat source.

3.3 SUMMARY AND DISCUSSION

In this Chapter, the temperature problem in both continuous and intermittent cutting processes has been presented. Several of the most significant investigations carried out to solve these problems have been discussed. Generally, the solution for a complete temperature distribution is advantageous for the study of many basic phenomena in metal cutting. However, most of the analyses were concentrated in solving the shear plane temperature and the tool/chip interface temperature.

In continuous cutting, the shear plane temperature and the tool/chip interface temperature were solved using two general methods. The first involved the heat transfer solution of stationary and moving heat sources. The second was based on an analytical or numerical solution of the relevant heat transfer equation and the associated boundary conditions. A complete temperature distribution on the tool, workpiece and chip was obtained experimentally by Boothroyd[36] and analytically by Tay et al.[37,38].

In intermittent cutting processes, the work was concentrated on determining the tool/chip interface temperature. McFeron and Chao[44] measured and calculated the tool/chip interface temperature. Okushima and Hoshi[19] measured the tool/chip interface temperature using a tool work thermocouple. They used the measurements to obtain the temperature distribution inside the tool based on a single dimensional model[20]. Wang et al.[45,46], used indirect measurement techniques to measure the tool/chip interface temperature. Recently, Wu and Mayer[9] used a two-dimensional tool model to compute the temperature cycling during the heating and cooling periods of a cutting cycle. The thermal loading was represented by a square-wave heat source. This representation of the thermal loading is inappropriate since the interaction between the tool/chip and workpiece is neglected.

A model which includes and represents all of the tool, chip and workpiece is required in order to adequately compute a complete temperature distribution in an intermittent cutting process.

CHAPTER 4

FINITE ELEMENT FORMULATION OF THE HEAT TRANSFER EQUATIONS IN INTERMITTENT CUTTING PROCESSES

This Chapter is devoted to the finite element formulation of the energy equation which governs the heat transfer mechanism in intermittent cutting processes. This chapter is divided into four major parts. The energy equation and the associated boundary conditions are derived in the first part of the chapter. The energy equation is the transient transport-convective heat transfer equation which is time dependent.

In the second part, the finite element formulation of the transient heat transfer problem is presented. The element equations are derived using the weighted residual approach. The result of the assembly of the element equations over a defined space domain is a system of ordinary differential equations (ODEs), which should be solved over the time domain.

In the third part, the two-point recurrence schemes which can be used to solve the above ODEs are presented and their numerical stability is discussed. For stability reasons, it has been found that an automatic step control algorithm should be used. Therefore, an automatic step control algorithm has been derived and is presented in the last part of this chapter. The algorithm has been implemented in the finite element program and has given successful results.

4.1 HEAT TRANSFER EQUATION IN INTERMITTENT CUTTING PROCESSES

In general, cutting tools in intermittent cutting experience a thermal cycle which consists of two distinguished periods, a cutting period (heating) and a non-cutting period (cooling-off). In the heating period the heat generation occurs in two main heat zones (Fig. 3.1); the shear zone (AB) and the tool/chip interface zone (BC). Some of the generated heat is carried away by the chip and the rest conducted to the tool and the workpiece, and also to the surroundings by convection and radiation. During the cooling-off period the tool tip or tool tooth loses the heat by conduction to the tool shank, and by both convection and radiation to the coolent and surroundings.

The temperature distribution in the cutting domain (workpiece, tool and chip) is governed by the energy balance according to the first law of thermodynamics for a differential element in the region. If the radiation is absent, the energy balance on the differential volume element $\Delta x\Delta y\Delta z$ about a point (x,y,z) may be stated as:

$$\left(\begin{array}{c}\text{Net rate of heat}\\ \text{entering by con-}\\ \text{duction into}\\ \text{element } \Delta x\Delta y\Delta z\\ \text{I}\end{array}\right) + \left(\begin{array}{c}\text{Rate of heat}\\ \text{generated in}\\ \text{element}\\ \Delta x\Delta y\Delta z\\ \text{II}\end{array}\right) = \left(\begin{array}{c}\text{Rate of increase of}\\ \text{internal energy}\\ \text{stored in element}\\ \Delta x\Delta y\Delta z\\ \text{III}\end{array}\right) \tag{4.1}$$

The mathematical expression for the three terms I, II, and III in this energy equation are derived below for a two-dimensional (orthogonal) cutting process.

The net rate of heat addition by conduction into the element (Δx, Δy, and unit thickness), can be deduced from Fig. 4.1 as:

$$I = \left[\frac{\partial}{\partial x}\left(k_x \frac{\partial T}{\partial x}\right) + \frac{\partial}{\partial y}\left(k_y \frac{\partial T}{\partial y}\right)\right]\Delta x\Delta y \tag{4.2}$$

where k_x and k_y are the thermal conductivities in the principal directions, and T is the temperature.

If the element is a heat source with uniform strength and $\tilde{Q}$ is the rate of heat generated per unit volume, then the rate of heat generated within the element is obtained by

$$II = \tilde{Q}\,\Delta x \Delta y \tag{4.3}$$

Let u and v be the velocity components in the x and y directions, and assume that they are constant across the moving chip. Then, the rate of energy stored in the moving chip element is defined as:

$$III = \rho\, C\, \left(\frac{\partial T}{\partial t} + u\,\frac{\partial T}{\partial x} + v\,\frac{\partial T}{\partial y}\right)\,\Delta x \Delta y \tag{4.4}$$

Substituting Equations (4.2), (4.3) and (4.4) in Equation (4.1), the energy equation governing the heat transfer mechanisms in a two-dimensional (orthogonal) cutting process can be obtained as:

$$\rho\, C\, \left(\frac{\partial T}{\partial t} + u\,\frac{\partial T}{\partial x} + v\,\frac{\partial T}{\partial y}\right) = \frac{\partial}{\partial x}\left(k_x\,\frac{\partial T}{\partial x}\right) + \left(k_y\,\frac{\partial T}{\partial y}\right) + \tilde{Q} \tag{4.5}$$

In the non-cutting period, the chip is absent and $\tilde{Q} = u = v = 0$ in the tool region. Thus, the energy Equation (4.5) reduces to

$$\rho\, C\, \left(\frac{\partial T}{\partial t}\right) = \frac{\partial}{\partial x}\left(k_x\,\frac{\partial T}{\partial x}\right) + \frac{\partial}{\partial y}\left(k_y\,\frac{\partial T}{\partial y}\right) \tag{4.6}$$

Equation (4.5) is the transient convective-transport equation, and Equation (4.6) is the Fourier equation of heat conduction.

The transient temperature distribution in the cutting field for a cutting cycle can be obtained from the solution of Equations (4.5) and (4.6). This requires specification of the initial and boundary conditions of the cutting field. The initial condition specifies the temperature distribution in the cutting region (Ω) at the origin of the time coordinate

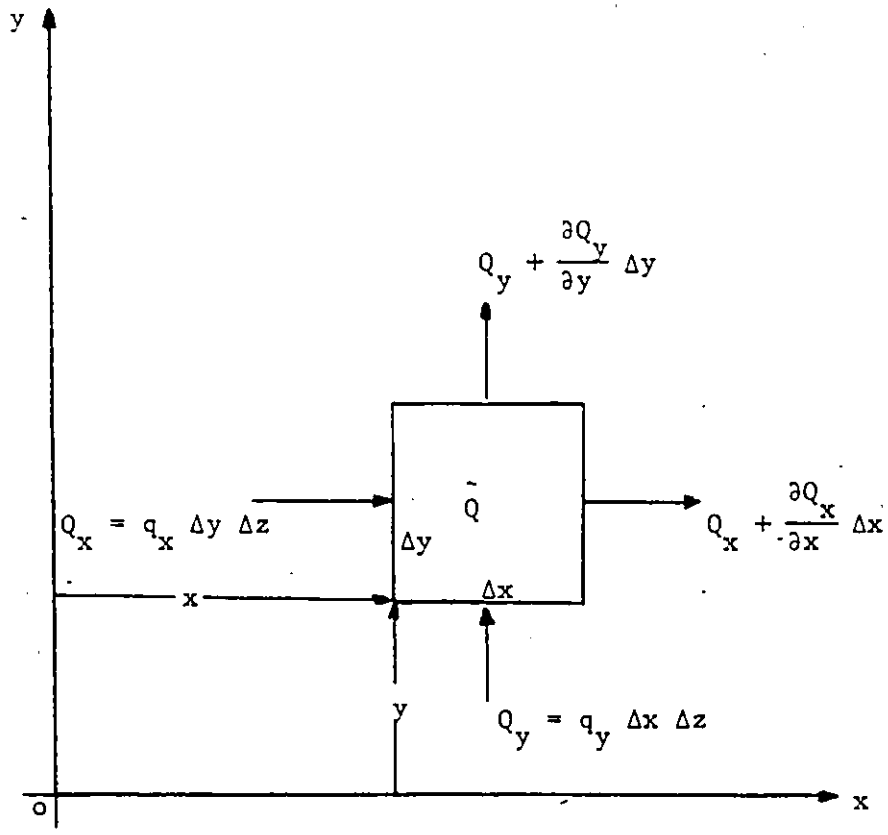

$$q_x = -k_x \frac{\partial T}{\partial x} \qquad \text{and} \qquad q_y = -k_y \frac{\partial T}{\partial y}$$

$\tilde{Q}$ rate of heat generated/unit volume

Fig. 4.1 Nomenclature for heat addition by conduction.

(that is t = 0). It is mathematically represented by

$$T = T_o\ (x,y,t) \quad \text{in } \Omega,\ t = 0 \tag{4.7}$$

The boundary conditions describe the heat flow or temperature situation on the boundary of the cutting region. The heat at the boundary of the cutting region transfers to the surroundings by the following:

(a) Conduction to the tool shank and workpieces.

(b) Radiation and convection from the tool, workpiece and chip surfaces. The part of the boundary (Γ_2) on which the heat flows by conduction or convection is called "Cauchy" boundary conditions and is represented mathematically as:

$$k_x \frac{\partial T}{\partial x} n_x + k_y \frac{\partial T}{\partial y} n_y + q + \bar{h}\ (T - T_\infty) = 0 \quad \text{on } \Gamma_2,\ t > 0 \tag{4.8}$$

where n_x and n_y are the unit, outward, normal vectors to the surface Γ_2 and $\bar{h}$ is the total heat transfer coefficient which includes the radiation effect.

(c) At a distance deep inside the tool or workpiece far from the heat generation zones, the temperature is equal to room temperature. This part of the boundary (Γ_1) is called the specified temperature boundary and represented mathematically as:

$$T = T\ (x,y,t) \quad \text{on } \Gamma_1,\ t > 0 \tag{4.9}$$

Energy Equation (4.5) governs the heat transfer mechanism during the cutting period, and Equation (4.6) governs the heat transfer mechanism in the tool during the non-cutting period. These equations must satisfy the initial condition (Equation (4.7)) and the boundary conditions (Equations (4.8) and (4.9)) on the domain Ω for the time span t.

This is a time dependent heat flow problem which can be solved to obtain the temperature distribution at different time intervals. The analytical solution of this problem is extremely complex. Therefore, the finite element method is employed.

4.2 FINITE ELEMENT FORMULATION OF TWO-DIMENSIONAL TRANSIENT CONVECTIVE-TRANSPORT PROBLEM

In general, the first step in the finite element method is to discretize the continuum or solution region into elements (Fig. 4.2). A variety of element shapes may be used such as the triangular, rectangular, etc. The elements are separated by fictitious boundaries and adjacent elements are connected at common points which are called "nodal points" or "nodes". Each node can have a certain number of degrees of freedom which represents the discretized field variables of the problem. The field variables could be temperature, displacements, etc. The next step is to assume an interpolation function to represent the variation of the field variables over the element. Once the element and the interpolation functions are selected, the next step is to determine the discretized equations for an individual element. For this task various approaches can be used, e.g. variational principles, weighted residual approach or energy balance. Using any of these approaches the individual element matrices can be formulated, then assembled together to obtain a global system of equations. This system of equations can also account for the boundary conditions, and then solved to obtain the nodal values of the field variable, i.e. temperature.

In this Section, the finite element discretization is applied to formulate the transient convective-transport problem.

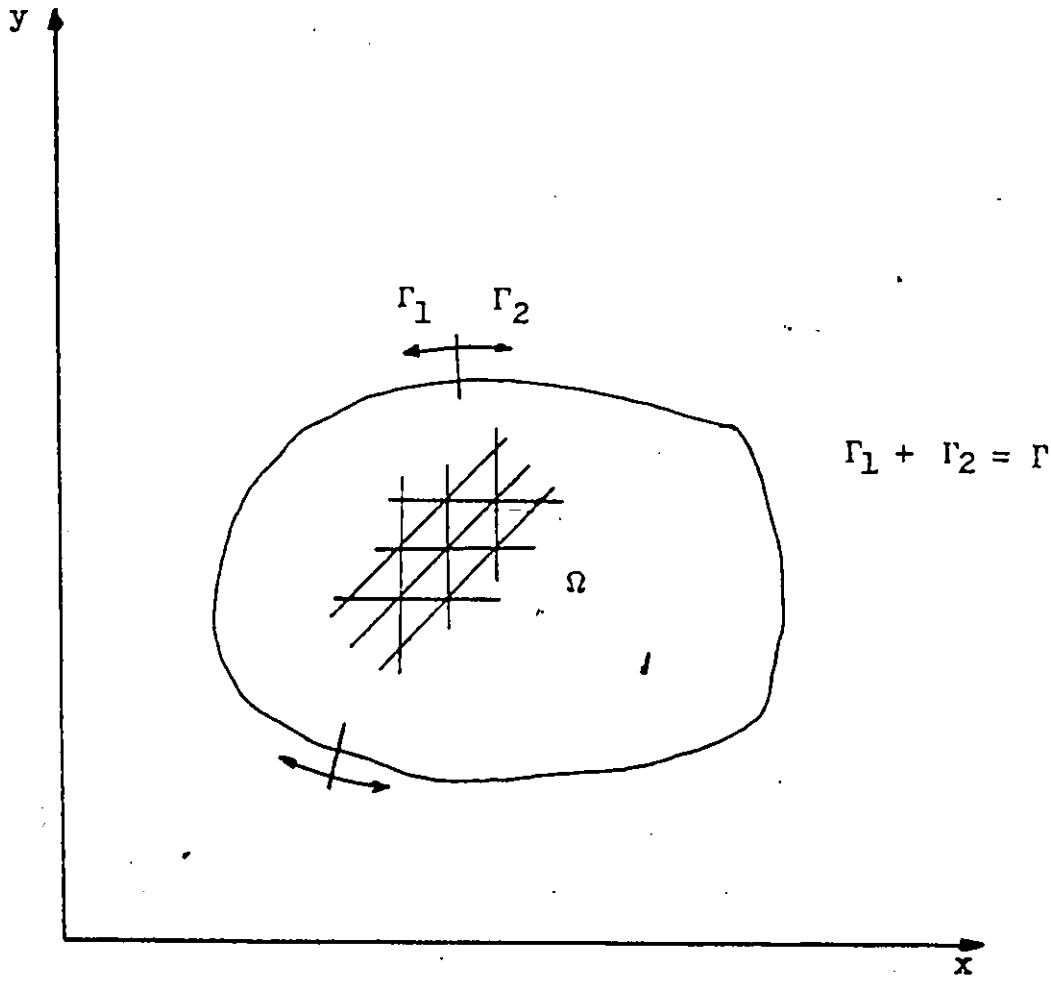

Fig. 4.2 Two-dimentional domain divided into triangular elements.

4.2.1 Procedure to Construct Finite Element Equations for Time Dependent Problem

Several approaches can be used to construct finite element equations for time dependent problems. The most common[47-50] one is to consider the problem at one instant of time. Then, a finite element model can be constructed by expressing the field variable for a typical element with m degrees of freedom as:

$$T^{(e)}(x,y,z,t) = \sum_{i=1}^{m} N_i(x,y,z)\ T_i(t) \qquad (4.10)$$

where $N_i(x,y,z)$ are the interpolation functions, and $T_i(t)$ are time dependent nodal parameters. At this point, the variational principle can be used to derive the element equation, if one exists, for the contrived steady state problem or one can resort to the method of weighted residuals with Galerkin's criterion. In either case, the assembly of the elements equations results in a system of ordinary differential equations in {T}, where {T} is the column vector of the nodal parameter. This system may be solved by variety of techniques to be discussed in Section 4.3.

4.2.2 Derivation of Finite Element Equations Using the Weighted Residuals Approach

The weighted residuals approach with Galerkin's criterion will be used to derive the finite element equations for the governing partial differential Equation (4.5), and the applicable boundary conditions (Equations (4.7) and (4.8)).

Let the unknown function within a typical element with m degrees of freedom, be approximated as:

$$T^{(e)} = \sum_{i=1}^{m} N_i(x,y)\, T_i(t) = [N]\, \{T\}^e \qquad (4.11)$$

where the interpolation functions N_i need only preserve C° continuity, and $\{T\}$ is a column vector of the field variable (temperature) at any instant t. Galerkin's method then requires that the following equation be satisfied, at any instant of time, within the domain of element e for node i.

$$\int_{A^e} N_i \left[\frac{\partial}{\partial x}\left(k_x \frac{\partial T^e}{\partial x}\right) + \frac{\partial}{\partial y}\left(k_y \frac{\partial T^e}{\partial y}\right) + Q - \rho\, C \left(\frac{\partial T^e}{\partial t} + u \frac{\partial T^e}{\partial x} + v \frac{\partial T^e}{\partial y}\right)\right] dxdy = 0 \qquad (4.12)$$

where A^e is the domain for element e.

In the above equation, second derivatives appear in the integral imposing unnecessary continuity restrictions between elements. Therefore, it is worth while to modify Equation (4.12) by integrating such terms by parts using Green's theorem[50]. Integrating the first term of Equation (4.12) by parts leads to

$$\int_{A^e} N_i \frac{\partial}{\partial x}\left(k_x \frac{\partial T^e}{\partial x}\right) dxdy = \oint k_x \frac{\partial T^e}{\partial x} N_i\, dy - \int_{A^e} k_x \frac{\partial T^e}{\partial x} \frac{\partial N_i}{\partial x}\, dxdy$$

$$= \oint_{\Gamma_2^e} k_x \frac{\partial T^e}{\partial x} n_x N_i\, d\Gamma^e - \int_{A^e} k_x \frac{\partial T^e}{\partial x} \frac{\partial N_i}{\partial x}\, dxdy \qquad (4.13)$$

where n_x is the x component of the outward unit vector normal to the boundary and $d\Gamma^e$ is the differential arc length along the boundary. Treating the second term in Equation (4.12) in the same way, Equation (4.12) takes the following form:

$$-\int_{A^e} \left(k_x \frac{\partial T^e}{\partial x} \frac{\partial N_i}{\partial x} + k_y \frac{\partial T^e}{\partial y} \frac{\partial N_i}{\partial y}\right) dxdy + \int_{A^e} N_i \tilde{Q}\, dxdy - \rho C \int_{A^e} N_i \left(\frac{\partial T^e}{\partial t} + u \frac{\partial T^e}{\partial x} + v \frac{\partial T^e}{\partial y}\right) dxdy + \oint_{\Gamma_2^e} \left(k_x \frac{\partial T^e}{\partial x} n_x + k_y \frac{\partial T^e}{\partial y} n_y\right) N_i\, d\Gamma^e = 0 \qquad (4.14)$$

The boundary integral (boundary residuals) in Equation (4.14) is used to introduce the natural boundary conditions. The following relation (Equation (4.8)) is applied for the elements on the boundary Γ_2:

$$k_x \frac{\partial T^e}{\partial x} n_x + k_y \frac{\partial T^e}{\partial y} n_y = -q^e - \bar{h} (T^e - T_\infty) \quad \text{on } \Gamma_2 \qquad (4.8)$$

Substituting Equation (4.8) in Equation (4.14) and noting that $T^e = [N]\{T\}^e$, Equation (4.14) may be rewritten as:

$$\int_{A^e} \left(k_x \left[\frac{\partial N}{\partial x}\right] \frac{\partial N_i}{\partial x} + k_y \left[\frac{\partial N}{\partial y}\right] \frac{\partial N_i}{\partial y}\right) \{T\}^e\, dxdy - \int_{A^e} N_i \tilde{Q}\, dxdy + \int_{A^e} \rho C \left(u\left[\frac{\partial N}{\partial x}\right] + v\left[\frac{\partial N}{\partial y}\right]\right) N_i \{T\}^e\, dxdy + \int_{A^e} \rho C N_i [N] \{\dot{T}\}\, dxdy + \int_{\Gamma_2^e} \left(q^e N_i + \bar{h} [N] \{T\}^e N_i - \bar{h} T_\infty N_i\right) d\Gamma^e = 0 \qquad (4.15)$$

in which the dot stands for time differentiation.

Now, the first order derivatives only have to be integrated and the continuity of N_i must be imposed. On boundary points where the value of T is prescribed, the equation is not formed. Thus, it is necessary to have prespecified temperature boundary to avoid solution singularity.

The element Equation (4.15) can be written in a matrix form as follows:

$$([K_c]^e + [K_t]^e + [K_v]^e)\ \{T\}^e + [K_h]^e\ \{\dot{T}\}^e - \{Q\}^e + \{q\}^e - \{C_v\}^e = 0 \tag{4.16}$$

where

$[K_c]^e$ is the conduction matrix and is defined by the coefficients:

$$k_{c_{ij}} = \int_{A^e} \left(k_x \frac{\partial N_i}{\partial x} \frac{\partial N_j}{\partial x} + k_y \frac{\partial N_i}{\partial y} \frac{\partial N_j}{\partial y}\right) dxdy \tag{4.17}$$

$[K_t]^e$ is the heat transport matrix and is defined by:

$$k_{t_{ij}} = \int_{A^e} \rho\ C\ N_i \left(u \frac{\partial N_j}{\partial x} + v \frac{\partial N_j}{\partial x}\right) dxdy \tag{4.18}$$

$[K_h]^e$ is the heat capacitance matrix and is defined by:

$$k_{h_{ij}} = \int_{A^e} \rho\ C\ N_i\ N_j\ dxdy \tag{4.19}$$

$\{Q\}^e$ is the internal heat generated matrix and is defined by:

$$Q_i = \int_{A^e} \tilde{Q}\ N_i\ dxdy \tag{4.20}$$

$\{q\}^e$ is the boundary heat flux matrix and is defined by:

$$q_i = \int_{\Gamma_2^e} q\ N_i\ d\Gamma^e \tag{4.21}$$

$[K_v]$ and $\{C_v\}$ are the convection boundary matrices and are defined by:

$$k_{v_{ij}} = \int_{\Gamma_2^e} \bar{h}\ N_i\ N_j\ d\Gamma^e \tag{4.22}$$

and

$$c_{v_i} = \int_{\Gamma_2^e} \bar{h}\ T_\infty\ N_i\ d\Gamma^e \tag{4.23}$$

and $\quad i = 1,2,3\text{--}m, \quad j = 1,2,3\text{--}m$

Equation (4.16) expresses the general behaviour of the two-dimensional thermal element. After selecting the element shape and an appropriate set of interpolation functions, the element equations can be explicitly evaluated. Then, following the usual global assembling method, a system of first order ordinary differential equations is obtained in the following form:

$$[C]\ \{\dot{T}\} + [K]\ \{T\} + \{F\} = 0 \tag{4.24}$$

where

$$[C] = \sum_{e=1}^{s} [K_h]^e \tag{4.25}$$

$$[K] = \sum_{e=1}^{s} ([K_c]^e + [K_t]^e + [K_v]^e) \tag{4.26}$$

$$\{F\} = \sum_{e=1}^{s} (\{q\}^e - \{Q\}^e - \{C_v\}^e) \tag{4.27}$$

and s is the total number of elements. Equation (4.24) subjected to the initial value (Equation (4.7)) can be solved using a suitable recurrence scheme to obtain the nodal temperature vector $\{T\}_i$ at any time (t_i).

At this point, it is important to mention that in order to satisfy the boundary conditions some of the parameters of $\{T\}_i$ have to be prescribed and the number of equations must be equal to the number of unknowns[49].

A further point concerning the coefficients of the matrix [K], in Equation (4.24), should be noted. The coefficients of the matrices

$[K_c]^e$ and $[K_v]^e$ are symmetrical while the coefficient of $[K_t]^e$ are not symmetrical. Consequently, the global matrix [K] will be non-symmetrical if $[K_t]^e$ has non zero values.

As previously noted, Equation (4.5) can reduce to Equation (4.6) if $u = v = \tilde{Q} = 0$. It can be seen that in the finite element formulation (Equation (4.12) to (4.15)), the terms containing u, v, and $\tilde{Q}$ do not contribute to the boundary terms. Also, when $u = v = \tilde{Q} = 0$, the element equations for the energy Equation (4.5) is reduced to the element equations of Equation (4.6), since $[K_t]^e = [0]$ and $\{\tilde{Q}\} = \{0\}$. Therefore, the temperature distribution for a cutting cycle can be obtained by solving Equation (4.5) for the cutting period, and Equation (4.6) for the non-cutting period, using the same finite element program.

4.3 TWO-POINT RECURRENCE SCHEMES FOR SOLVING SYSTEM OF ORDINARY DIFFERENTIAL EQUATIONS

In the previous section, the finite element discretization of the two-dimensional transient convective-transport partial differential equation and the associated boundary conditions over the domain Ω have been presented. The result is a system of first order ordinary differential equations (ODEs) which is expressed as follows:

$$[C]\{\dot{a}\} + [K]\{a\} + \{F\} = 0 \qquad (4.28)$$

where a(x,y,t) denotes the field variable (temperature),

[K] is the convective-transport element matrix,

[C] is the heat capacitance matrix,

and {F} is the global load vector.

When [K] and [C] are constant, the ODEs are linear.

A recurrence scheme can be used to find an approximate solution for Equation (4.28) subjected to the initial condition $\{a\} = \{a(x,y,0)\}$ in the time interval $(0,t_o)$, at times $t = t_1, t_2, \text{---} t_n$, $0 < t_1 < t_2 \text{---} t_m = t_o$. Such a scheme transforms the system of ODEs into a system of algebraic equations of the following form:

$$[H]\ \{a\}_{n+1} = \{b\} \qquad n = 0,1,2\text{---}m-1 \tag{4.29}$$

in order to maintain the sparse (banded) characteristic matrices. Here, [H] is the characteristic matrix of the scheme[51].

In the next two subsections, two point recurrence schemes are derived based on both of finite difference formulation and the finite element formulation.

4.3.1 Finite Difference Formulae[52]

4.3.1.1 Euler forward difference scheme:

The Euler forward difference scheme is known to be an explicit linear one step method, with local truncation error $O(\Delta t^2)$. Using this scheme, Equation (4.28) takes the form.

$$\frac{1}{\Delta t}\ [C]\ (\{a\}_{n+1} - \{a\}_n) + [K]\ \{a\}_n + \{F\}_n = 0 \tag{4.30}$$

where $n = 0,1,2\text{---}(m-1)$.

Denoting

$$[H] = \frac{1}{\Delta t}\ [C] \tag{4.31}$$

and

$$\{b\} = \left(\frac{1}{\Delta t}\ [C] - [K]\right)\{a\}_n - \{F\}_n \tag{4.32}$$

then Equation (4.29) is obtained.

4.3.1.2 Euler backward difference scheme:

Here, an implicit linear one-step method with a local truncation error $O(\Delta t^2)$ is used. Equation (4.28) will be transformed to the following form by the Euler backward difference scheme:

$$\frac{1}{\Delta t}[C](\{a\}_{n+1} - \{a\}_n) + [K]\{a\}_{n+1} + \{F\}_{n+1} = 0$$

$$n = 0,1,---(m-1) \tag{4.33}$$

which is the form (4.29), where

$$[H] = [K] + \frac{1}{\Delta t}[C] \tag{4.34}$$

and

$$\{b\} = \frac{1}{\Delta t}[C]\{a\}_n - \{F\}_{n+1} \tag{4.35}$$

4.3.1.3 Crank-Nicholson-Galerkin scheme (trapezoidal rule):

This scheme is defined by

$$\{a\}_{n+1} = \{a\}_n + \frac{1}{2}\Delta t(\{\dot{a}\}_{n+1} + \{\dot{a}\}_n) \tag{4.36}$$

Applying this relation to Equation (4.28) yields

$$(\frac{1}{\Delta t}[C] + \frac{1}{2}[K])\{a\}_{n+1} = (\frac{1}{\Delta t}[C] - \frac{1}{2}[K])\{a\}_n - \frac{1}{2}(\{F\}_{n+1} + \{F\}_n) \tag{4.37}$$

which again is of the form (4.29) with

$$[H] = \frac{1}{\Delta t}[C] + \frac{1}{2}[K] \tag{4.38}$$

and

$$\{b\} = (\frac{1}{\Delta t}[C] - \frac{1}{2}[K])\{a\}_n - \frac{1}{2}(\{F\}_{n+1} + \{F\}_n) \tag{4.39}$$

The trapezoidal rule is an implicit linear two-step method with local truncation error of order $O(\Delta t^3)$.

4.3.2 Finite Element Formulation[49,52]

Following the usual procedure of finite element discretization, with time as the independent variable, we can write:

$$\{a\} \simeq \{\hat{a}\} = \sum_{i=1}^{m} N_i(t)\,\{a\}_i \quad , \qquad i = 1,2,\text{---}m \tag{4.40}$$

where $\{a\}_i$ stands for the nodal set of $\{a\}$ at time t_i,

m is the number of nodes per time element, and

$N_i(t)$ are the shape functions and they are scalers.

Since only the first order derivatives are involved in Equation (4.28), then the first order polynomials are sufficient for the shape function $N_i(t)$.

Let the time domain be divided into time elements of length Δt with $\{a\}_i$ taking on nodal values $\{a\}_n$ and $\{a\}_{n+1}$, as shown in Fig. 4.3. The shape functions and their derivatives can be written in terms of local variables as:

$$\begin{aligned} &0 \le \xi \le 1 && \xi = \frac{t-t_n}{\Delta t} \\ &N_n = 1 - \xi && \dot{N}_n = -\frac{1}{\Delta t} \\ &N_{n+1} = \xi && \dot{N}_{n+1} = \frac{1}{\Delta t} \end{aligned} \tag{4.41}$$

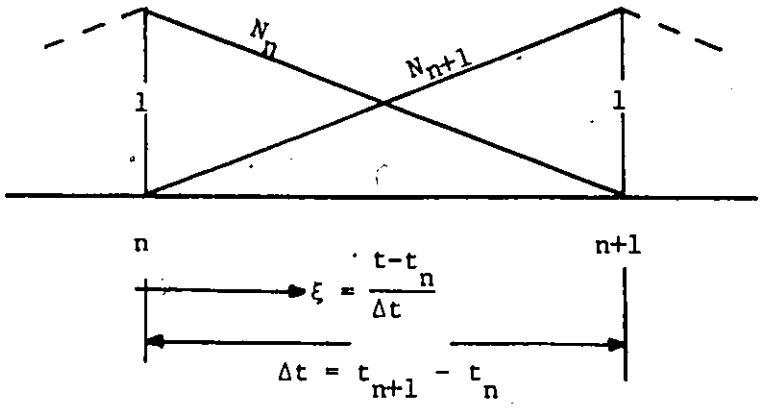

Fig. 4.3 Shape functions for two-point recurrence formulae.

Now, a typical weighted residual equation can be written, assuming that the full domain of investigation corresponds to that of one time element. The equation is:

$$\int_0^1 w_j \left[[C]\left(\dot{N}_n \{a\}_n + \dot{N}_{n+1} \{a\}_{n+1}\right) + [K]\left(\{a\}_n N_n + \{a\}_{n+1} N_{n+1}\right) + \{F\}\right] d\xi = 0 \qquad j = 1 \tag{4.42}$$

Inserting the values of $\dot{N}_n$, $\dot{N}_{n+1}$, N_n and N_{n+1}, the recurrence relation (4.42) can be written as:

$$\left([K] \int_0^1 w_j \, \xi d\xi + [C] \int_0^1 w_j \, d\xi/\Delta t\right) \{a\}_{n+1} + \left([K] \int_0^1 w_j \, (1-\xi) \, d\xi - [C] \int_0^1 w_j \, d\xi/\Delta t\right) \{a\}_n + \int_0^1 w_j \, \{F\} \, d\xi = 0 \tag{4.43}$$

In the relation (4.43) various weight functions (w_j) can be inserted. Also, the matrices [K] and [C] are assumed to be time independent.

Generally, relation (4.43) can be written for any weight function as:

$$\left(\frac{1}{\Delta t} [C] + \theta [K]\right) \{a\}_{n+1} + \left(-\frac{1}{\Delta t} [C] + (1-\theta) [K]\right) \{a\}_n + \{\bar{F}\} = 0 \tag{4.44}$$

where

$$\theta = \left(\int_0^1 w_j \, \xi d\xi\right) / \int_0^1 w_j \, d\xi \tag{4.45}$$

and

$$\{\bar{F}\} = \left(\int_0^1 w_j \, \{F\} \, d\xi\right) / \int_0^1 w_j \, d\xi \tag{4.46}$$

If we assume that the interpolation functions used for the unknown {a} is applied to the function $\{\bar{F}\}$, Equation (4.46) can be written as

$$\{\bar{F}\} = \left(\int_0^1 w_j \left(\{F\}_n N_n + \{F\}_{n+1} N_{n+1}\right) d\xi\right) \Big/ \int_0^1 w_j \, d\xi$$

$$= \left(\int_0^1 w_j \left(\{F\}_n (1-\xi) + \{F\}_{n+1} \xi\right) d\xi\right) \Big/ \int_0^1 w_j \, d\xi$$

$$\{\bar{F}\} = (1-\theta) \{F\}_n + \theta\{F\}_{n+1} \tag{4.47}$$

Equations (4.44) and (4.47) are such that

$$[H] = \frac{1}{\Delta t} [C] + \theta[K] \tag{4.48}$$

and $$\{b\} = \left(\frac{1}{\Delta t} [C] - (1-\theta) [K]\right) \{a\}_n - \left((1-\theta) \{F\}_n + \theta\{F\}_{n+1}\right) \tag{4.49}$$

which yield Equation (4.29).

Note: Setting $\theta = 0$ in Equations (4.48) and (4.49) yields the Euler forward difference scheme, while $\theta = \frac{1}{2}$ gives the Crank-Nicholson representation and $\theta = 1$ yields the Euler backward difference scheme.

4.4 CHOICE OF RECURRENCE SCHEME AND STABILITY CRITERION

In the preceding Section, it has been shown that the use of a recurrence scheme can transform the system of ODE's to a system of algebraic equations. Then, the system of algebraic equations can be solved at every time step to obtain the nodal values of the field variable. In most cases, the nature of the problem requires a small steplength in the initial phase of the numerical solution to maintain stability. This restriction can be overcome by employing a time step control scheme which controls step size and stability[53]. Therefore, the objective of this section is to discuss the stability of the aforementioned two point

recurrence schemes and the possibility of deriving automatic steplength scheme.

The system of ODEs (Equation (4.28)) can be rewritten in the following form:

$$\{\dot{a}\} = - [A] \{a\} - \{\bar{F}\} \tag{4.50}$$

where

$$[A]_{mxm} = [C]^{-1} [K]$$

$$\{\bar{F}\}_{1xm} = [C]^{-1} \{F\} \quad , \text{ and}$$

m is the number of equations constituting the ODEs system. The above system can be transformed to the following canonical form,

$$\{\dot{X}\}_{mx1} = - [\Lambda]_{mxm} \{X\}_{1xm} - \{\bar{F}\}_{1xm} \tag{4.51}$$

where $\{X(0)\} = \{1\}$.

This is equivalent to the system of an uncoupled equations

$$\dot{x}_i = - \lambda_i x_i - f_i \qquad i = 1;2,---m \tag{4.52}$$

and $x(0) = 1$.

In Equation (4.52), when the forcing term $f_i = 0$ (i.e. free response), the λ_i's are the eigenvalues of the matrix $[A] = [C]^{-1} [K]$ which are generally complex numbers.

Following the mathematical steps to analyze the aforementioned recurrence schemes, the following stability conditions can be derived[53,54]:

i - The explicit forward Euler scheme is absolutely stable in the interior of the unit circle centered at $\sigma = 1 + J0$ as shown in Fig. 4.4a).

ii - The implicit backward Euler scheme is absolutely stable in the exterior of a unit circle centered at $\sigma = -1 + J0$ as

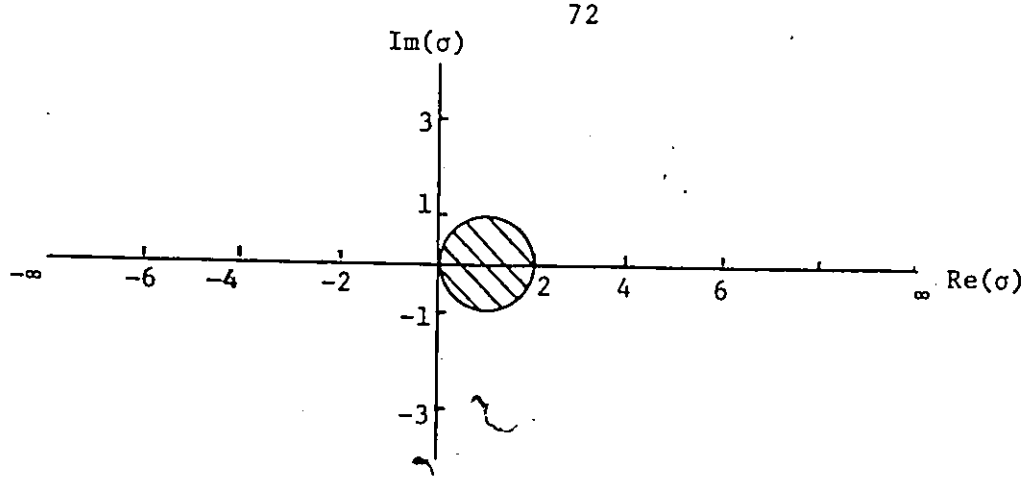

(a) Forward Euler $\theta = 0$

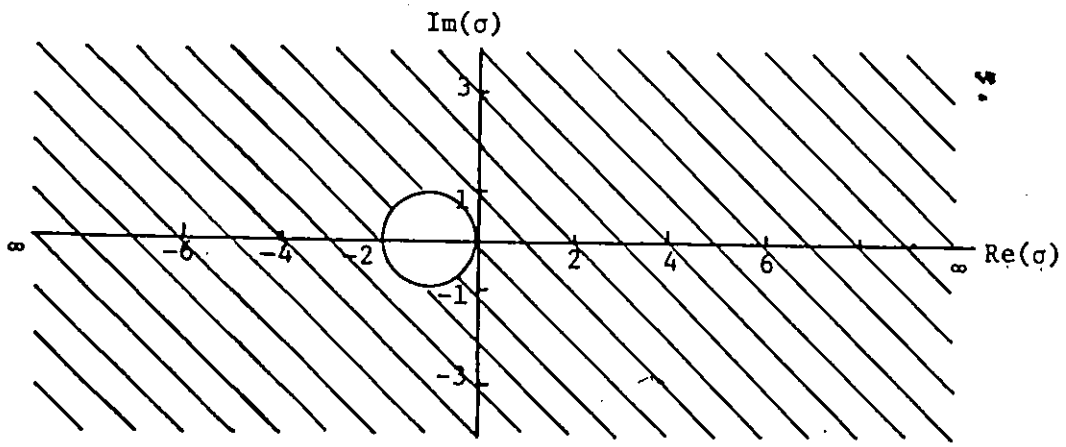

(b) Backward Euler $\theta = 1$

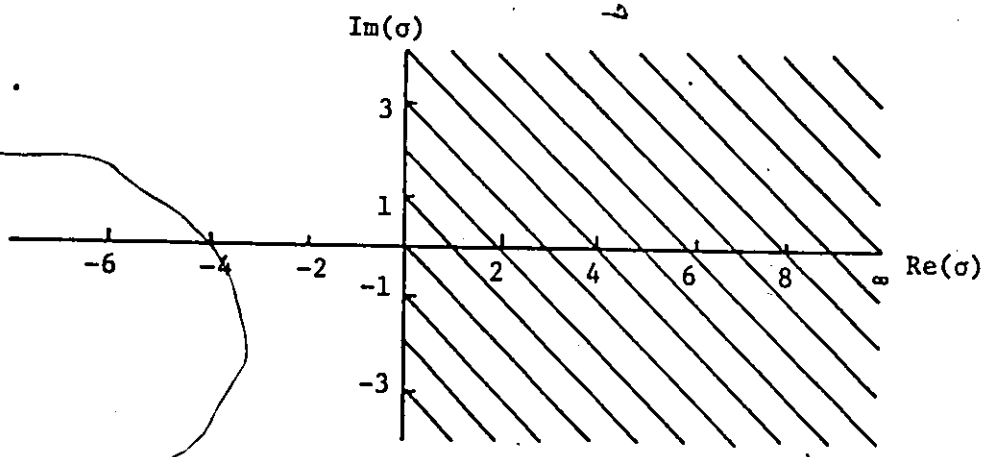

(c) Trapezoidal Rule $\theta = \frac{1}{2}$

Fig. 4.4 Regions of absolute stability for two-point recurrence schemes.

▨ Regions of absolute stability

shown in Fig. 4.4 b).

iii - The trapezoidal rule is absolutely stable in the right half plane as shown in Fig. 4.4 c).

In fact, for any given $\lambda > 0$, the implicit schemes ($\theta \geq 1/2$) are stable for any step size Δt. Hence, the choice of step size Δt is restricted only by accuracy - the maximum allowable local truncation error - and not by stability.

Now, recall the system of ODEs which were obtained with the finite element discretization of Equation (4.5) and Equation (4.6), and the associated boundary conditions. The finite element discretization of Equation (4.5) on the cutting field yields a system of ODEs in which the [K] matrix is non-symmetrical, while the discretization of Equation (4.6) yields a system in which [K] is symmetrical. In both systems the [C] matrix is symmetrical. In the latter system, if [K] and [C] are constants (i.e. time, temperature, and space independent), they are then positive definite. Consequently, the eigenvalues λ_i's are real positive numbers.

Thus, the stability condition for the forward Euler scheme is $\lambda_{max} \Delta t \leq 2$. The estimate of the critical time step for this scheme apparently necessitates the solution of the eigenvalue problem for the whole system. This is not the case, since the bound on the highest eigenvalue can simply be obtained by consideration of an individual element. This is established by an important theorem proposed by Iron, which proves that the highest eigenvalue must always be less than the highest eigenvalue of the individual elements. This allows a very easy estimate of the critical time step. However, it is important to observe here that for such a system of ODEs the element eigenvalues increase as h^2

(h = element size). This means a very rapid decrease of stable Δt with mesh subdivision and explicit schemes are, therefore, seldom used for such problems[49,55].

The trapezoidal rule is absolutely stable for all values of $\sigma_i = \lambda_i \Delta t$ (Fig. 4.4c). For $\lambda_i > 0$, it is stable for any step size Δt. However, oscillatory results have been noticed when the trapezoidal rule was applied using a moderate steplength in the initial phase of the numerical solution.

Zlàmal[56] reported that the trapezoidal rule does not give good results for a moderate step size if the exact solution is not smooth at $t = 0$. Ziewkiewicz, also, noted that oscillatory results occur with abrupt changes of the forcing term. The effect of the above reasons can be eliminated either by choosing a very small steplength in the initial phase or by using a moderate steplength and applying a smoothing procedure in the initial phase[53]. That is $\{a\}_n$ is replaced by $\{\hat{a}\}_n$, where

$$\{\hat{a}\}_n = \frac{1}{4}\{a\}_{n+1} + \frac{1}{2}\{a\}_n + \frac{1}{4}\{a\}_{n-1} \qquad (4.53)$$

An alternative procedure which helps to iron out the oscillation is to use $\theta > \frac{1}{2}$. In this context a useful compromise, which was proposed by Ziewkiewicz[52], is to use $\theta = 2/3$. Lambert[53] proves that $\theta = .878 \simeq 7/8$ is the optimal.

The implicit backward difference scheme ($\theta = 1$) is absolutely stable for any steplength. Although, the error is of lower order than for the trapezoidal rule, it gives better results for a relatively larger steplength.

From the above discussion, we may decide to choose a recurrence scheme with $\theta > 1/2$. However, the implicit schemes usually do not give the correct answers with moderate starting step sizes. Therefore, a very small steplength should be used in the initial phase, then the steplength should be automatically increased using a proper steplength control algorithm. In this work, an algorithm has been derived to control the steplength for the implicit two-point recurrence schemes ($\theta > \frac{1}{2}$). This algorithm has been implemented successfully with the finite element program. Section (4.7) is devoted to the derivation and discussion of this algorithm.

The system of ODEs obtained from the finite element discretization of Equation (4.5) has a non-symmetric [K] matrix. This is because of the convective-transport part of the partial differential Equation (4.5). This results in complex eigenvalues which are scattered. Thus, the system of ODEs is "stiff" which necessitates a very small steplength at the initial phase of the numerical solution. Hence an automatic steplength control becomes strongly recommended. Further, the finite element solution of the steady state for the convective-transport problem gives oscillatory results if the mesh size exceeds certain critical value[57]. Therefore, a discussion of this problem is given in the succeeding Section.

4.5 STABILITY OF THE STEADY CONVECTIVE-TRANSPORT PROBLEM

The numerical solution of the steady convective-transport partial differential equation,

$$\rho C \left(u \frac{\partial T}{\partial x} + v \frac{\partial T}{\partial y}\right) = k_x \frac{\partial^2 T}{\partial x^2} + k_y \frac{\partial^2 T}{\partial y^2} \qquad (4.54)$$

presents serious difficulties when the left hand (convective) side is dominant. These difficulties arise from the combination of the elliptic and parabolic nature of the two terms and manifest themselves in an oscillatory nature of the solution whenever the element size (characteristic length of the element h) exceeds a certain value[57,58]. This critical value is defined by the local Peclet number (thermal number) and governs the type of approximation to be used with the finite element formulation. The critical value is defined by

$$R = \frac{\bar{V} h}{k/\rho C} < 2 \qquad \bar{V} = \max[|u|, |v|] \qquad (4.55)$$

where R = local thermal number,

u,v = velocity components in x and y directions, respectively

and $k/\rho C$ = thermal diffusivity.

Zienkiewicz[49,57] recognized the above difficulties with the finite element formulation using the standard Galerkin procedure and a bilinear isoparametric element mesh. He found that reasonable results are obtained for R = 3.75, but when R increases the results deteriorate until R = 37.5, when meaningless oscillations are obtained. Zienkiewicz et al.[57,58] solved this problem by modifying the weight function. Ben-Saber and Rassnell[59] noted that this problem is not serious if a triangular element is used instead of an isoparametric element. They tested the triangular element against the isoparametric element when both were used to solve the same problem demonstrated by Zienkiewicz[57,58]. The triangular element provided better stability in the sense of smaller oscillation with high thermal number (R), even with unrealistic boundary

conditions. Thus, the triangular element is recommended for this type of problem.

In this work, the triangular element has been used and the finite element program has been developed. The detailed finite element formulation for the triangular element and the program block diagram are given in Appendix A and Appendix B, respectively.

4.6 STEPLENGTH CONTROL ALGORITHM FOR TWO-POINT RECURRENCE SCHEME

In general, the strategy of controlling the steplength for certain recurrence scheme is to choose the largest possible steplength (Δt) for which the local truncation error (E_T) remains upper bounded by a certain specified maximum allowable error[53,54]. The local truncation error for the linear multi-step recurrence schemes can be expressed in the form,

$$E_T = C_S \, \hat{x}^{(S+1)}_{(\tau)} \, (\Delta t)^{S+1} = O(\Delta t^{S+1}) \qquad (4.56)$$

where S is the scheme order, $\hat{x}^{(S+1)}_{(\tau)}$ denotes the $(S+1)^{th}$ derivatives of the solution $\hat{x}(t)$ at $t_n = \tau$ and $t_n < \tau < t_{n+1}$, and C_S is the error constant that depends on the order of the scheme. For the two-point recurrence schemes (θ-method) of Equation (4.43), the values of C_S, S and error formulae are given in Table 4.1.

Table 4.1 Error Formulae for θ-Scheme

θ	S	C_S	E_T
$\frac{1}{2}$	2	$-\frac{1}{12}$	$-\frac{1}{12} \hat{x}^{(3)}_{(\tau)} \Delta t^3$
$\theta > \frac{1}{2}$	1	$\frac{1}{2} - \theta$	$(\frac{1}{2} - \theta) \hat{x}^{(2)}_{(\tau)} \Delta t^2$

Assuming that the allowable truncation error per step is E, then for a steplength Δt used with first order schemes, we have

$$|E_T| = |C_S \hat{x}^{(2)}_{(\tau)} (\Delta t)^2| < E \tag{4.57}$$

Let the steplength be changed to $\Delta t_1 = \alpha \Delta t$, then

$$|E_{T_1}| = C_S \hat{x}^{(2)}_{(\tau)} (\Delta t_1)^2 = C_S \hat{x}^{(2)}_{(\tau)} (\alpha \Delta t)^2 = \alpha^2 |E_T| < E \tag{4.58}$$

and α can be determined from the relation

$$\alpha = \sqrt{\frac{E}{A|E_T|}} \tag{4.59}$$

where A is taken as a factor of safety, which can be determined experimentally to keep the error below the limits.

Once E_T is determined for the n^{th} step, the value of α and the new steplength can be approximated using the backward difference formula as follows:

$$X'(t_n - \Delta t) = X'(t) - \Delta t\, X''(t) + 0(\Delta t) \tag{4.60}$$

Hence,

$$x''_n = \frac{x'_n - x'_{n-1}}{\Delta t_n} \tag{4.61}$$

Similarly, x'_n and x'_{n-1} can be determined from the following equations:

$$x'_n = \frac{x_n - x_{n-1}}{\Delta t_n} \tag{4.62}$$

$$x'_{n-1} = \frac{x_{n-1} - x_{n-2}}{\Delta t_{n-1}} \tag{4.63}$$

Substituting (4.62) and (4.63) in (4.51), we get

$$x''_n = \frac{x_n - (1 + \alpha_n)\, x_{n-1} + \alpha_n\, x_{n-2}}{\Delta t_n^2} \tag{4.64}$$

If we consider $x''_n(\tau) = x''_n$, i.e. taking $\tau = t_n$, then we can write the formula to estimate E_T for the two-point recurrence schemes of $\theta > \frac{1}{2}$ as follows:

$$E_T = (\tfrac{1}{2} - \theta)\ (x_n - (1 + \alpha_n)\ x_{n-1} + \alpha_n\ x_{n-2}) \qquad (4.65)$$

Estimating the error E_T at the starting point is not an easy task because three values of x (x_n, x_{n-1} and x_{n-2}) are required. Therefore, a starting routine should be established to begin the iteration. The starting procedure is to choose any steplength Δt and move two steps, then estimate E_T. If $|E_T| < E$ determine the new steplength and the solution can be proceeded. But, if $|E_T| > E$, determine (α) and a new starting steplength and repeat the starting steps until $|E_T|$ becomes less than E.

For a system of equations, the error is equal to the L_2 norm of the individual elements of E_T, which is defined by

$$\| E_T \|_{L_2} = \sqrt{\{E_T\}^T\ \{E_T\}} \qquad (4.66)$$

The relative error is usually used with "stiff" system of ODEs instead of the absolute error. The relative error is defined as:

$$\| E_T \| = \frac{\| E_T \|}{\| x_n \|} = \sqrt{\frac{\{E_T\}^T\ \{E_T\}}{\{x_n\}^T\ \{x_n\}}} \qquad (4.67)$$

where $\{x_n\}$ are the values of the function at $t = t_n$.

The above algorithm has been implemented in the finite element program and tested with $\theta = 2/3$, $7/8$ and 1. The algorithm provided stable and accurate results. The $\theta = 7/8$ gave the largest steplength and consequently was the most economical to use. Appendix C provides an example illustrating the above algorithm and presents the results.

CHAPTER 5

SOLUTION OF THE TRANSIENT TEMPERATURE DISTRIBUTION IN INTERMITTENT CUTTING PROCESSES

The temperature distribution in a cutting tool is essential to compute the thermal stresses associated with the cutting process. Most of the research work (see Chapter 3) has been directed towards the solution of the shear plane temperature and the tool/chip interface temperature problems, in both continuous and intermittent cutting processes. Less effort was directed towards the transient temperature distribution problem, particularly in intermittent cutting processes.

Since our primary objective is to study the thermal cycling in peripheral milling, this chapter is devoted to presenting the solution of the transient temperature distribution in intermittent cutting processes with specific reference to the peripheral milling operation.

Peripheral milling is the process in which the intermittent cutting action between the rotating cutter and the stationary workpiece takes place on the outer periphery of the cutter. The three basic modes of peripheral milling are presented in Fig. 5.1. These modes are up-milling, down-milling and slotting. The parameter of "immersion" (i) is defined as the ratio of the radial depth of cut a_r to the cutter diameter d; $i = a_r/d$.

In peripheral milling operation, the thickness of the undeformed chip varies with the angle of rotation during the cut. Thus, not only

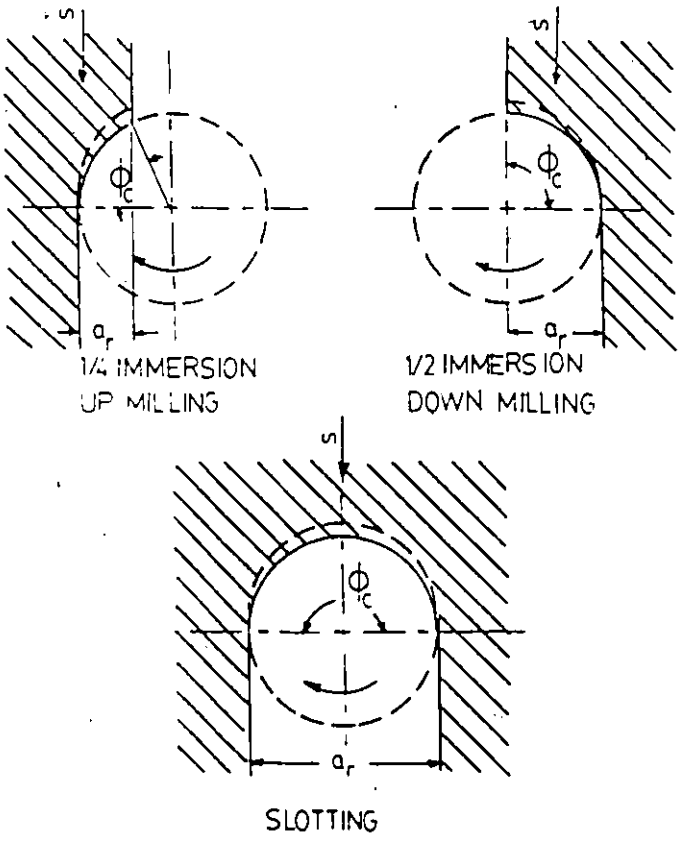

Fig. 5.1 Geometry of peripheral milling.

the cutting action is intermittent, but also the cutting conditions are continuously changing. The shear plane heat source as well as the friction heat source vary in both length and intensity with the angle of rotation. This transient behaviour renders the problem rather complex.

The thermal conditions in the cutting process are described by two models; the first for the cutting period, and the second for the non-cutting period. Also, the tool/chip interface heat source is modelled so that it can distinguish the difference between up- and down-milling processes.

These models are presented here, together with a summary of the computed results for typical cases.

5.1 MODELLING OF THE INTERMITTENT CUTTING PROCESS

5.1.1 Assumptions

The assumptions which were made for this analysis can be outlined as follows:

a) The cutting process is orthogonal; i.e., two-dimensional.

b) The tool tip is sharp.

c) The shear plane is a plane uniform heat source.

d) The friction zone is a plane uniform heat source.

e) The chip region is a homogeneous and isotropic continuum.

f) The chip velocity is constant across the chip, and the chip curl is neglected.

g) The material density, specific heat, thermal conductivity and heat transfer coefficient are constant for both the chip and the tool.

h) The chip ratio is constant.

i) The tool/chip contact area is linearly proportional to the chip thickness.

j) The tooth path is an arc of a circle.

The main advantages of these assumptions are to simplify the modelling of the cutting process, and to permit a detailed theoretical analysis, which might otherwise be difficult. For instance, we have assumed that the cutting process is orthgonal and the tool is sharp. These assumptions neglect the influence of the helix angle, and, the fact that the cutting edge of the tool is round or chamfer. Considering these effects call for three-dimensional analysis, which is laborious and requires extensive computational effort.

Regarding assumptions (c) and (d), it is conventional in the theoretical analysis of cutting temperature to assume that the work material was sheared at a plane and that the heat source due to this shearing was a plane heat source of uniform strength. It was also assumed that the heat source due to friction between the chip and tool was a plane heat source of uniform strength. In previous investigations[60,61,62], for chip formation in orthogonal continuous cutting operation, it was demonstrated that the chip deforms plastically at the shear plane over a thick zone rather than a plane. A thick-shear-zone appears at low cutting speeds, particularly when cutting metals which are in the annealed condition. However, the plastic deformation occurs on a thin shear plane at high cutting speeds. Nakayama[63], using the quick-stop technique, demonstrated that the chip deforms over a wide area at the tool/chip interface. In milling, the undeformed chip is very thin. Therefore, adopting the conventional assumptions in this

analysis is not a gross simplification.

It is also assumed that the chip ratio is constant. This assumption was made following Boothroyd's experiment which assumes that the chip ratio is constant with varying chip thickness when the chip thickness is small[64].

In this analysis, the tooth path has been assumed to be an arc of a circle. Mortellotti[65] showed that the path of a milling cutter tooth is trochoidal. With practical cutting conditions, the error in assuming the tooth path to be an arc of a circle is negligible[62].

5.1.2 Models

In order to study the thermal conditions in the cutting and the non-cutting periods of the cutting process, two models were devised. The first is a two-dimensional tool/chip model to be used to obtain the temperature distribution in the cutting period. The second is a two-dimensional tool model which is used to compute the temperature distribution in the non-cutting period.

5.1.2.1 Cutting period model

During the cutting period, the chip deforms plastically and all the deformation energy is assumed to be converted into heat. The energy conversion takes place in three zones, which are considered as heat sources. These are the shear plane source, the tool/chip interface source, and the third source which forms as the cutting progresses and the tool flank is worn out. However, if the tool is sharp the last heat source is negligible and it has been neglected in this study.

A part of the heat generated in the shear zone is carried away by the chip, and the other part goes to the workpiece. At any instant, it is assumed that while passing through the shear plane, the chip acquires a uniform temperature. Hence, the shear plane defines a distinguished boundary which reflects the interaction between the chip and the workpiece. Therefore, a tool/chip model is sufficient to describe the thermal conditions in the cutting period.

Figure 5.2 a) shows a two-dimensional tool/chip model together with the thermal boundaries. The shear plane boundary is a prescribed temperature boundary which has the average instantaneous shear plane temperature (T_s). Deep enough into the tool, it is assumed that room temperature (T_r) is reached in the shank of the tool. Along the contact length ℓ_c, between the chip and the tool, friction power is generated, which provides for a plane heat source with conduction both into the chip and into the tool. The tool/chip interface heat source defines a conduction boundary. Heat is convected away from the rake and flank faces of the tool, which define convection boundaries.

The energy equation describing the heat transfer mechanism in the cutting period is the transient convective-transport equation (Equation (4.5)). If the tool has a zero rake angle, the energy equation reduces to:

$$\rho\, C\, \left(\frac{\partial T}{\partial t} + v_c \frac{\partial T}{\partial x}\right) = k\, \left(\frac{\partial^2 T}{\partial x^2} + \frac{\partial^2 T}{\partial y^2}\right) \qquad (5.1)$$

where the second term of the left hand side is applied over the chip domain only. The chip velocity is v_c. The thermal conductivity (k), specific heat (C) and density (ρ) are assumed constant, i.e. temperature

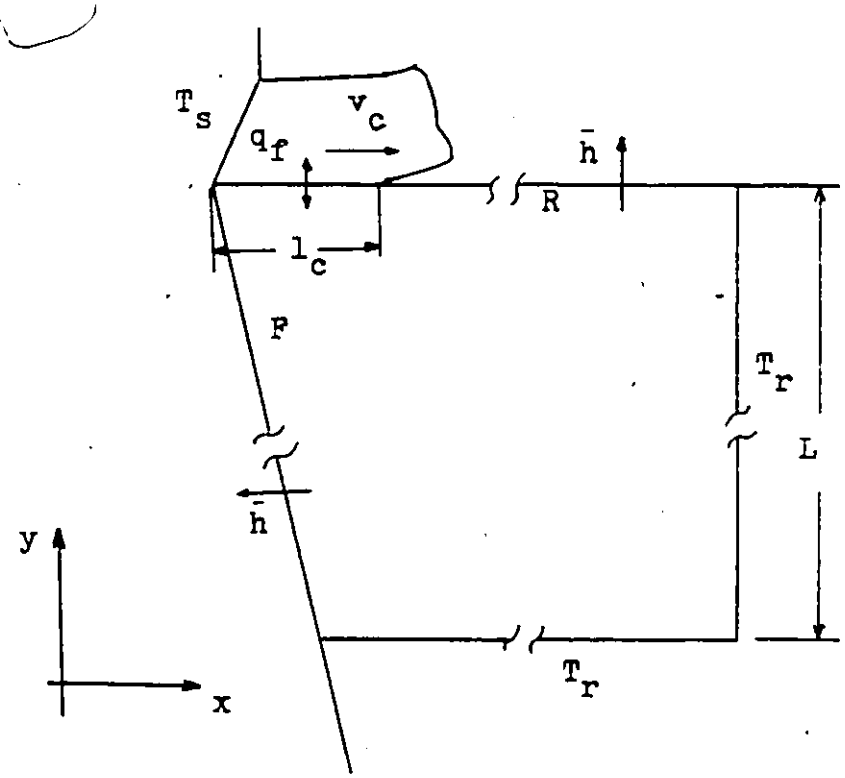

(a) Tool/chip model.

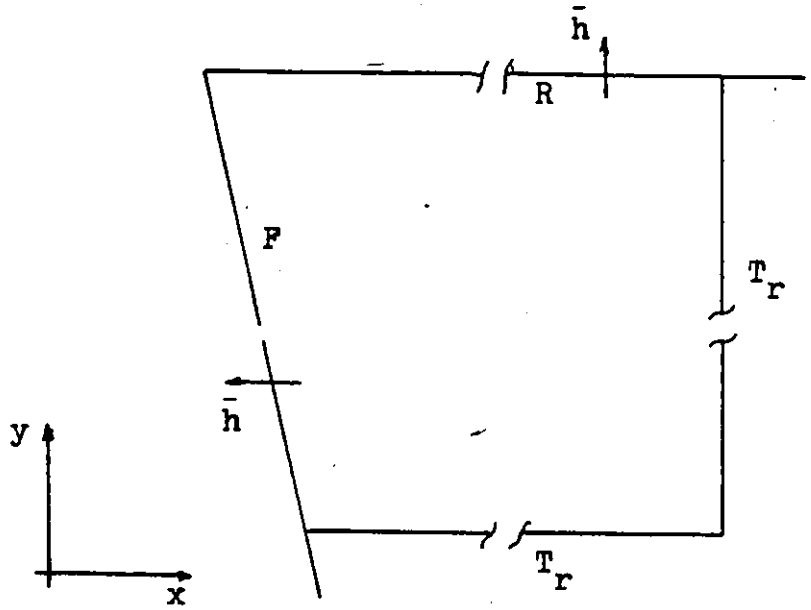

(b) Tool model.

Fig. 5.2 Temperature computational models showing thermal boundaries.

and space independent. The heat generation is on the plane heat source and there is no internal energy generation, i.e., $\bar{Q} = 0$.

The boundary conditions are partly the prescribed temperature, and partly the convective and conductive boundaries. These thermal boundaries are expressed mathematically as follows:

(a) Prescribed temperature boundaries:

The prescribed temperature boundary is defined as

$$T = T(x,y,t) \qquad t > 0 \tag{5.2}$$

on surfaces where temperature is specified. On the shear plane, we have

$$T = T_s(x,y,t) \qquad t > 0 \tag{5.2a}$$

On surfaces deep enough in the tool shank, we have

$$T = T_r(x,y,t) \qquad t > 0 \tag{5.2b}$$

where the room temperature is reached.

(b) Convection boundaries:

On the rake and flank surfaces of the tool where heat is convected away, we have

$$k \left(\frac{\partial T}{\partial x} n_x + \frac{\partial T}{\partial y} n_y\right) = \bar{h} (T - T_r) \tag{5.3}$$

(c) Conduction boundaries:

On the tool/chip interface region, where friction heat is generated, we have

$$k \left(\frac{\partial T}{\partial x} n_x + \frac{\partial T}{\partial y} n_y\right) = q_f \tag{5.4}$$

where q_f is the heat flux of the friction heat source.

With peripheral milling, the chip thickness varies with the angle of rotation, and consequently, the contact length and the heat intensity

are time dependent. With up-milling, the undeformed chip thickness varies from zero to a maximum at the start and end of a cut, respectively, while with down-milling it is the opposite. Consequently, if the contact length is proportional to the undeformed chip thickness, the length of the friction heat source is expected to vary in the same manner. Therefore, during the cutting period, the friction heat source has been varied with time as shown in Fig. 5.3. In case of up-milling (Fig. 5.3 a)), heat flux is indicated by a rectangle q_1 in the first instant, by q_2 in the second instant, and q_n in the n^{th} instant. The same sequence is considered with down-milling (Fig. 5.3 b)), except that the first instant starts with a rectangle covering the full contact length. With slotting, the heat source varies as in up-milling in the first half then as in down-milling in the second half.

5.1.2.2 Non-cutting period model

Following the cutting period is the non-cutting period, during which there is no chip, and the whole rake face and the flank are exposed to the cooling air or to the cutting fluid. The energy equation describing the heat transfer mechanism in this period is the Fourier Equation of heat conduction, which is:

$$\rho\, C\, \frac{\partial T}{\partial t} = k\, \left(\frac{\partial^2 T}{\partial x^2} + \frac{\partial^2 T}{\partial y^2}\right) \qquad (5.5)$$

Figure 5.2 b) shows a two-dimensional tool model together with the thermal boundaries. The thermal boundaries are a prescribed temperature boundary defined by Equation (5.2b), and the convection boundaries on the rake face and the flank are defined by Equation (5.3).

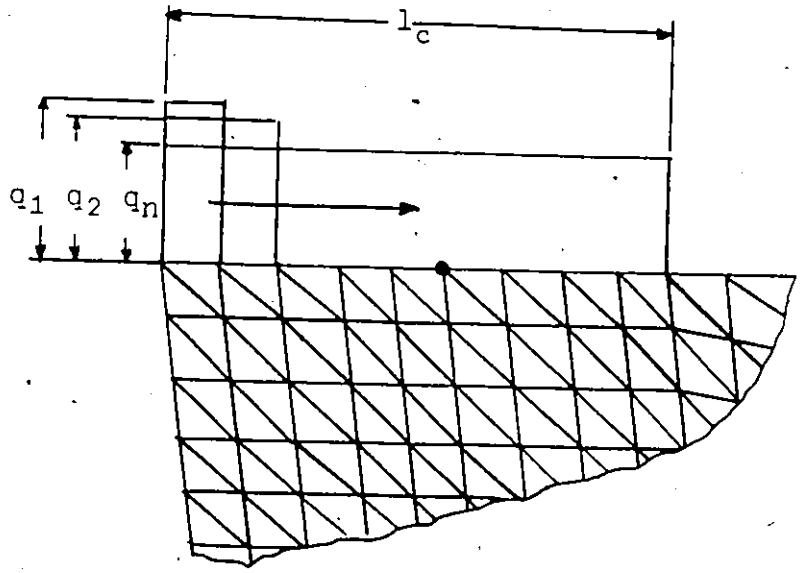

(a) Up-milling

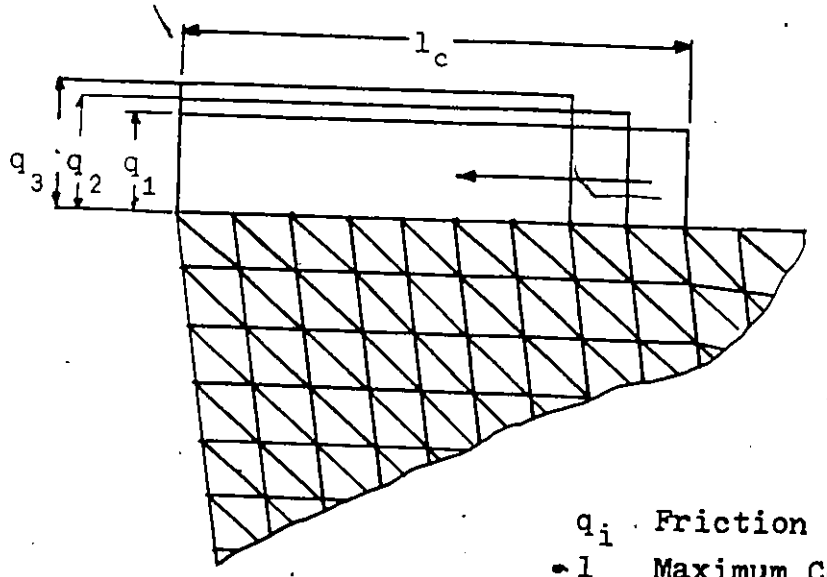

q_i Friction Heat Flux

l_c Maximum Contact Length

(b) Down-milling

Fig. 5.3 Friction heat source models.

The transient temperature distribution in a cutting cycle is obtained using the above two models to solve the following two problems:

a) The convective-transport energy equation (Equation (5.1)) with the associated boundary conditions (Equations (5.2), (5.3) and (5.4)) is to be solved over the tool/chip domain (Fig. 5.2 a)) in a heating period of a time span t_h. The initial condition at the beginning of the first cycle ($t = 0$) is assumed to be a uniform temperature, which is defined by:

$$T = T_r(x,y,0) \tag{5.6}$$

b) The Fourier Equation of heat conduction (Equation (5.5)), with the associated boundary conditions (Equations (5.2b) and (5.3)), is to be solved on the tool domain (Fig. 5.2 b)) in a cooling period of a time span t_c. The initial condition is the temperature distribution on the tool wedge at the end of the heating period.

The temperature distribution at the end of a cycle is used as an initial condition for problem a) to obtain the solution for the temperature distribution in the subsequent cycles.

A finite element computer program (Heat Transfer Program) has been developed for this purpose. The program is designed to solve the above two problems in sequence for a finite number of cycles. The detailed flow chart and the description of the program are given in Appendix B.

5.1.3 Determination of the Boundary Conditions

In order to solve the aforementioned problems, the following boundary conditions should be determined:

(a) The shear plane temperature (T_s).

(b) The heat flux of the friction heat source (q_f).

(c) The coefficient of heat transfer ($\bar{h}$) on the rake face and the flank of the tool.

(d) Location of the room temperature boundaries.

5.1.3.1 Determination of the shear plane temperature and the friction heat flux

The shear plane temperature and the heat flux of the friction heat source are determined based on the energy consumed on cutting. The rate of energy consumption during machining is the product of the tangential cutting force (F) and the cutting speed (v). The tangential cutting force depends on the material of the workpiece, on the dimension of the chip: its thickness (h) and width (b), on the geometry of the tool, and on the cutting speed. At practical cutting speeds, the tangential force component varies slightly with cutting speed[65].

Quite generally, the following formula is recognized for the relationship between the tangential cutting force and the basic parameters[65]:

$$F = K_s \; b \; h \qquad \text{Newton (N)} \qquad (5.7)$$

where K_s is the specific cutting force in N/mm^2. The specific cutting force is a function of the chip thickness according to the relationship:

$$K_s = C_1 \; h^{-x} \qquad (5.7a)$$

where C_1 and x are constant, depending on the workpiece material and on the milling cutter.

Sabberwal[66] demonstrated that the specific cutting force is independent of the width of cut, helix angle and chip section. Therefore, the tangential cutting force in the peripheral milling has been determined using the cutting force formula given in Equation (5.7).

It is extremely difficult to include the chip variation in a finite element model. Therefore, the procedure described below was adopted to determine the shear plane temperature and the flux of the friction heat source.

The cutting period has been divided into a finite number of intervals. In each interval, the cutting is considered as a continuous cut having the average chip thickness. This simplification is depicted in Fig. 5.4.

Consider the time interval (i) in which the tool advances from ψ_1 to ψ_2 as shown in Fig. 5.4. Then, the cutting energy can be determined for a cutting condition described by cutting speed (v), width of cut (b) and feed/tooth (s_t), as follows:

The instantaneous chip thickness h in mm is given by

$$h = s_t \sin \psi \tag{5.8}$$

The instantaneous tangential cutting force F in Newton (N) is given by

$$F = K_s \, b \, s_t \sin \psi = C_1 \, b \, (s_t \sin \psi)^{1-x} \tag{5.9}$$

Assuming that the tool has a zero rake angle, and that the coefficient of friction (μ) and chip ratio (r) are constant for a cutting condition, then the instantaneous friction F_f, and shear force F_s in N are

$$F_f = \mu \, F = \mu \, C_1 \, b \, (s_t \sin \psi)^{1-x} \tag{5.10}$$

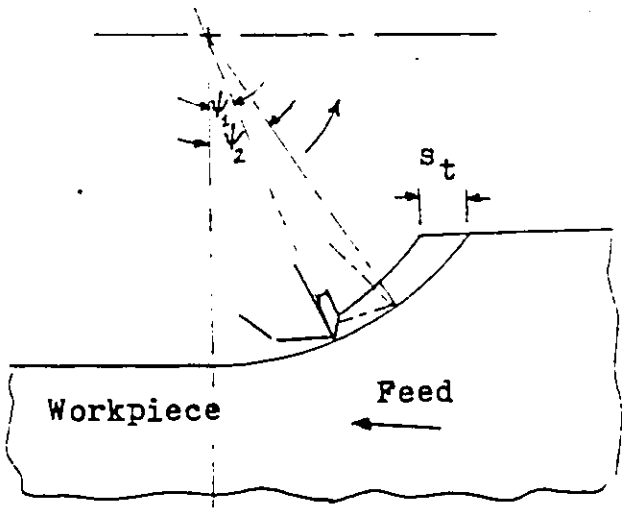

(a) Actual.

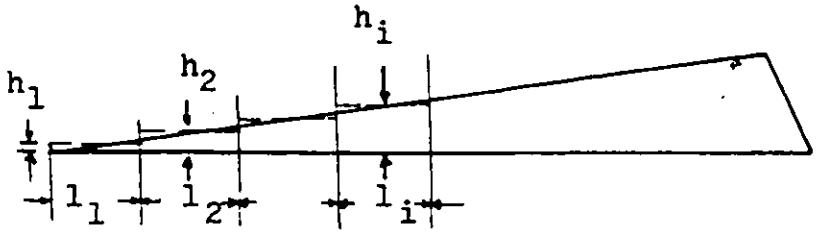

(b) Approximation.

Fig. 5.4 Variation of undeformed chip thickness in peripheral milling.

$$F_s = F \cos \phi - F_f \sin \phi$$

$$= C_1 \, b \, (s_t \sin \psi)^{1-x} \, [\cos \phi - \mu \sin \phi] \qquad (5.11)$$

where

ϕ = the shear angle = $\tan^{-1} r$.

The instantaneous gross rate of energy liberation on the shear source P_s in J/s, and friction source P_f in J/s are

$$P_s = F_s \, v_s = v_s \, C_1 \, b \, (s_t \sin \psi)^{1-x} \, [\cos \phi - \mu \sin \phi] \qquad (5.12)$$

$$P_f = F_f \, v_c = v_c \, C_1 \, b \, (s_t \sin \psi)^{1-x} \qquad (5.13)$$

where v_s = the shearing velocity = $v_c/\cos \phi$ in m/s

and v_c = the chip velocity = rv in m/s.

The instantaneous average shear plane temperature is determined from the simple equation derived for the steady cutting operation. This is in accordance with the findings of McFeron and Chao[44]. The average temperature rise θ_s in °K at the shear plane at any instant is determined from the expression

$$\theta_s = \frac{(1-\lambda_s) \, P_s}{\rho \, C \, v \, A_c}$$

$$= \frac{(1-\lambda_s) \, r \, C_1 \, (s_t \sin \psi)^{-x} \, [\cos \phi - \mu \sin \phi]}{\rho \, C \cos \phi} \qquad (5.14)$$

where

λ_s = the proportion of the shear heat source conducted back to the workpiece,

A_c = the instantaneous chip cross sectional area in mm^2, and

$\rho \, C$ = volumetric specific heat KJ/mm^3 °K.

The proportion of the shear heat source λ_s conducted back to the workpiece is determined using the formula (Equation (3.1)) after Weiner[34].

The heat flux of the friction heat source $\dot{q}_f$ in J/s.mm^2 at any instant is

$$q_f = \frac{P_f}{A_{ct}} = \frac{r^2 \, v \, C_1 \, (s_t \sin \psi)^{-x}}{a} \tag{5.15}$$

where A_{ct} is the instantaneous tool/chip contact area in mm^2, which is proportional to the chip thickness and can be determined as follows:

$$A_{ct} = \frac{b \, a \, s_t \sin \psi}{r} \tag{5.16}$$

and a is a constant.

The mean values of the boundary conditions in the interval i is determined by integration from ψ_1 to ψ_2. The temperature rise at the shear plane $\bar{\theta}_i$ is:

$$\bar{\theta}_i = \frac{r \, C_1 \, (\cos \phi - \mu \sin \phi)}{\rho \, C \, (\psi_2 - \psi_1) \cos \phi} \int_{\psi_1}^{\psi_2} (1 - \lambda_s)(s_t \sin \psi)^{-x} \, d\psi \tag{5.17}$$

and the shear plane temperature T_{si} is

$$T_{si} = \bar{\theta}_i + \theta_o \tag{5.17a}$$

where θ_o is the room temperature.

The friction heat flux q_{fi} in the interval i is determined from:

$$q_{fi} = \frac{r^2 \, v \, C_1}{a \, (\psi_2 - \psi_1)} \int_{\psi_1}^{\psi_2} (s_t \sin \psi)^{-x} \, d\psi \tag{5.18}$$

The integrals in Equation (5.17) and Equation (5.18) are determined numerically using Simpson's rule.

The above procedure has been followed to determine the boundary conditions for all the cases studied in this work. The boundary conditions are calculated and given in Table 5.1 for a typical case; half immersion cut, H.S.S. end mill cutter diameter d = 25 mm, cutting speed 40 m/min, feed/tooth S_t = .1 mm, and unit width of cut b = 1 mm. The workpiece material was SPS steel (equivalent to AISI 4140) in the annealing condition with tensile strength σ_β = 700 N/mm^2. The thermal properties for both the H.S.S. and the AISI 4140 steel are given in Table 5.2. The specific cutting force K_s (Equation (5.7a)) is determined using the parameters C_1 = 1520 N/mm^2 and x = .305. The coefficient of friction μ and the chip ratio r are 0.52 and 0.37, respectively.

Table 5.1 Boundary Conditions for Typical Cutting Condition

(v = 40 m/min and s_t = .1 mm/tooth)

Iteration Number	Angle range $\psi_1 \rightarrow \psi_2^0$	Shear Temp T_s °C	Friction Power q_f J/s.mm^2	λ_s
1	0→7.18	329	63.8	0.68
2	7.18→14.5	379	71.45	0.48
3	14.5→22.0	388	68.12	0.41
4	22→30	389	64.6	0.36
5	30→38.7	388	61.6	0.32
6	38.7→48.6	385	59.0	0.28
7	48.6→61.0	381	56.9	0.25
8	61→90	376	55.7	0.23

Table 5.2 Thermal Properties of Tool and Workpiece Materials*

Property	H.S.S.	AISI 4140 steel
Thermal conductivity W/m.°K BTU/ft hr °F	36.34 (21)	38 (22)
Volumetric specific heat (C_p) KJ/m^3 °C BTU/in^3 °F	4800 (.041)	5800 (.05)

*H.S.S. properties are at 400 °K and workpiece properties are at 600 °K.

5.1.3.2 The coefficient of heat transfer on the rake face and the flank of the tool

The rake face and the flank of the tool lose the heat to the surrounding and to the coolent by radiation and convection. The coefficient of heat transfer should be the combined convection and radiation heat transfer coefficient. It is usually called the total heat transfer coefficient. This coefficient is a function of many parameters and it is difficult to determine theoretically, and therefore, should be determined experimentally. Despite an extensive search in literature, no data could be found for the heat transfer coefficient in milling processes for different kinds of tools. Okushima and Hoshi[20] calculated a value for the total heat transfer coefficient $\bar{h}$. In their simplified one-dimensional model, they found various values for $\bar{h}$ ranging from 0.01 W/mm^2 °K to .016 W/mm^2 °K, depending on the cutting ratio. In view of this uncertainty over the precise value of the heat transfer coefficient, the mean value of $\bar{h}$ = .013 W/mm^2 °K has been used in this study.

5.1.3.3 Location of the room temperature boundaries

The location of the room temperature boundaries can be determined based on the concept of heat penetration as discussed in Ref. (67). The time (t_o) necessary for the heat to reach a certain point inside the tool at depth (L) can be determined from the relation

$$t_o = \frac{L^2}{6\alpha} \tag{5.19}$$

where α is the thermal diffusivity of the tool material. Hence, the location of the room temperature boundary can be determined upon deciding the number of cycles for which the transient temperature is to be computed. The location of the room temperature boundaries is taken at L = 10 mm (Fig. 5.2) which corresponds to 30 cycles each of 120 milliseconds span.

5.2 SUMMARY OF THE RESULTS OF THE COMPUTATION

The transient temperature distribution in peripheral milling has been computed for the cutting conditions given in Table 5.3. The tool was H.S.S. end mill 25 mm diameter. The workpiece material was AISI 4140 steel. In this section a summary is given in which the highlights of the computed results are presented.

5.2.1 Cyclic Temperature Change of Tool/Chip Interface

In Fig. 5.5 the cyclic temperature variation of a point on the rake face in the middle of the fully established contact length is given for the first four cycles of three milling operations. These are; case a) is 0.25 immersion up-milling, case b) is 0.5 immersion

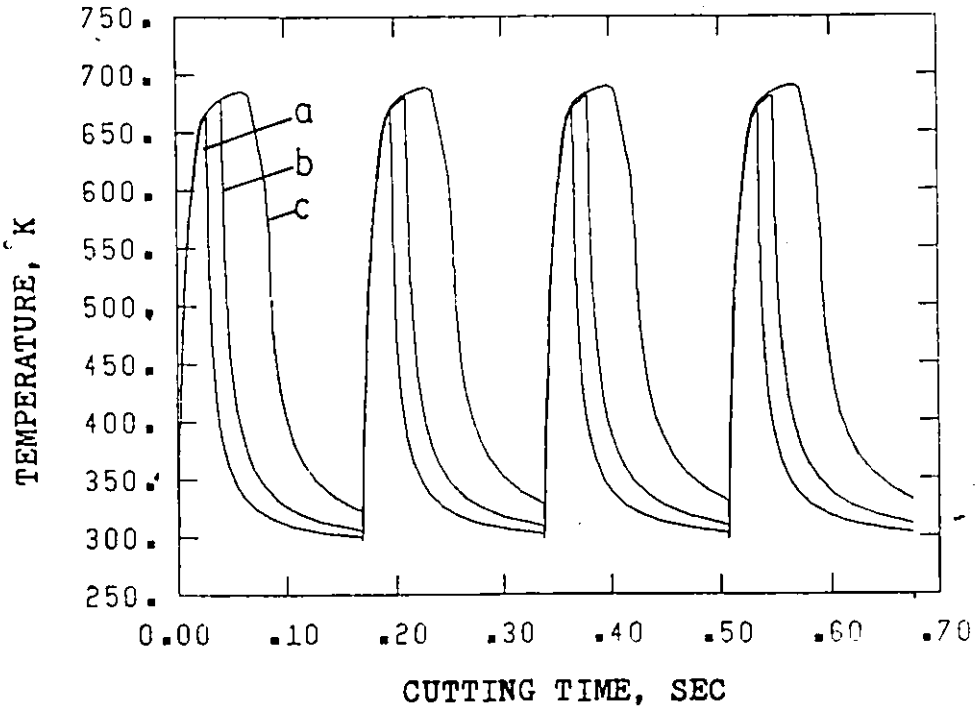

Fig. 5.5 Temperature variation for the first four cycles of:(a)quarter, (b) half and (c) full immersion.

up-milling, and case c) is slotting. The cutting conditions are: cutting speed v = 28.5 m/min and feed per tooth s_t = .05 mm. The graph is a typical temperature cyclic change and very similar results were obtained with other cutting conditions. This indicates the most important conclusion, one which will be reiterated later on by using also other characteristic parameters: there is very little difference between the three cases in the maximum and minimum temperatures reached during the cycle. The temperature cycle is almost fully established already in the first cycle (first revolution of the cutter from the start of cutting). Both the heating and cooling processes are rather fast.

The above results are in agreement with the results obtained by previous investigators[44,19,20]. McFeron and Chao[44] investigated the transient temperature rise in the plain peripheral milling through both mathematical model and experiments. They reported an abrupt temperature rise within a few milliseconds in conventional plain milling of AISI 4140 steel at two cutting speeds; 80 and 100 m/min (see Fig. 3.3). The tool was 260 mm diameter carbide tipped milling cutter.

Okushima and Hoshi[19,20], also, investigated the cyclic temperature change of tool/chip interface in face-milling using carbide tools in machining a medium carbon steel. They reported that the tool/chip interface temperature builds up very rapidly in a few milliseconds. Also, there was no significant difference in the maximum tool/chip interface temperature obtained in machining a narrow (width = 27 mm) and a wide (width = 164 mm) workpiece, under identical conditions.

Table 5.3 Cutting Edge Temperatures in Different Cutting Conditions

Cutting Tool: H.S.S. End Mill 25 mm Diameter

Case No.	Cutting Condition			Peak Temp. °K	Min. Temp. °K	Temp. Range
	Immersion a/d	Feed (s_t) mm/tooth (in/tooth)	Speed m/min (sfpm)			
1	1/2 up	.05 (.002)	28.5 (93.5)	650	310	340
2	slot (full)	.05 (.002)	28.5 (93.5)	660	330	330
3	1/4 up	.05 (.002)	28.5 (93.5)	647	303	344
4	1/2 up	.1 (.004)	28.5 (93.5)	647	321	326
5	1/2 up	.1 (.004)	40 (130)	699	335	354
6	1/2 up	.1 (.004)	55.8 (183)	747	356	391
7	slot	.1 (.004)	40 (130)	715	375	340
8	1/2 down	.1 (.004)	40 (130)	692	332	360

5.2.2 Transient Temperature Distribution in Tool Wedge

In Figs. 5.6 a) through h), the transient temperature fields are given for the fourth cycle of a half immersion up cut with cutting speed v = 40 m/min and feed per tooth s_t = .1 mm. The cutting period is 30 milliseconds. The chip thickness during this period increases

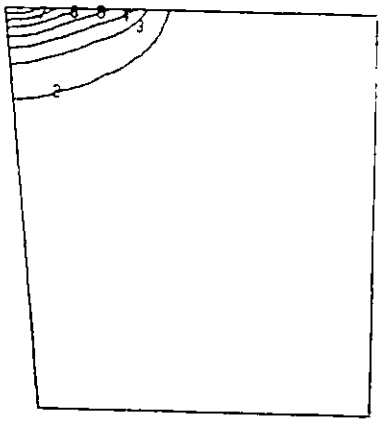

(a) t_h= 5 msec

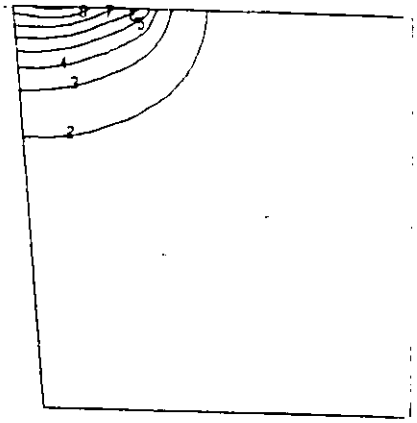

(b) t_h= 10 msec

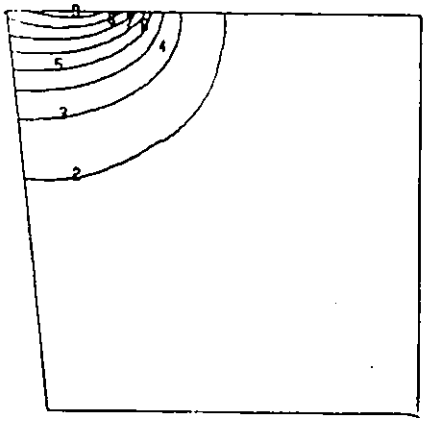

(c) t_h= 15 msec

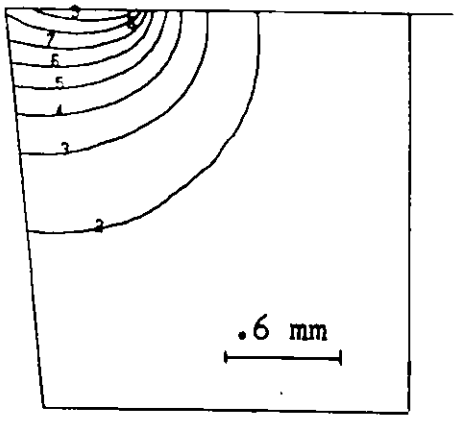

(d) t_h= 30 msec

Fig. 5.6 Temperature fields in a cutting cycle for half immersion up-milling.
Graphs a,b,c and d for the heating period at times t_h.

Key to Contours

Contour	1	2	3	4	5	....
Temp. K	300	350	400	450	500	....

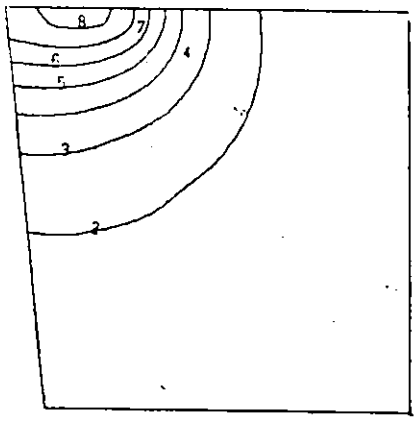

(e) $t_c = 0.6$ msec

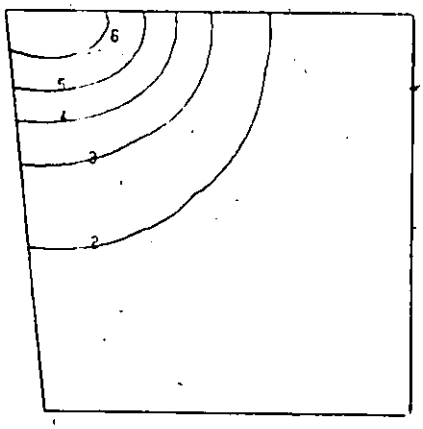

(f) $t_c = 4$ msec

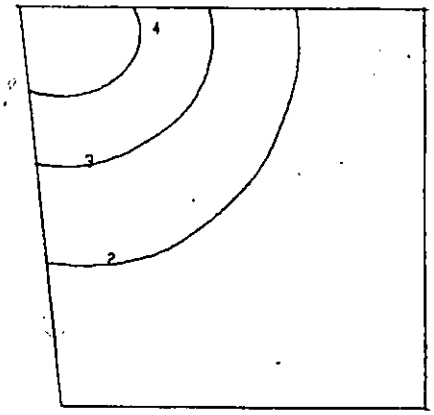

(g) $t_c = 14$ msec

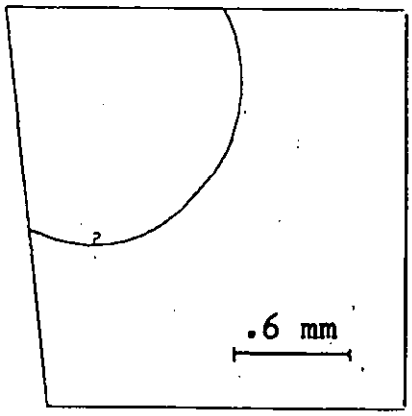

(h) $t_c = 54$ msec

Continued Fig. 5.6 :Graphs e,f,g and h are for the cooling period at cooling times t_c.

gradually from zero to s_t, and the contact length on the tool face spreads from 0.0 to 0.7 mm. The temperature field spreads accordingly. The temperature contours show that the temperature field, also, spreads inside the tool with the cutting time (see Fig. 5.6 a) through d)). The temperature gradient is very high in the direction perpendicular to the rake face. The tool/chip interface temperature is increasing to its maximum value at the end of the heating period. Thus, it is anticipated that high compressive stress is induced in the tool/chip interface area in the cutting period. This should be balanced with tensile stress in the cold area underneath.

The temperature fields at four time instants in the cooling period are shown in Fig. 5.6 e) through h). The cooling period lasts for 90 milliseconds. It is shown that the temperature field continues to spread inside the tool. The tool temperature is decreasing rapidly. As shown in Fig. 5.6 h), the tool has cooled considerably after 54 milliseconds.

The cooling rate of the tool wedge depends not only on the heat transfer coefficient, but also on the volume of the metal which has been heated (the area of heat penetration in the vicinity of the cutting edge). It is shown that, in the heating period a small area is heated up while the rest of the tool is still cold. Therefore, it is anticipated, under these conditions, that the tool wedge loses the gained heat very rapidly. Then, the tool/chip interface temperature reaches a temperature very close to the temperature at the start of the cycle.

For further illustrations of the temperature field in the tool, temperature profiles along the rake face, the flank and a section

perpendicular to the rake face are shown in Fig. 5.7, Fig. 5.8 and Fig. 5.9, respectively. Figures 5.7 a) and b) present temperature profiles along the rake face at four instants of the heating period, and four instants in the cooling period, respectively. The vertical line in the figures indicates the end of the fully established contact length. It is seen that the maximum temperature shifts away from the cutting edge as each of the chip thickness and the contact length increases. The maximum temperature at the end of the heating period occurred at a point close to the end of the contact length (about 3/4 of the fully established contact length).

The curves in Figs. 5.8 a) and 5.8 b) present temperature profiles along the flank. During the heating period (Fig. 5.8 a)), the cutting edge maintains the temperature of the shear plane and the flank heats up with its temperature falling off with distance from cutting edge. During the cooling period (Fig. 5.8 b)), the cutting edge cools down faster than the flank at a small distance from the cutting edge. The temperature gradient is reversed in the part of the flank close to the cutting edge.

The temperature profiles along a section perpendicular to the rake face are shown in Figs. 5.9 a) and 5.9 b). The section is at a point in the middle of the fully established contact length. It is seen that during the heating period (Fig. 5.9 a)), the temperature gradients from the rake face to the inside layers are very high, and the heat has penetrated to a small area underneath the rake face. During the cooling period (Fig. 5.9 b)), the heat continues to penetrate to the inside layers while the tool wedge is cooling down very fast. Also, the tool

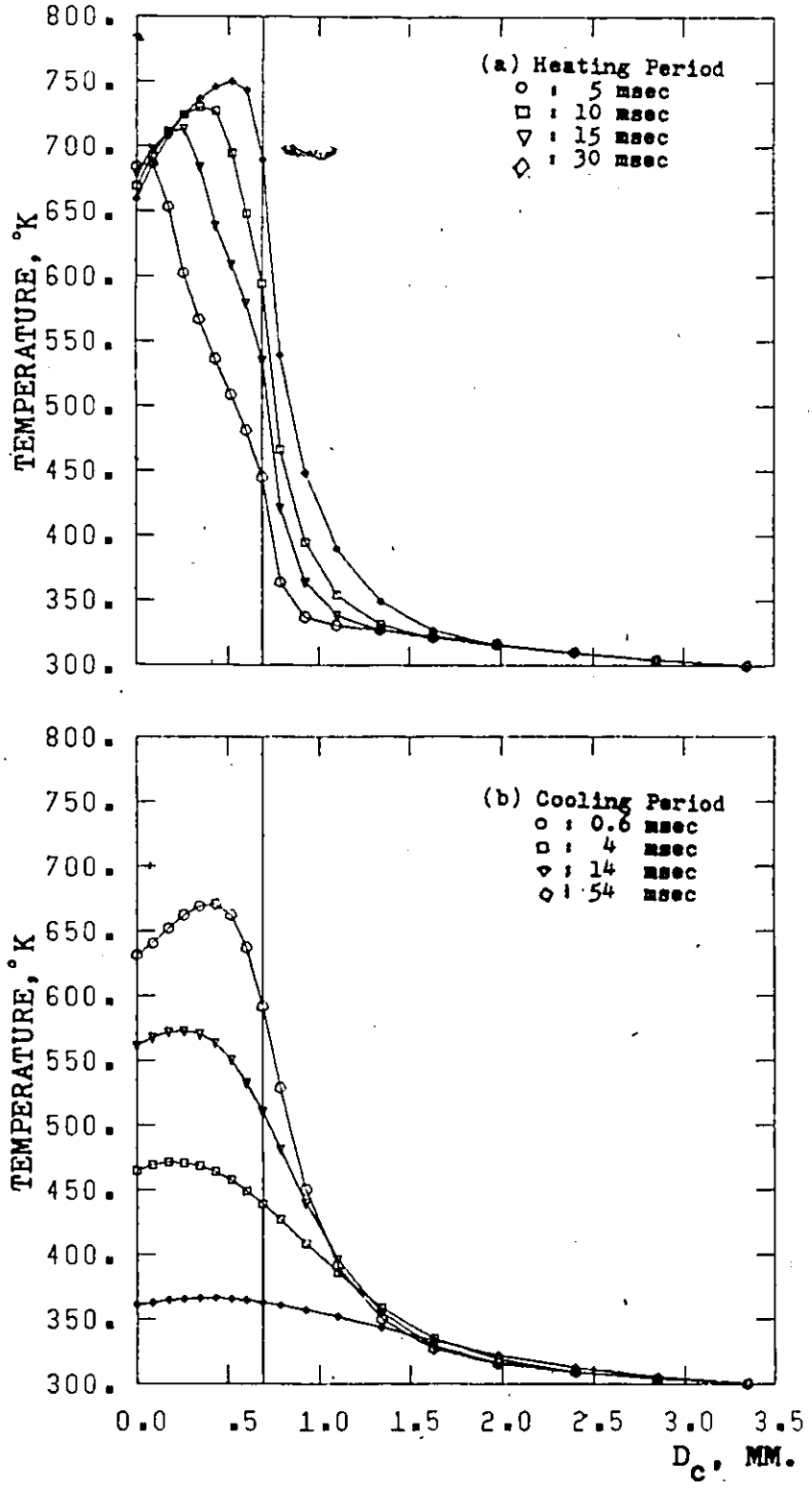

Fig. 5.7 Temperature distribution on the rake face for a cutting cycle of a half immersion up-milling. D_c is the distance from the cutting edge.

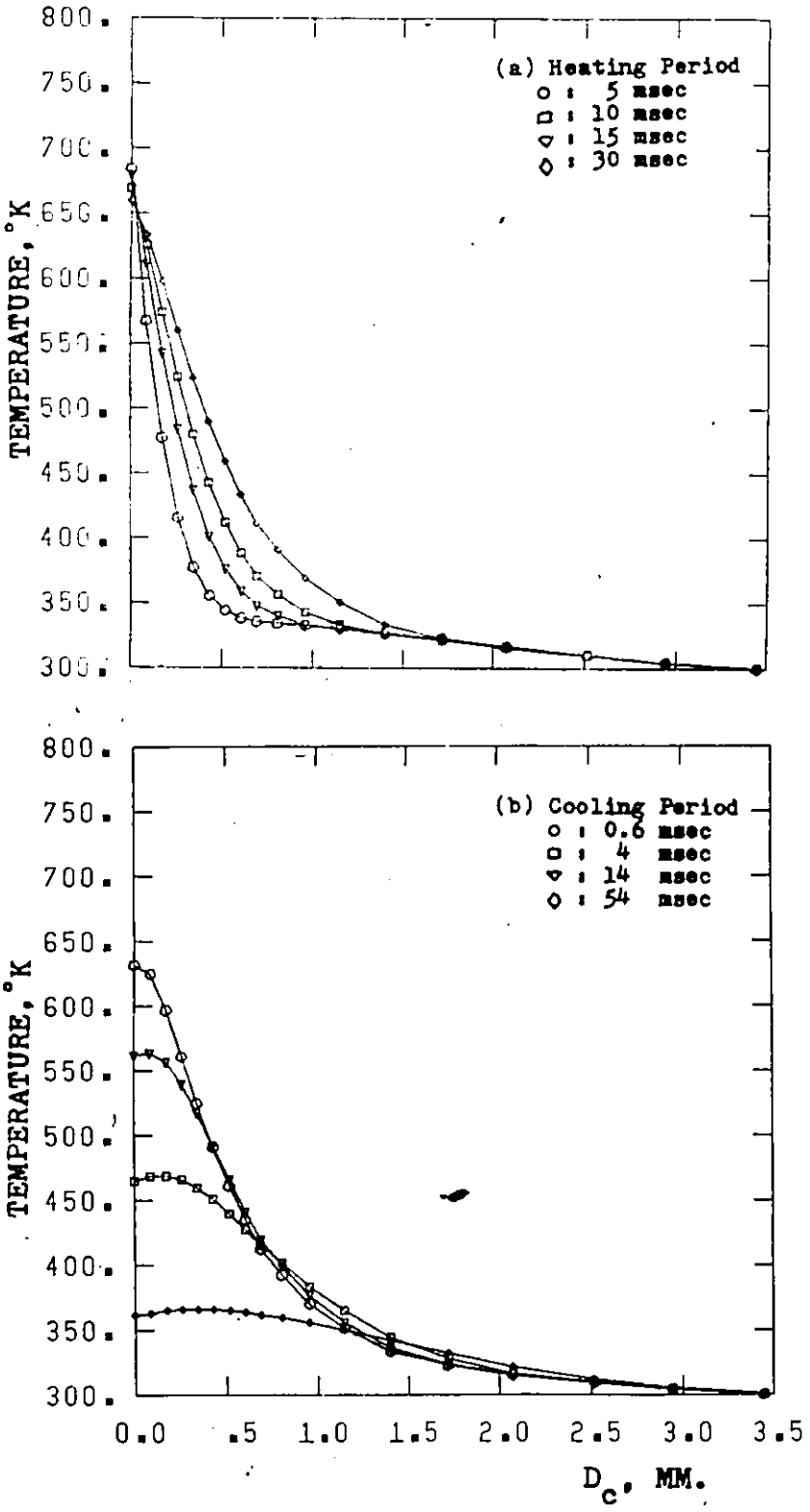

Fig. 5.8 Temperature distribution on the flank for a cutting cycle of a half immersion up-milling. D_c is the distance from the cutting edge.

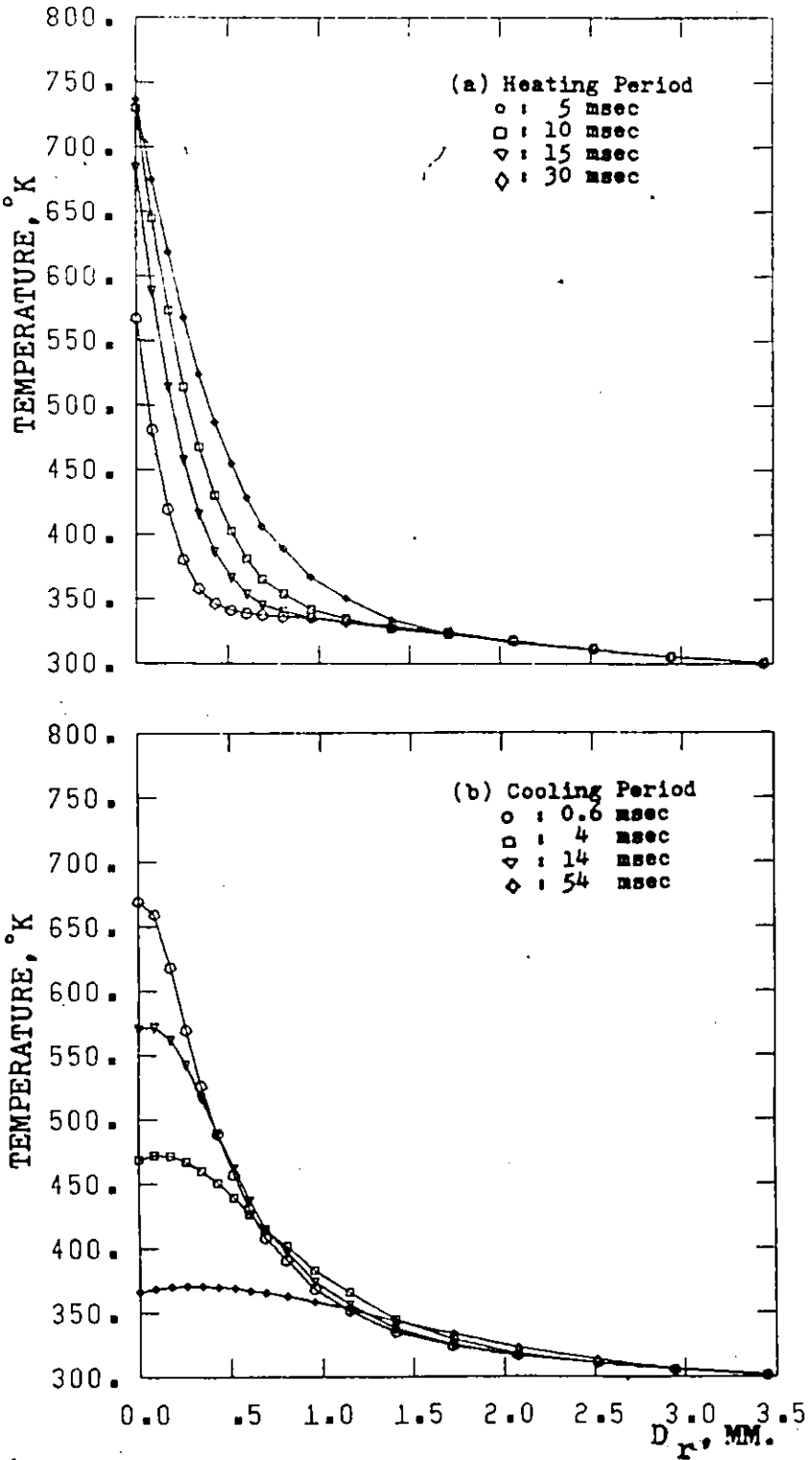

Fig. 5.9. Temperature distribution on a plane perpendicular to the rake face at the middle of the contact length for a cutting cycle of a half immersion up-milling.

D_r is the distance from rake face.

rake face cools faster than inside at some distance from the surface. The temperature gradient is reversed at a point very close to the surface. This indicates that tensile stresses might develop on the rake face during the cooling period.

In Figs. 5.10 a) through h), selected temperature contours are shown for the fourth cycle of half immersion down-milling. The cutting parameters are identical to the half immersion up-cut. Here, with down-milling, the cutting starts with maximum chip thickness which decreases with tool advancement. Thus, in applying the thermal load, the tool/chip interface heat source is assumed to spread over the full contact at the start of cutting, and to decrease with the cutting time.

In Fig. 5.10, the temperature fields a), b), c) and d) are for four time instants in the heating period. It is seen that the tool/chip interface temperature reaches its maximum value at a time instant during the heating period, then decreases. This can be seen clearly in Fig. 5.11 where it is shown that the maximum temperature is reached after 17 milliseconds, and then starts to decrease. This phenomenon was noticed by Okushima and Hoshi[19]. They reported that, in face milling, the tool/chip interface temperatures varied according to the instantaneous thickness of the metal to be removed. The tool/chip interface increased to maximum with cutting progress, then starts to decrease as the tool passes the centerline.

Figures 5.10 e) through h) show the temperature fields at four time instants in the cooling period. The tool cools very rapidly as in up-milling cut. It has cooled considerably after 45 milliseconds (Fig. 5.10 h)) to a temperature between 350 °K and 400 °K.

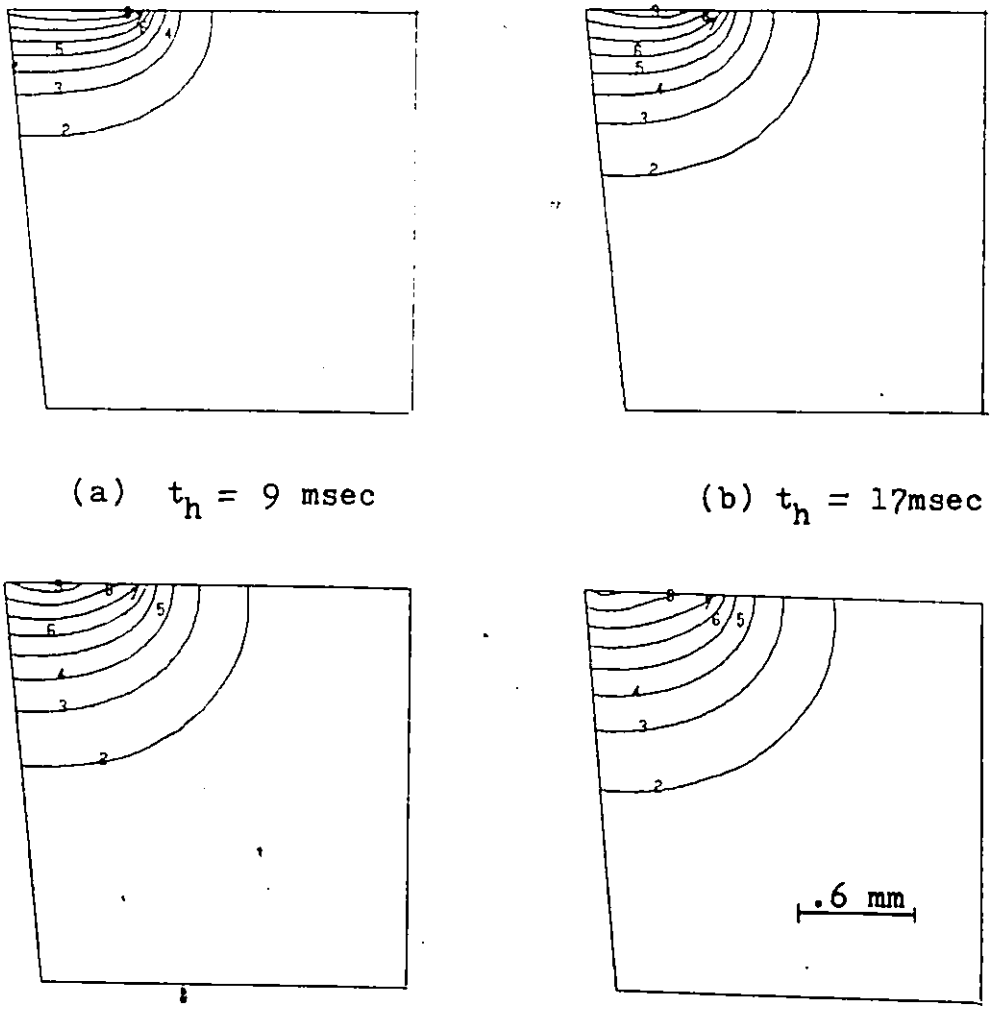

(a) t_h = 9 msec

(b) t_h = 17msec

(c) t_h = 23 msec

(d) t_h = 28 msec

Fig. 5.10 Temperature fields in a cutting cycle for half immersion down-milling. Graphs a, b, c and d are for the heating period at times t_h .

Key to Contours

Contour	1	2	3	4	5	.....
Temp. °K	300	350	400	450	500	.....

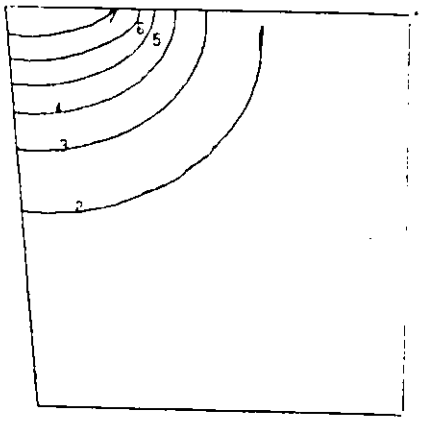

(e) t_c = .35 msec

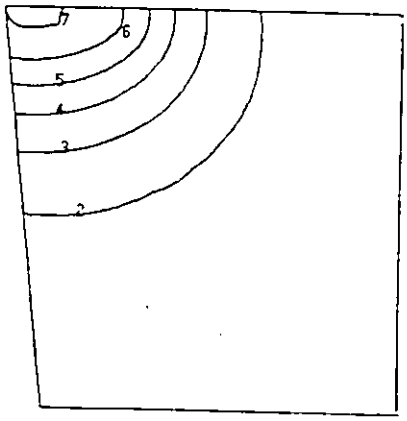

(f) t_c = 1. msec

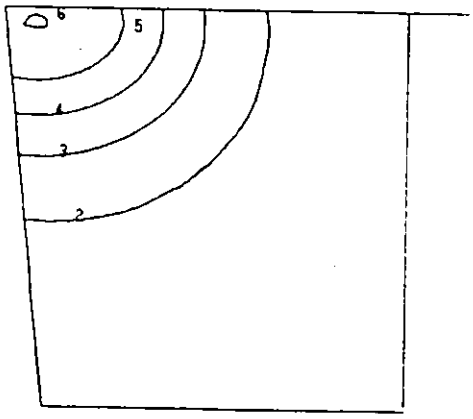

(g) t_c = 4 msec

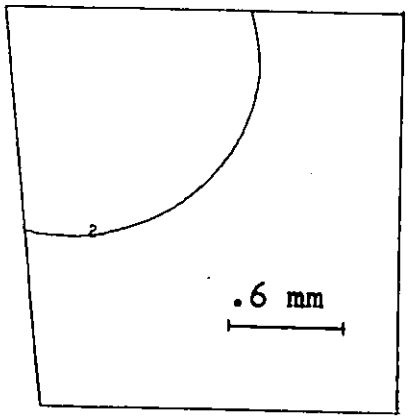

(h) t_c = 45 msec

Continued Fig. 5.10 : Graphs e, f, g and h are for the cooling period at cooling times t_c.

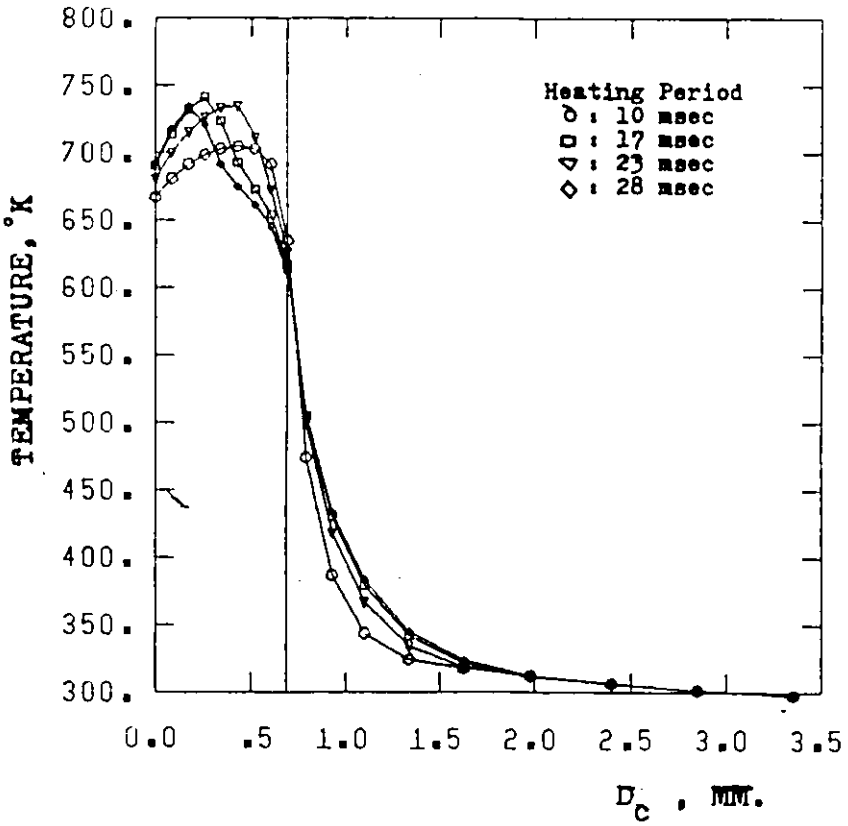

Fig. 5.11 Temperature distribution on the rake face for a cutting period of a half immersion down-milling.

D_c is the distance from the cutting edge.

The maximum tool/chip interface temperature obtained in up-milling is a few degrees higher than that in down-milling (750 °K for up-milling compared to 742 °K for down-milling). On the other hand, the minimum interface temperature in up milling is 335 °K while in down milling it is 332 °K. It is evident that there is no substantial difference in the range of temperature. However, the distribution of temperature is quite different in both cases, and it may create difference in the magnitudes of the stresses and the strains.

It should be mentioned that we have not considered in this analysis the difference in the cutting mechanics between up- and down-milling processes. The two processes differ in the following manner:

a) Entry and exit which lead to differences in the mechanics of chip formation at the initial and final stage of a cut.

b) The varying chip thickness in both cases causes variation in the shear angle and coefficient of friction. The magnitudes of these variations differ in the two processes.

The assessment of these differences is extremely complex and difficult to model.

5.2.3 Effect of Cutting Speed on Cutting Edge Temperature

The cutting edge temperature was determined for half immersion cut at three cutting speeds and a constant feed of .1 mm/tooth. The maximum temperature (at the end of the cutting period) and the minimum temperature (at the end of the cooling period) are plotted against the speed, and shown in Fig. 5.12. Both temperatures increase linearly with logarithmic increase of the speed. This result is in agreement,

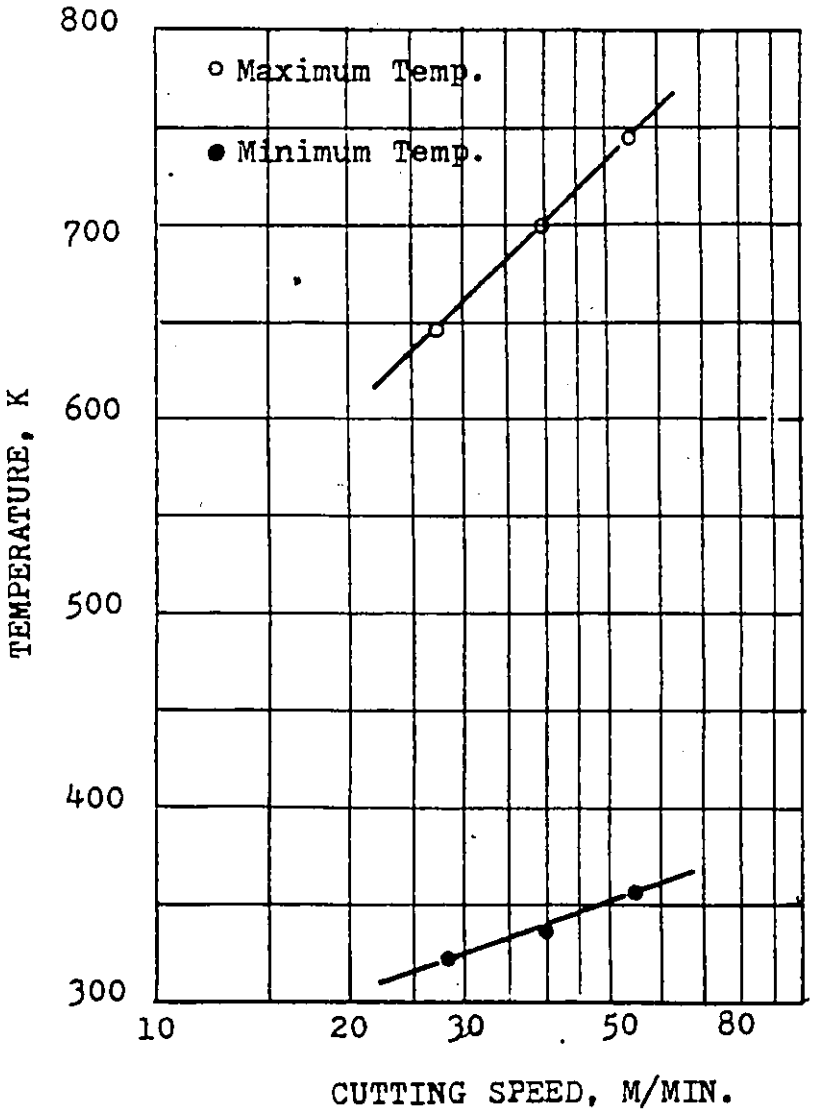

Fig. 5.12 Effect of cutting speed on the maximum and the minimum temperatures of the cutting edge.

in trend, with the experimental measurements of Okushima and Hoshi[19].

5.3 SUMMARY AND CONCLUSIONS

In this Chapter, a procedure to compute the transient temperature distribution in peripheral milling has been established. The cutting process has been modelled based on several assumptions which are necessary to permit detailed theoretical analysis, and to simplify applying the finite element technique. The computations of the transient temperature distribution for several cutting conditions are based on two-dimensional finite element models. These are a tool/chip model for the cutting period, and a tool model for the non-cutting period.

The results of the computation have been analyzed and a summary of the computed results has been presented. The major conclusions which can be extracted may be summarized as follows:

a) There is very little difference between a quarter, half and full immersion in the maximum and minimum temperatures reached during a cycle.

b) The tool/chip interface area experiences an abrupt temperature increase in the heating period, and a rapid temperature decrease in the cooling period.

c) The significant parameters which might influence the tool wear in milling include the following:

   i) Peak temperature; it may affect the level of stresses in heating and cooling.

   ii) Temperature range; the cyclic temperature change causes, upon heating, high compressive strain and stress, and upon

cooling, low compressive or tensile stress on the vicinity of the cutting edge. Hence, the temperature range influences the range of strain and the magnitude and type of stress induced.

CHAPTER 6

STRESS CYCLING IN INTERMITTENT CUTTING PROCESSES

In the preceding Chapter, the results of the computation of temperature cycling in peripheral milling operations were presented. It is seen that the tool temperature abruptly increases or decreases, respectively, at the beginning of both the heating and cooling periods. Hence, the tool experiences a compressive stress in the heating period and tensile stress in the cooling period. Further, the tool is exposed to the cutting forces in the heating period. Therefore, in intermittent cutting processes, the tool must support the cutting forces at the high temperature attained during cutting, and it must also endure the cyclic thermal stresses induced by the heating/cooling cycle. In these conditions of loading and temperature, the study of the stress cycling is very important in order to explain the tool failure phenomenon.

This Chapter is devoted to the study of the stress cycling in peripheral milling operations. The stress computation is based on a two-dimensional finite element tool model. The thermal stresses are computed using the temperature distribution on the tool. The mechanical stresses in the cutting period are computed and combined with the associated thermal stresses. A summary of the computed results is given and the important parameters which may affect the tool wear in milling are presented.

6.1 FINITE ELEMENT MODEL

The stresses induced on the tool in a cutting cycle have been computed based on the two-dimensional finite element model shown in Fig. 6.1. The tool is considered as a plate of dimension L × L × 1 (the same dimensions of temperature computation model where L = 10 mm).

For simplicity, the case is assumed to be a plane strain. This simplification is acceptable for two reasons; (a) the chip width is very large compared to the chip thickness (ratio more than 20), and (b) the heated spot is restricted to expand by the surrounding cold material, which means that the strain in the z-direction is very small, i.e. $\varepsilon_{zz} = 0$, which is the plane strain basic requirement. In addition, the following simplifications are applied:

(a) the tool material is considered to be homogeneous and isotropic, and

(b) the material properties; modulus of elasticity, thermal expansion, and Poisson's ratio are assumed to be temperature independent.

The boundary conditions involved in the computation are:

(a) Prescribed displacement boundary.

(b) Prescribed force boundary.

(a) Prescribed displacement boundary

Sufficient displacements may be prescribed to prevent rigid body motion. The displacements in x and y directions along the lines bc and ab (Fig. 6.1), respectively, are assumed restricted. This means that

$$u = 0 \quad \text{along bc} \tag{6.1a}$$

and

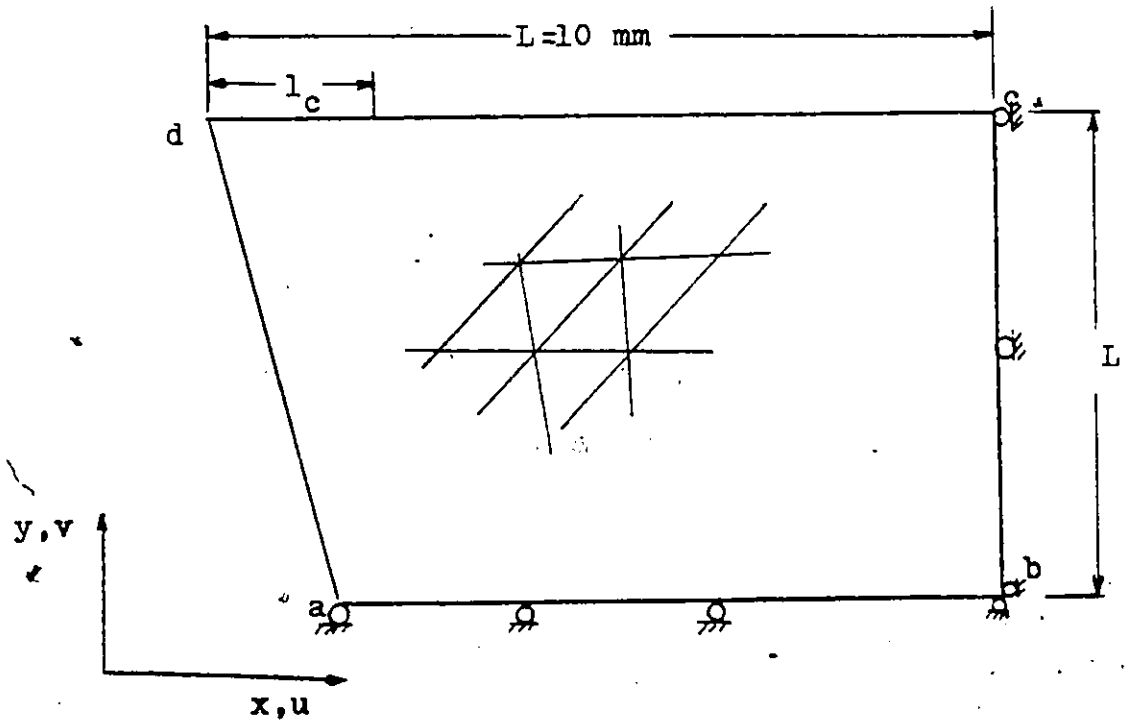

Fig. 6.1 The tool model for the stress computations.

$$v = 0 \qquad \text{along ab} \qquad (6.1b)$$

(b) Prescribed force boundary

In milling, the tool tooth is exposed to cutting forces when it engages in cutting. The cutting force cycling is shown schematically in Fig. 6.2. The cutting force, as discussed previously in Chapter 5, is a function of the instantaneous chip thickness. Thus, in up-milling, the cutting force increases gradually to a maximum at the end of the cutting period (Curve (a)). In down-milling, the cutting force starts at maximum and decreases gradually as cutting progresses (Curve (b)).

The instantaneous force distribution on the rake face of the tool is considered to be similar to the force distribution in continuous cutting. This is not a gross simplification. The forces' distributions are shown in Fig. 6.3 at different time instants in the cutting period. At any instant during cutting, the normal stress distribution on the tool rake face varies linearly, from a maximum value at the cutting edge to zero at the end of tool/chip contact. The shear stress is assumed to be uniformly distributed from the cutting edge to half the contact length ($\ell_c/2$), and decreasing linearly to the end of the tool/chip contact.

In order to combine the mechanical stresses with the thermal stresses, the loading sequence a, b, c, d (Fig. 6.3) is applied for up-milling, while the sequence d, c, b, a is applied for down-milling.

6.2 STRESS COMPUTATION

In general, the material within an element boundary on the tool body is subjected to thermal strain due to temperature changes. In the problem of stress solution, the thermal strains are treated as "initial

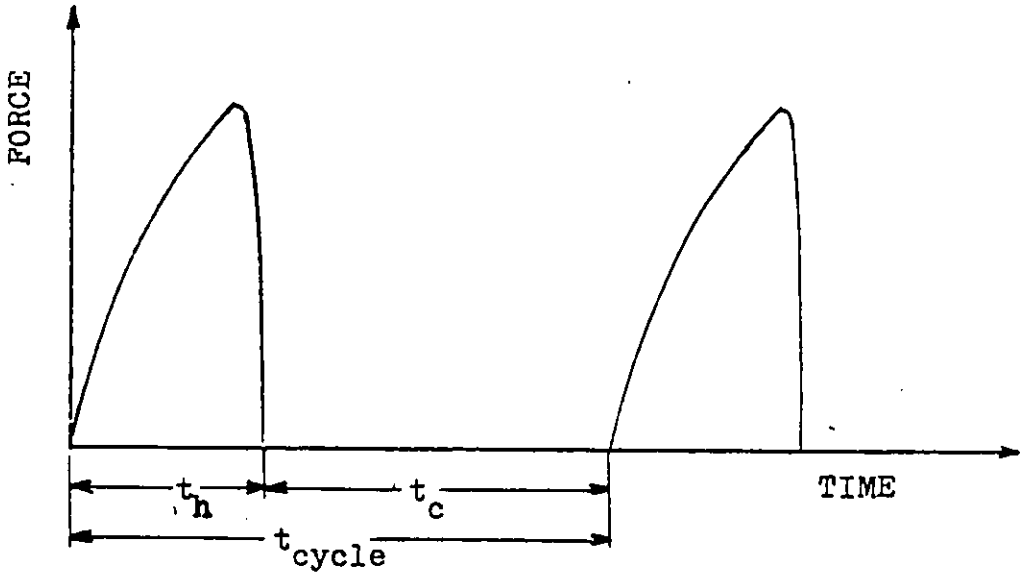

(a) Up-milling

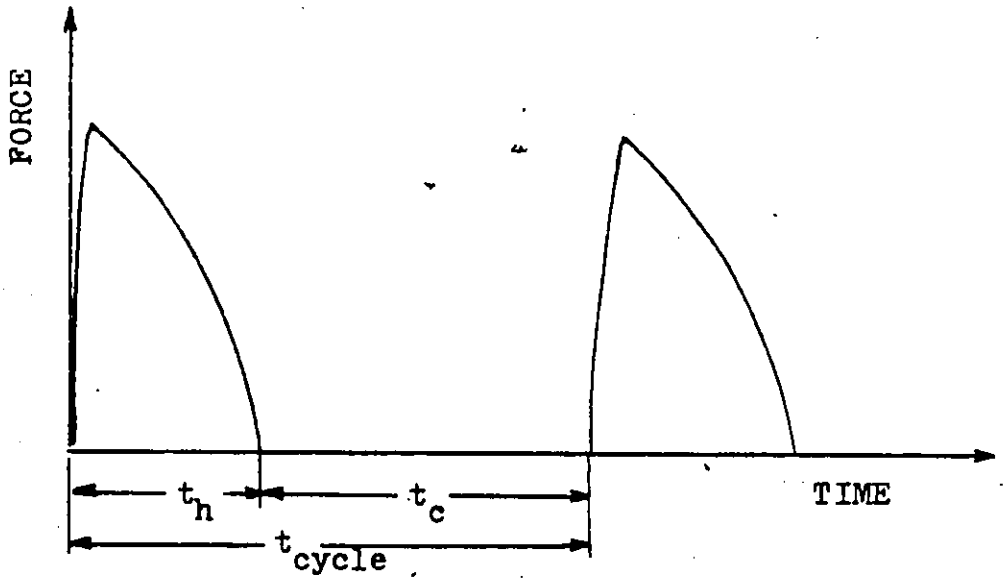

(b) Down-milling

Fig. 6.2 Cutting force cycle in milling.

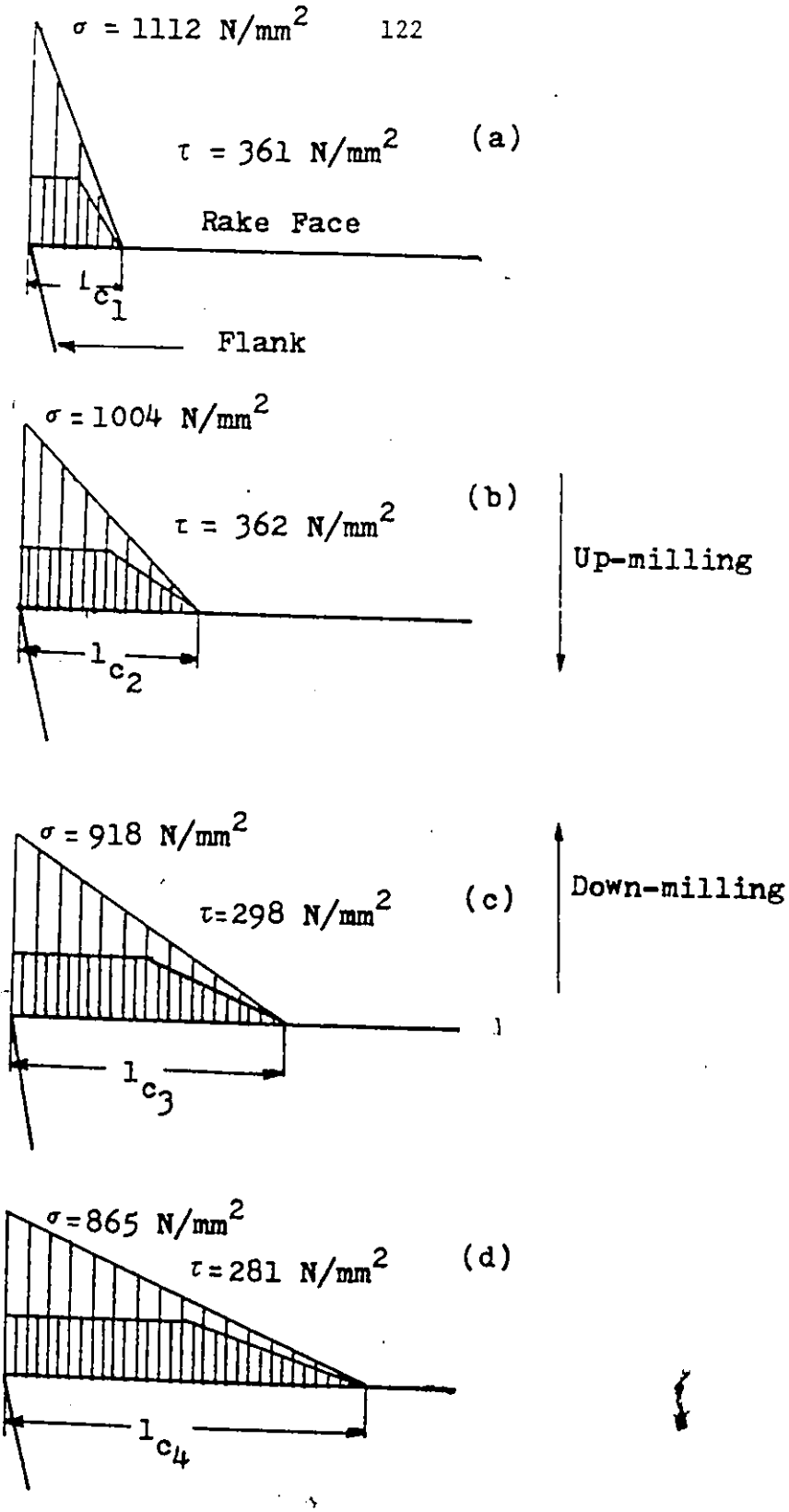

Fig. 6.3 Load distribution on tool tip at four time instants in the cutting period for half immersion, v = 40 m/min. and s_t = .1 mm.

strains" and denoted by $\{\varepsilon_o\}$. The stresses will be caused by the difference between the actual strain (due to mechanical loads) and the initial strain. Thus, assuming general linear elastic behaviour, the relationship between stresses and strains is linear. For two-dimensional plane strain, the relationship between stress and strain is of the form:

$$\{\sigma\} = [D]\ (\{\varepsilon\} - \{\varepsilon_o\}) \tag{6.2a}$$

and

$$\sigma_{zz} = \nu\ (\sigma_{xx} + \sigma_{yy}) - \alpha E\ (T_m - T_o) \tag{6.2b}$$

in which the stress vector $\{\sigma\}$ is defined as:

$$\{\sigma\} = \begin{Bmatrix} \sigma_{xx} \\ \sigma_{yy} \\ \tau_{xy} \end{Bmatrix} ,$$

the strain vector $\{\varepsilon\}$ is

$$\{\varepsilon\} = \begin{Bmatrix} \varepsilon_{xx} \\ \varepsilon_{yy} \\ \gamma_{xy} \end{Bmatrix} , \qquad \varepsilon_{zz} = 0 \quad ,$$

the initial strain vector $\{\varepsilon_o\}$, as no shear strains are caused by thermal dilation, is

$$\{\varepsilon_o\} = (1 + \nu) \begin{Bmatrix} \alpha(T_m - T_o) \\ \alpha(T_m - T_o) \\ 0 \end{Bmatrix}$$

and the elasticity matrix [D] is

$$[D] = \frac{E(1-\nu)}{(1+\nu)(1-2\nu)} \begin{bmatrix} 1 & \nu/1-\nu & 0 \\ \nu/1-\nu & & 0 \\ 0 & 0 & (1-2\nu)/2(1-\nu) \end{bmatrix}$$

where

E = modulus of elasticity,

ν = Poisson's ratio,

α = coefficient of thermal expansion,

T_m = mean temperature of the element, and

T_o = reference temperature at which the body is stress free.

The finite element formulation procedure for the plane elasticity problem in Zeinkiewicz's book[49] has been closely followed. Based on this formulation, a finite element program has been developed for the constant strain triangular element, i.e. the displacement is assumed linearly distributed over the element. The finite element formulation, and the block diagram describing the program are given in Appendices A and B, respectively. The program can be used to find the solution for the plane strain and plane stress problems. It is designed to compute the mechanical stresses only, the thermal stresses only, and the combined mechanical-thermal stresses.

The computation procedure starts with the selection of the number of iterations in a cutting cycle sufficient to represent the stress cycling. The instantaneous stresses at each iteration are then computed after reading the temperature file and the mechanical loads. The temperature files were written previously by the heat transfer program.

For the purpose of this study the thermal stresses have been computed for all the cutting conditions in Table 5.3. The mechanical stresses have been combined with the associated thermal stresses for only two cutting conditions for comparison purposes. A summary of the computed results is given in the next Section.

6.3 SUMMARY OF THE COMPUTED RESULTS

The following results are typical for all cases computed. The cases selected for this purpose are half immersion up- and down-milling with a 25 mm diameter H.S.S. cutter. The cutting speed and feed were $v = 40$ m/min and $s_t = .1$ mm/tooth, respectively. Consequently, the heating period is 30 msec, and the cooling period is 90 msec. The properties of the tool material were: modulus of elasticity $E = 20.7 \times 10^4$ N/mm^2, Poisson's ratio $\nu = .28$ and coefficient of thermal expansion $\alpha = 1.44 \times 10^{-5}$ mm/mm°C.

6.3.1 Maximum Normal Stress (σ_1)

Selected stress contours for the maximum normal thermal and combined mechanical-thermal stresses are shown in Fig. 6.4 at time instants in the fourth cutting cycle. Diagrams a), b) and c) are for the thermal stresses during the heating and cooling periods. Diagrams d) and e) are for the combined thermal-mechanical stresses.

In diagram a) and b), which are for two time instants in the heating period, the maximum normal stresses are tensile inside the tool and compressive at the tool faces (flank and rake faces). The maximum tensile stress occurs at 5 msec (diagram a) from the start of the heating period. The maximum tensile stress of over 95 N/mm^2 is found inside the tool wedge about 0.4 mm from the tool rake face. In diagrams d) and e), the combined mechanical and thermal stresses at the same time instants show that the tensile stress still exists in the same area but is reduced to about 70 N/mm^2. Furthermore, tensile stresses appear in the tool shank which can be attributed to the mechanical loads.

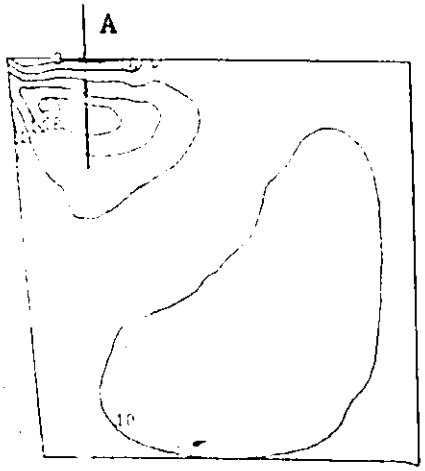

(a) Thermal stress for t_h = 5 msec.

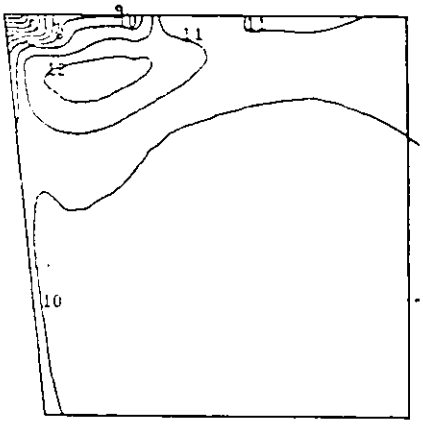

(d) Thermal/Mechanical stresses for t_h = 5 msec.

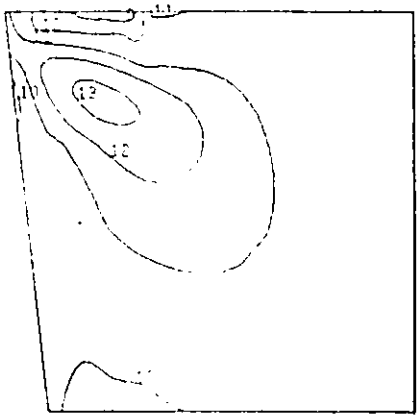

(b) Thermal stress for t_h = 16 msec.

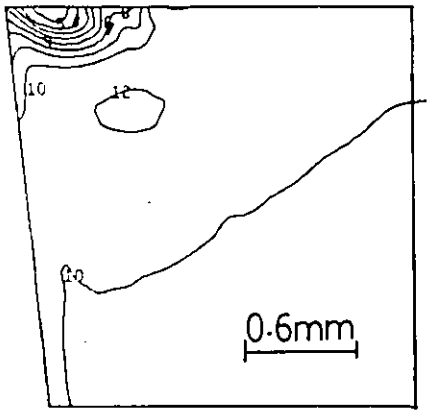

(e) Thermal/Mechanical stresses for t_h = 16 msec.

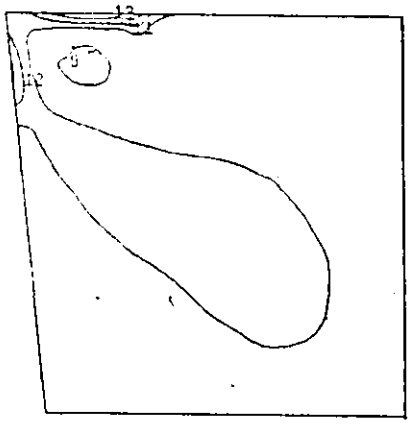

(c) Thermal stress for t_c = 4 msec.

Key: Contour	N/mm^2
8	-50
9	-25
10	0
11	25
12	50
.	.
.	.

Fig. 6.4 Normal stress contours for thermal and thermal/mechanical stresses in up-milling.

Diagram c) is the stress contours at 4 msec into the cooling period. The tensile stress has developed on the rake face and the maximum value is approximately 100 N/mm^2 at a distance of 0.6 mm from the cutting edge. Also, tensile stress has developed on the flank as well, and the maximum value is approximately 75 N/mm^2 at a distance of 0.3 mm from the cutting edge.

More details about these stresses are given in Figs. 6.5, 6.6, and 6.7. The stress profiles at various instants of heating and cooling periods are given along selected lines on the tool wedge area. Figure 6.5 corresponds to a section through the tool wedge along line A in graph a) of Fig. 6.4. Graphs a) and b) are for the thermal stress profiles at various instants of the heating and cooling periods, respectively. Graph c) is for the combined thermal and mechanical stress profiles at the same time instants in the heating period. The maximum tensile stress reached is $\sigma_1 = 95\ N/mm^2$ due to thermal effect (graph a)), and when the mechanical stress is combined it decreased to approximately $\sigma_1 = 70\ N/mm^2$ (graph c)). In the cooling period (graph b)), it reached only 50 N/mm^2.

Although the tensile stresses developed inside the tool appear to be low, but it could be serious if the material is inhomogeneous such as sintered carbide tools. This observation could be very useful in explaining the development of some kinds of cracks which appear with carbide tools. Okushima and Hoshi[1,2,5], in their studies of the cracking of carbide tools in face milling carbon steel, observed the formation of submerged cracks underneath the tool rake face. The development of this tensile stress in a non-homogeneous tool material,

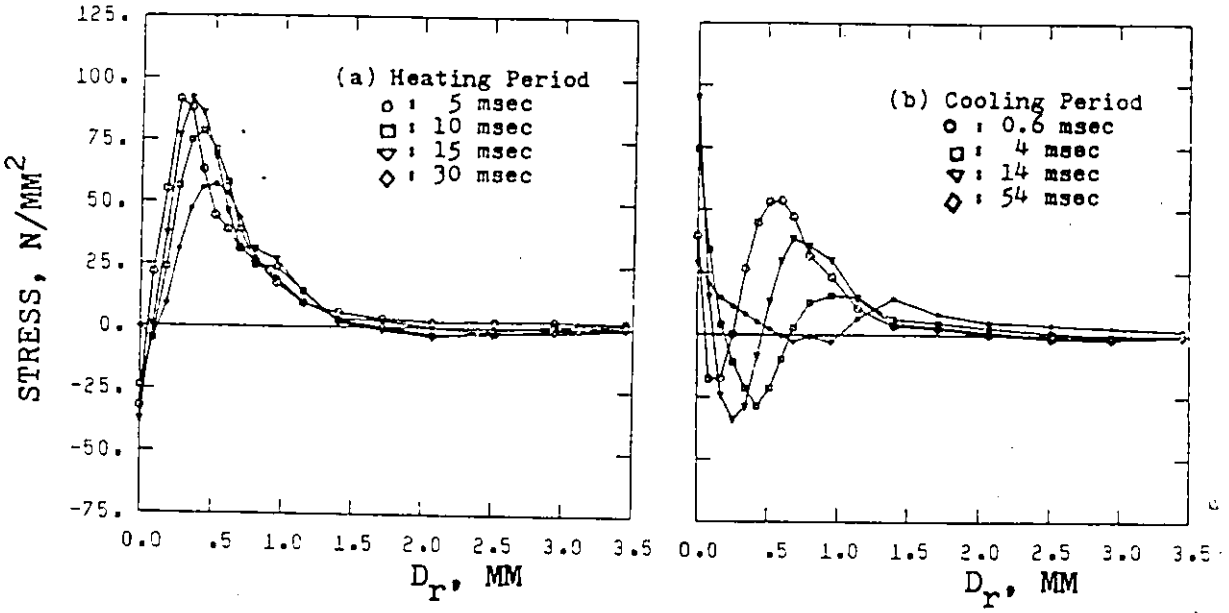

(a) Thermal.

(b) Thermal.

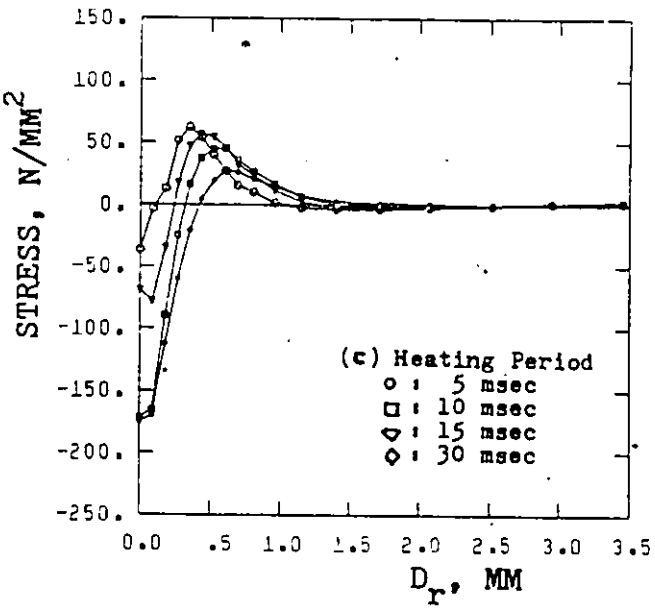

(c) Thermal/Mechanical.

Fig. 6.5 Maximum normal stress distribution on section 'A' for a cutting cycle of a half immersion up-milling.

D_r is the distance from the rake face.

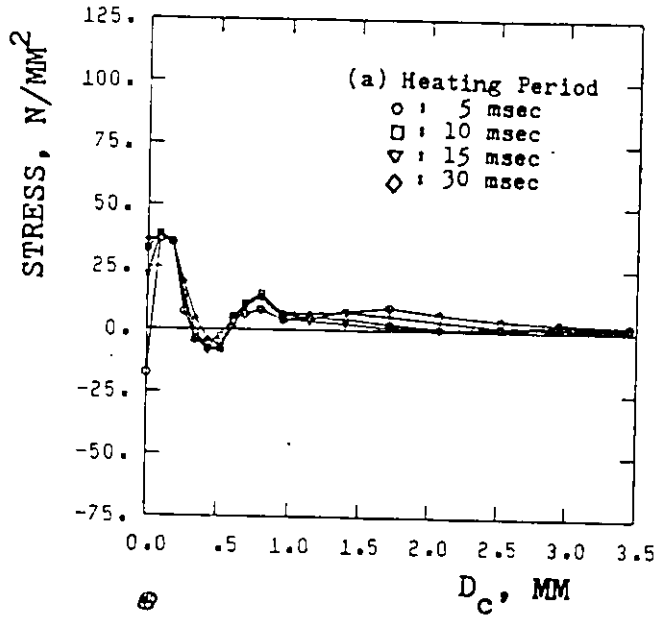

(a) Thermal.

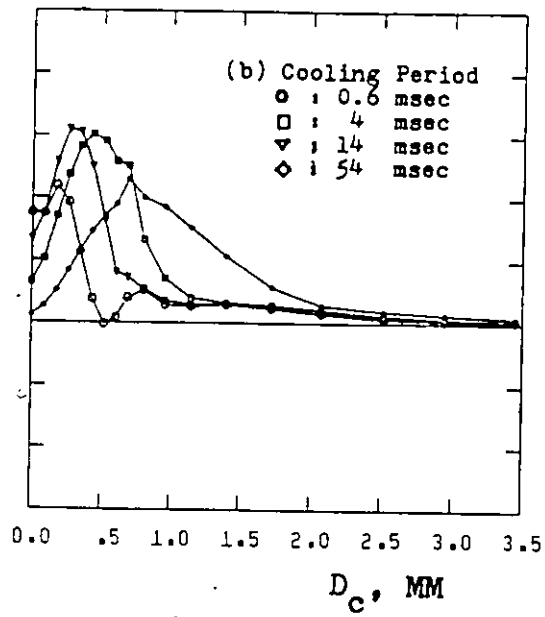

(b) Thermal.

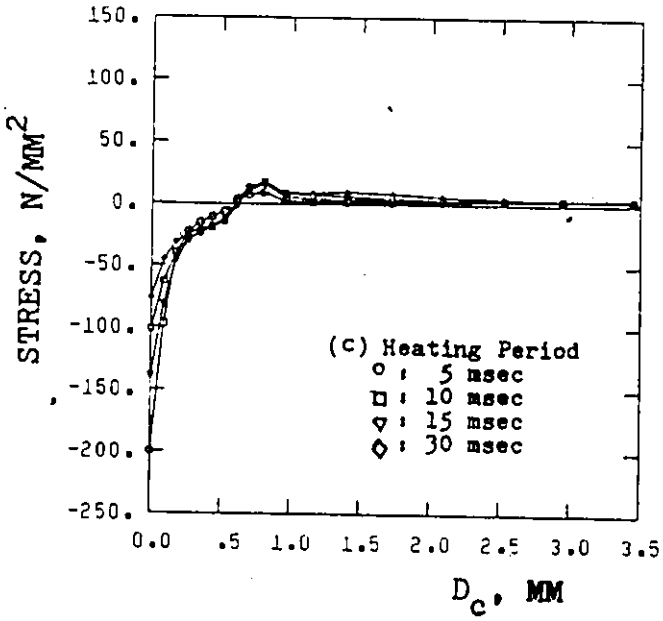

(c) Thermal/Mechanical.

Fig. 6.6 Maximum normal stress distribution on tool flank for a cutting cycle of a half immersion up-milling.

D_c is the distance from the cutting edge.

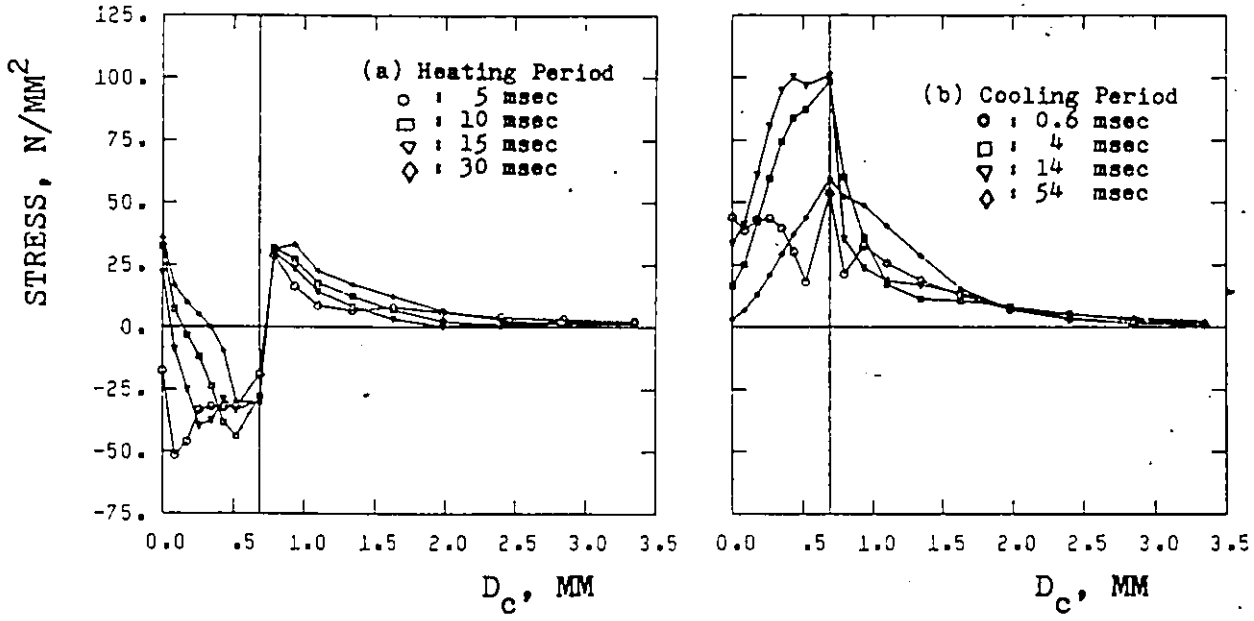

(a) Thermal. (b) Thermal.

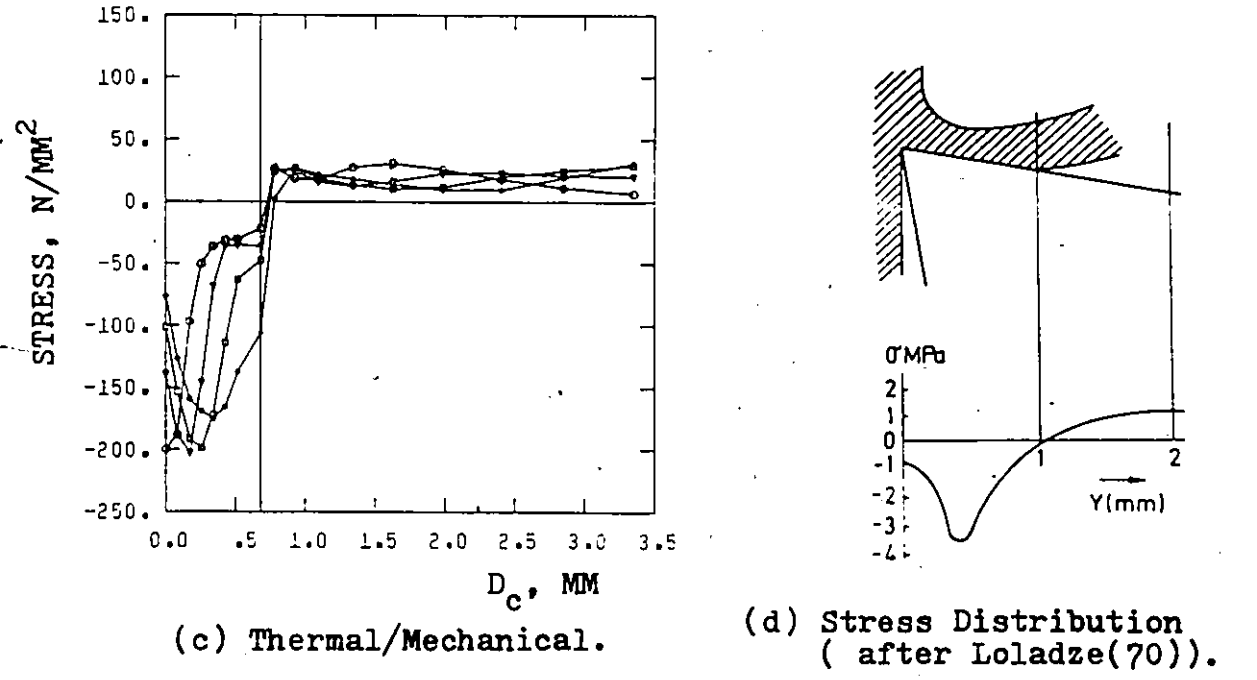

(c) Thermal/Mechanical. (d) Stress Distribution (after Loladze(70)).

Fig. 6.7 Maximum normal stress distribution on the rake face for a cutting cycle of a half immersion up-milling.

D_c is the distance from the cutting edge.

such as sintered carbide or ceramics, could cause the formation of such kind of cracks.

The maximum normal stress profiles on the flank face are shown in Fig. 6.6 for time instants in a cutting cycle. During the heating period, the thermal stresses only (graph a)) are tensile at the cutting edge. After combining the mechanical loads the flank face, up to .5 mm, is under compressive stress of $\sigma_1 = -200$ N/mm^2 at 5 msec in the cutting period. In the cooling period (graph b)), the stresses are tensile and the maximum stress is 75 N/mm^2.

In Figs. 6.7 a) and b), the thermal stress profiles on the rake face are given at time instants in the heating and cooling periods. The maximum tensile stress on the rake face is $\sigma_1 = 100$ N/mm^2 in the cooling period. In graph c) the profiles of the combined mechanical/thermal stresses are given. It is seen that the tool/chip interface area is under compressive stress and the shank is under tensile stress. The stress profile shown in graph c) is in agreement with the photoelasticity analysis results shown in graph d). The photoelasticity analysis was conducted by Loladze[70] who used plastic tools to cut lead, and applied photoelasticity analysis to determine the stress distribution in the tool wedge. He found that tensile stresses were developed at distances from the cutting edge greater than the tool/chip interface contact length. The maximum tensile value is at about twice the contact length. Comparing graphs a) and c), we find that the tensile stress on the tool shank is mainly due to the mechanical load. Hence the tool breakage may be related to mechanical stresses rather than thermal stresses.

Finally, it can be detected that there are tensile stresses developed during the heating period inside the tool and during the cooling period in the tool faces, and all are in the vicinity of the cutting edge. The maximum tensile stress of about $\sigma = 105\ N/mm^2$ arose in the cooling period on the tool rake face. It should be noted that the cutting speed and feed are fairly low.

6.3.2 Stresses in the z-Direction (σ_{zz})

The stresses in the z-direction (σ_{zz}) are the stresses on the plane perpendicular to the cutting edge. The stress in this direction is called the minimum normal stress since $\sigma_{zz} < \sigma_2 < \sigma_1$. In Fig. 6.8, selected stress contours for the thermal stresses in z-direction are given at time instants in a cutting cycle. It is seen that thermal stresses in this direction are always negative, i.e. compressive. In the vicinity of the cutting edge high compressive stress has developed during the cutting period, and its maximum value was reached at the end of the heating period. In the cooling period, the compressive stress decreases rapidly with cooling and reached a very low value at the end of the cycle. This means that the compressive stress is fluctuating in a wide range, and a high alternating stress is developed due to heating and cooling.

More details about σ_{zz} on the rake face and the flank are shown in Fig. 6.9 and Fig. 6.10, respectively. It is seen that the cutting edge region is exposed to high compressive stress, and its maximum value reached at a point on the rake where the maximum temperature almost occurs. Figures 6.9 a) and 6.9 c) are for the thermal and thermal/mechanical

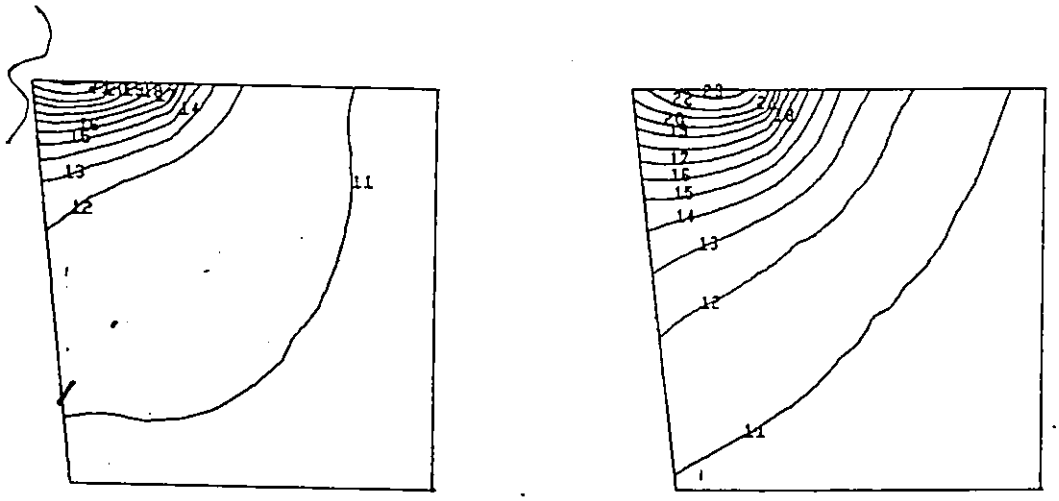

(a) $t_h = 10$ msec

(b) $t_h = 30$ msec

(c) $t_c = 4$ msec

(d) $t_c = 54$ msec

Fig. 6.8 Minimum normal stress fields for a cutting cycle of a half immersion up-milling.

Key to contours:

Contour	8	9	10	11	12 .....
σ_{zz} N/mm^2	200	100	0	-100	-200

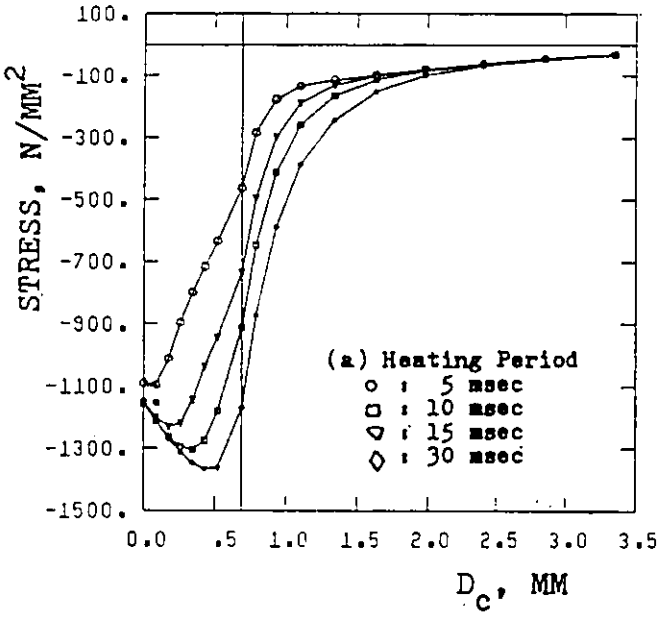

(a) Thermal.

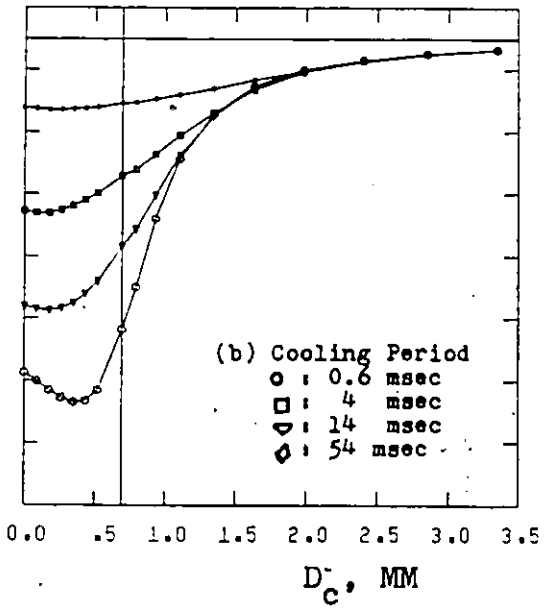

(b) Thermal.

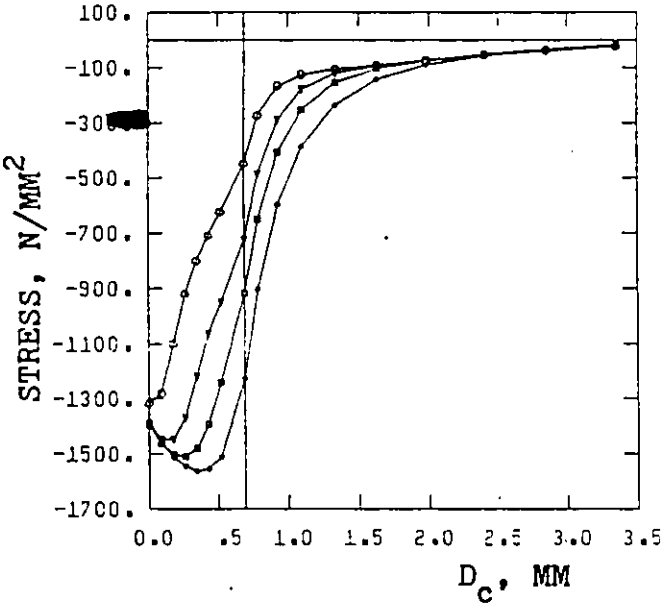

(c) Thermal/Mechanical.

Fig. 6.9 Minimum normal stress distribution on the rake face for a cutting cycle of a half immersion up-milling.

D_c is the distance from the cutting edge.

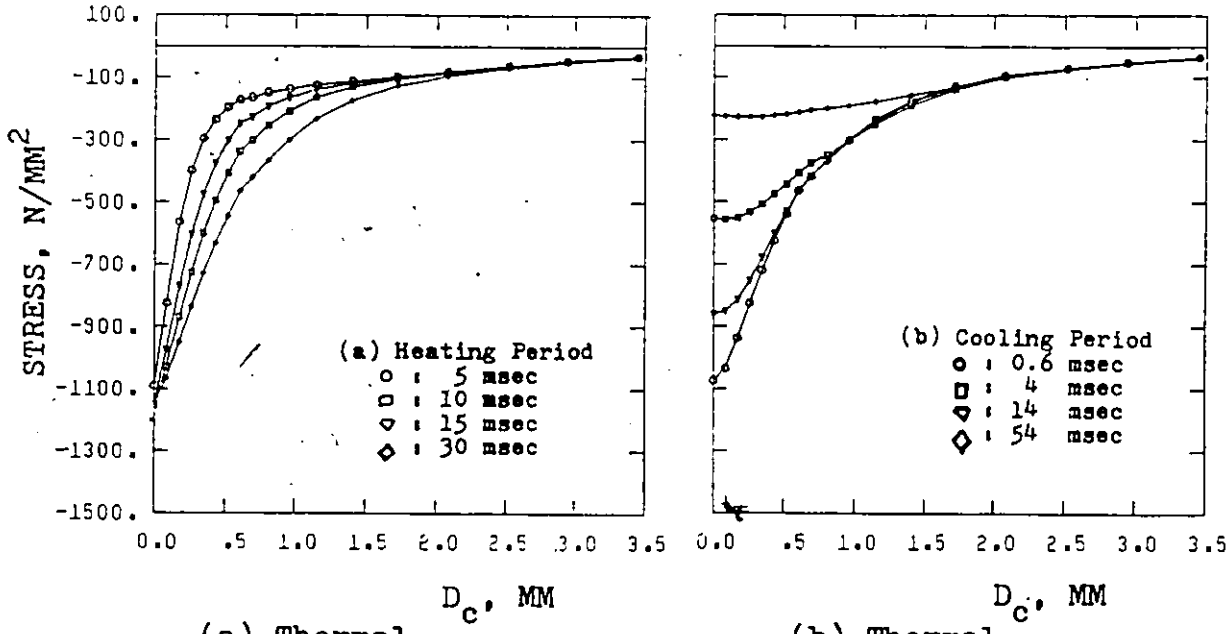

(a) Thermal. (b) Thermal.

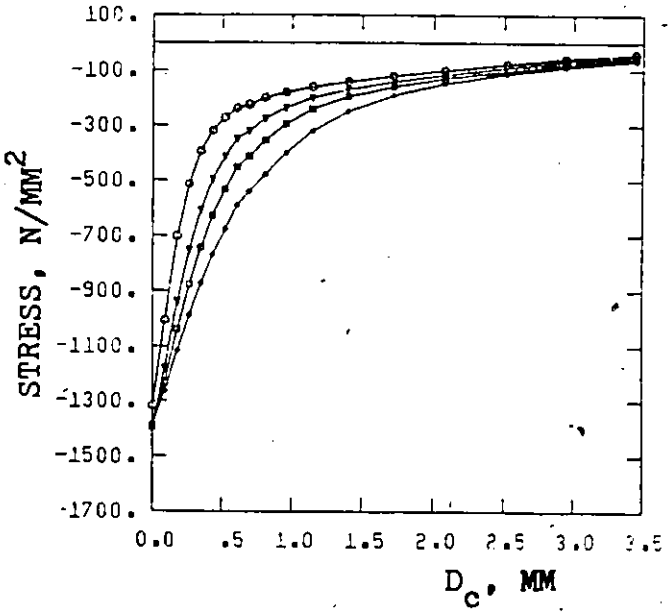

(c) Thermal/Mechanical.

Fig. 6.10 Minimum normal stress distribution on tool flank for a cutting cycle of a half immersion up-milling.

D_c is the distance from the cutting edge.

combined stress, respectively. The maximum thermal compressive stress reached is $\sigma_{zz} = -1400$ N/mm^2, while the maximum combined mechanical and thermal stress is $\sigma_{zz} = -1600$ N/mm^2. Hence, the contribution of the mechanical load is very little (12%) compared to the thermal load.

6.3.3 Maximum Shear Stress (τ_{max})

The maximum shear stress is defined by the relationship:

$$\tau_{max} = \frac{1}{2} (\sigma_1 - \sigma_3)$$

where

σ_1 is the maximum normal stress, and

σ_3 is the minimum normal stress (σ_{zz}).

The maximum shear stress contours at selected time instants in a cutting cycle is shown in Fig. 6.11. The contours shown are for the thermal stresses only. Observe that the highest values of τ_{max} are concentrated on the tool/chip interface area. Clearly, this is due to the combination of the maximum normal stress (σ_1) and the minimum normal stress (σ_{zz}). This means that the maximum shearing stresses occur in a plane parallel to the cutting edge.

More details of the maximum shear stress on the tool rake face are shown in Fig. 6.12. Graphs a) and b) present the thermal stress profiles on the tool rake face at time instants in the heating and cooling periods. The maximum of τ_{max} occurs at the end of the heating period inside the tool/chip interface area. The maximum stress is of the order of 700 N/mm^2. Graph c) is the shear stress profiles for the combined thermal-mechanical stresses on the rake face. The combined

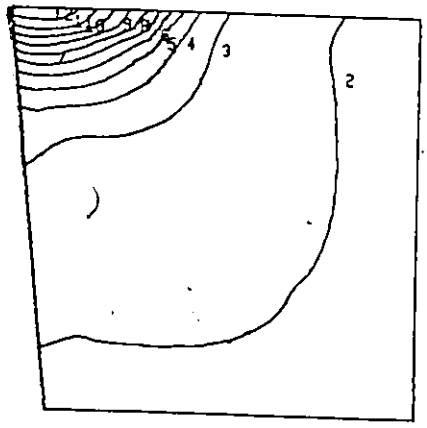

(a) t_h = 10 msec

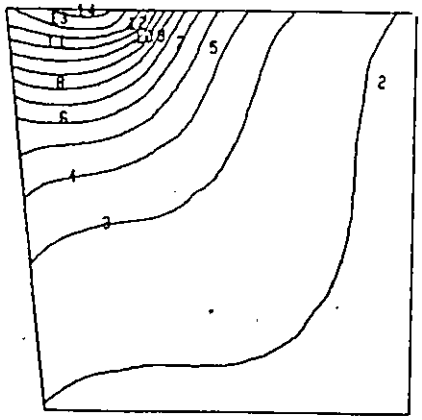

(b) t_h = 30 msec

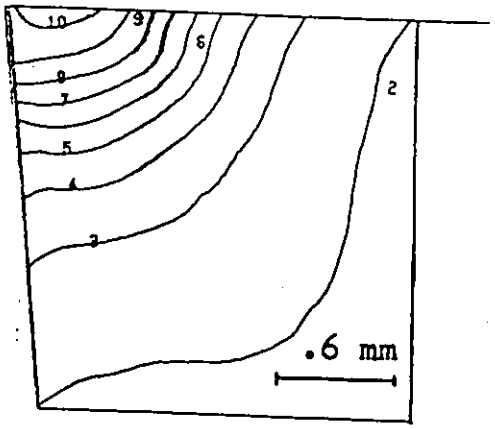

(c) t_c = 4 msec

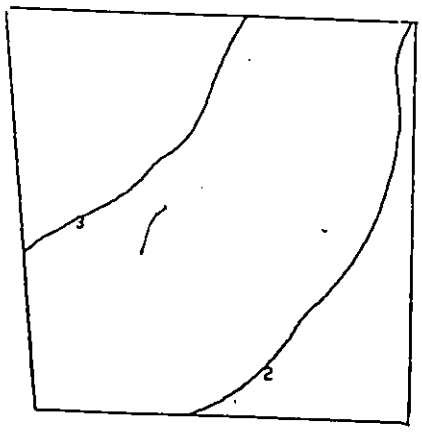

(d) t_c = 54 msec

Fig. 6.11 Maximum shear stress fields for a cutting cycle of a half immersion up-milling.

Key to contours:

Contour	1	2,	3	4	5 ...
τ_{max} N/mm^2	0.0	50	100	150	200

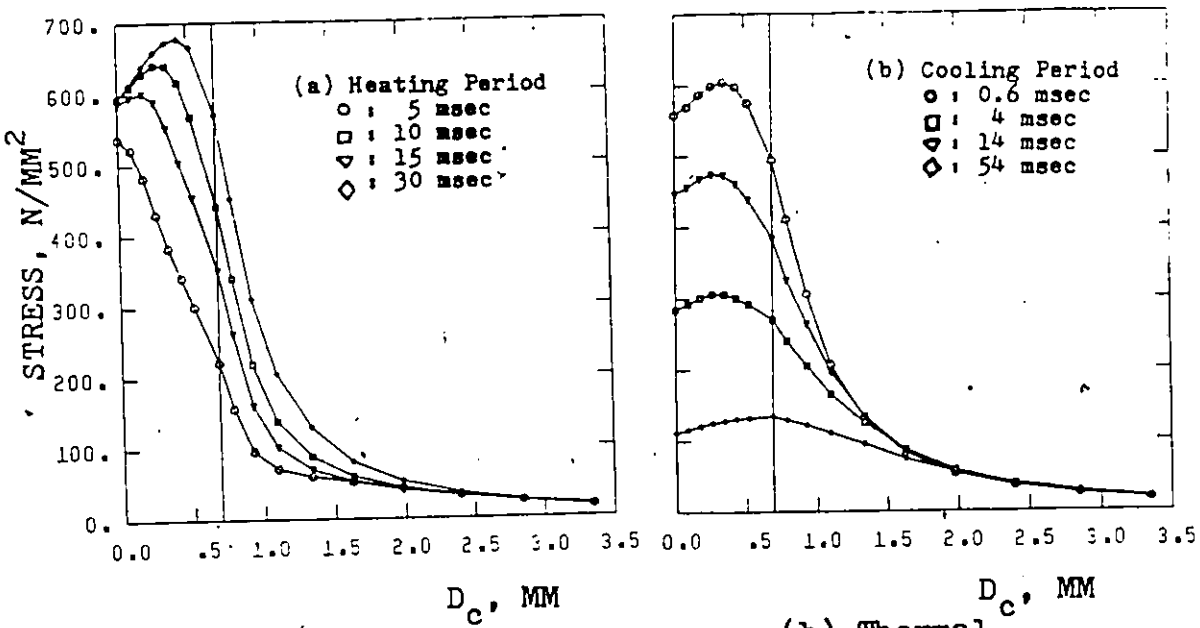

(a) Thermal. (b) Thermal.

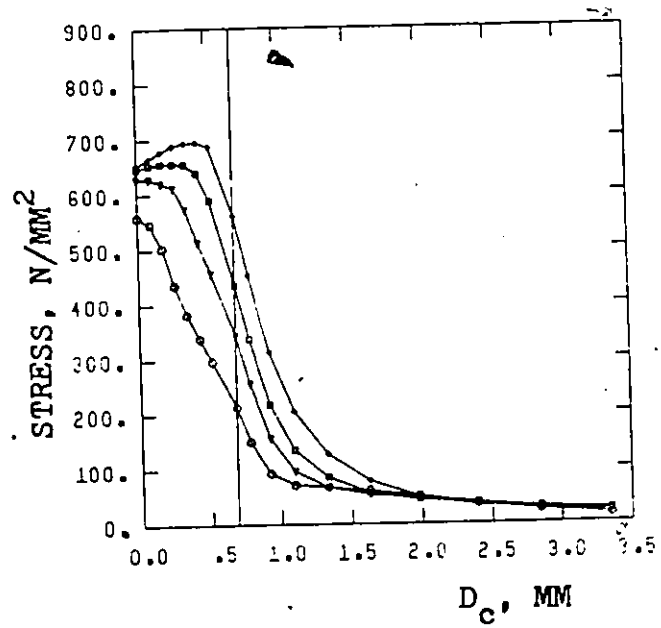

(c) Thermal/Mechanical.

Fig. 6.12 Maximum shear stress distribution on the rake face for a cutting cycle of a half immersion up-milling.

D_c is the distance from the cutting edge.

shear stress is slightly increased, and it is of the order of τ_{max} = 750 N/mm^2. Again, it is seen that the mechanical load contribution is very small compared to the thermal load.

6.3.4 Analysis of the Stress in Down-Milling

In down-milling, the stresses induced are found to be more or less similar to the ones in the case of up-milling with the same cutting speed and feed. The only difference is the instant of occurrence. The maximum stresses in up-milling normally occur at the end of the heating period. But, in down-milling, the maximum stresses occur at time instants in the heating period.

For comparison purposes Fig. 6.13 and Fig. 6.14, which illustrate stress profiles for the combined thermal-mechanical stresses at time instants in the heating period, are provided. Figure 6.13 shows the maximum normal stress profiles along the rake face and the line A in Fig. 6.4 a). Comparing Fig. 6.13 a) and Fig. 6.7 c), it is seen that the maximum normal stress in the case of down-milling is more compressive, and the maximum value occurs at time instant t = 10 msec early in the cutting period. In Fig. 6.13 b), the tensile stress inside the tool is of the same order as with up-milling (see Fig. 6.5 c)).

Figure 6.14 presents the stress profiles along the rake face where graph a) shows σ_{zz} profiles and graph b) shows τ_{max} profiles. The maximum values of these stresses occur at time instant t = 17 msec in the heating period, while with up-milling the maximum values of both σ_{zz} and τ_{max} occur at the end of the heating period (see Figs. 6.9 c) and 6.12 c)). The maximum values of σ_{zz} and τ_{max} in down-milling are slightly lower

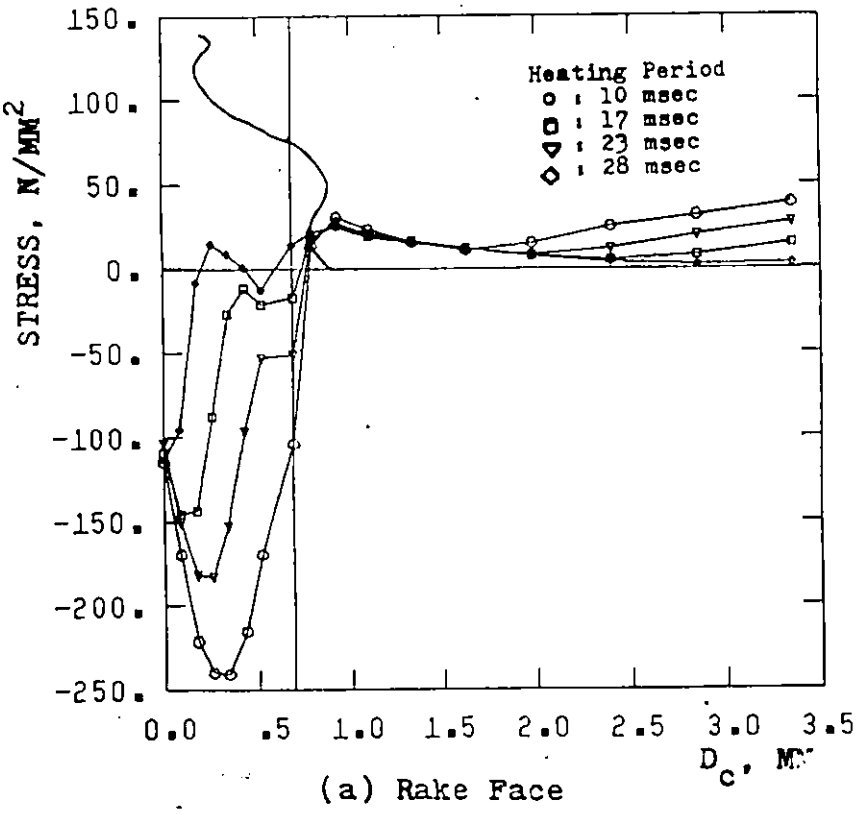

(a) Rake Face

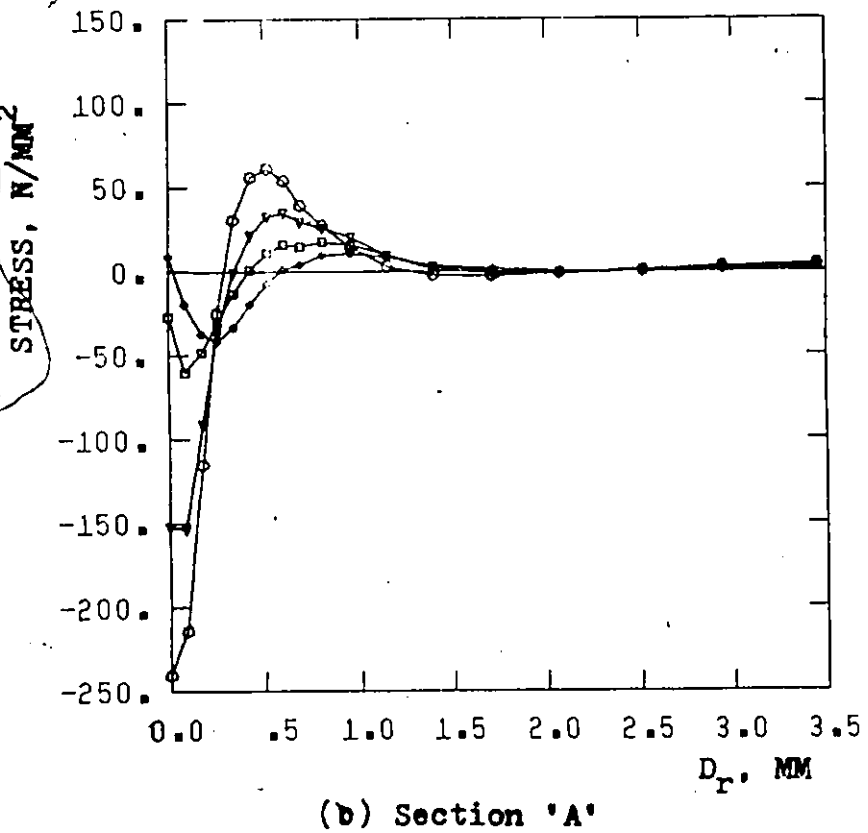

(b) Section 'A'

Fig. 6.13 Maximum normal thermal/mechanicl stress distribution for the heating period of a half immersion down-milling.

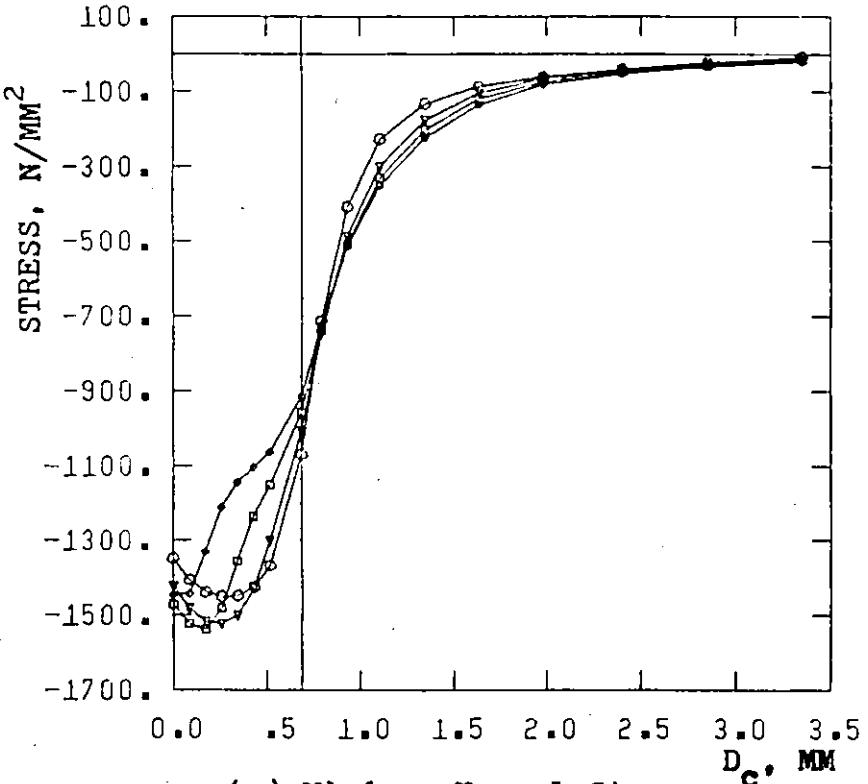

(a) Minimum Normal Stress

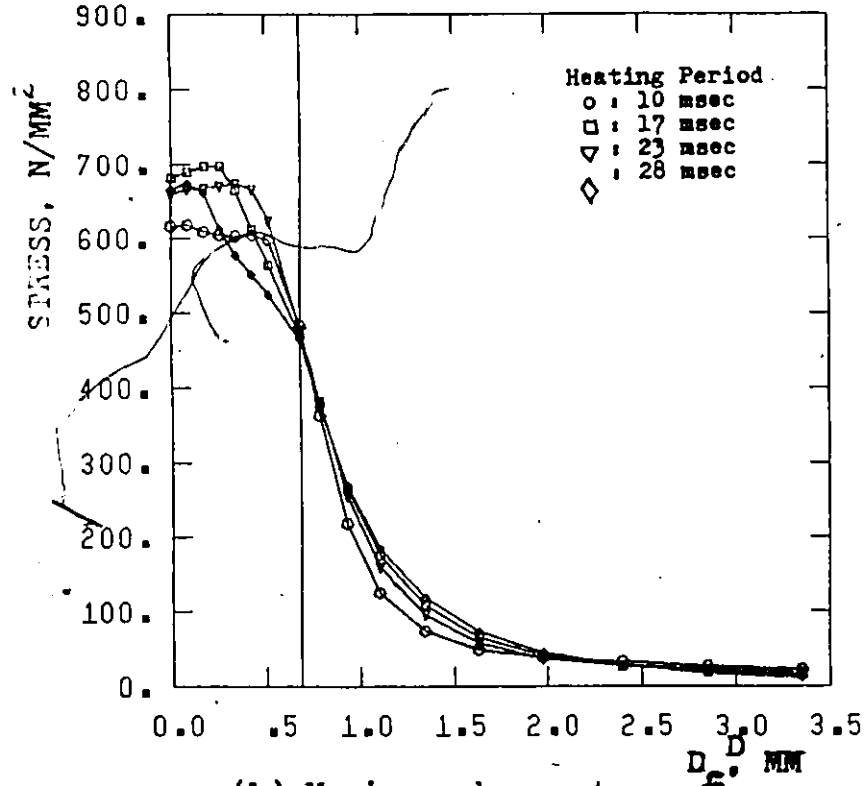

(b) Maximum shear stress.

Fig. 6.14 Thermal/mechanical stress distribution on the rake face for the heating period of a half immersion down-milling.

than in up-milling). The difference is about 100 N/mm^2 and 50 N/mm^2 in σ_{zz} and τ_{max}, respectively.

6.4 DISCUSSION AND CONCLUSIONS

Tensile stresses are developed in the vicinity of the cutting edge during both the heating and the cooling periods. Those developed during the cutting period occur inside the tool about 0.4 mm under the tool/chip interface area. These tensile stresses could be very important in analyzing the occurrence of submerged cracks in carbide tools. The tensile stresses induced during the cooling period occurred on both the rake and the flank close to the cutting edge. These stresses could be the reason for the formation of a kind of microcracks which might accelerate the tool wear on the flank and rake faces.

The tool wedge is also exposed to compressive stresses on the plane perpendicular to the cutting edge. The maximum compressive stresses occurred on the rake face at the tool/chip interface contact area. On this position, the crater wear, and the comb and cross cracks usually occur. The maximum stress developed is about $\sigma_{zz} = -1700\ N/mm^2$ which is much less than the yield strength of the H.S.S. However, with carbide, where the temperature is much higher and the product of the modulus of elasticity (E) and the coefficient of thermal expansion (α) is also much higher ($E\alpha$/carbide:$E\alpha$/H.S.S. = 2:1) and considering the inhomogeneity of the material, these compressive stresses may exceed the yield strength of the material.

Even with H.S.S., the compressive stress could help in the wear of the cutting tools where it fluctuates in a very wide range. Thus,

the cutting edge is exposed to fatigue. Similarly, the highest shear stress usually occurs on the tool cutting edge region.

In the previous analysis, it is found that the mechanical loads contribution is very small compared to the thermal load (10-12%) for these particular cutting conditions. Thus, the tool wear or cracking which occur after repeated number of cycles may not be related to the mechanical loads, i.e. cutting forces. Therefore, for comparison reasons, the thermal stresses could only be considered.

Based on the foregoing analysis, we deduce that the following parameters might affect the rate of flank wear in peripheral milling:

a) Tensile stresses on the tool flank.

b) Maximum shear stress.

c) Maximum range of compressive stresses.

The study of the influence of these parameters on the tool wear in peripheral milling is the subject of the next chapter.

CHAPTER 7

INFLUENCE OF THERMAL CYCLING ON TOOL LIFE IN PERIPHERAL MILLING

In the preceding two Chapters, the results of the thermal cycling computation were presented. These results can be used to try to explain various experimentally determined characteristics of tool wear, cracking and breakage in milling. In this Chapter, we are aiming at correlating the aforementioned results with the tool life tests conducted mostly by Yellowley and Barrow[12], and partly by the author. These tests concentrated on the flank wear of both high speed steel and sintered carbide milling cutters. The experimental results led to the conclusion that the cutting time ratio has a strong effect on the tool life.

7.1 EXPERIMENTAL WORK

In a rather large experimental program, Barrow and Yellowley conducted milling tests for full immersion (slotting) and half-immersion up- and down-cut operations[12]. The tool materials were H.S.S. grades M2 and T1, and several grades of sintered carbides, i.e., most of the existing tool materials. Workpiece materials were, in British standard, En 28 (equivalent to AISI 4140), En 30B (AISI E9310), and IMI 550 (titanium base alloy). The chemical compositions of these materials are given in Table 7.1.

Several cutting tests were performed with different cutting conditions; speed range 11-140 m/min, feed per tooth (s_t) range .05-.125

TABLE 7.1 Chemical Composition and Properties of Workpiece Materials

Work Material	Nominal Chemical Composition											Condition and Approx. Hardness BHN
	C	Fe	Ni	Cr	Mo	P	Aℓ	Ti	Mn	Si	Sn	
En 28	.3	Bal	3.5	1.25	0.4					.2		Hard and Temp (280)
En 30B	.3	Bal	4.1	1.3	.3				.5	.2		Hard and Temp (431 and 486)
IMI 550					4.0		4.1	Bal		.58	1.86	Soak, air cool, age (360)
SPS	0.4	Bal	1.25	0.6	.15	.02			0.75			Annealed (202)

mm. The cutters were end mills with 25 and 32 mm diameters. The tool life was based on flank wear as a mode of failure. The results of these tests are presented in Fig. 7.1 in which "active" tool life is shown. The "active" tool life (t_{ac}) is the actual cutting time which is defined as:

$$t_{ac} = (\phi_c/360) \times t \qquad (7.1)$$

where t is the total elapsed time to cause flank wear of V_B = .015 inches, and ϕ_c is the angle of immersion. Thus the active tool life is 0.25 t for half immersion, and 0.5 t for slotting.

Figure 7.2 shows the results of two sets of tests conducted by the author. The tool material was H.S.S. grade M2 and work material was SPS alloy steel (equivalent to AISI 4140) in the annealing condition. The properties of SPS are given in Table 7.1. The two sets of experiments were conducted using two flywheel cutters. Each cutter has a slot on the periphery to hold a 10 mm turning tool. The cutters' diameters were 65.5 mm and 127 mm. The cutting speed, feed and depth of cut were: v = 45 m/min, S_t = .113 mm, and d = 1.5 mm, respectively.

7.2 DISCUSSION OF THE EXPERIMENTAL RESULTS

The features of the experimental data, shown in Fig. 7.1 and Fig. 7.2, can be summarized as follows:

a) The most significant feature of the data is the large increase in the active tool life which occurred when going from half immersion to slotting. The tool life is more than doubled, i.e. in slotting twice as much metal is

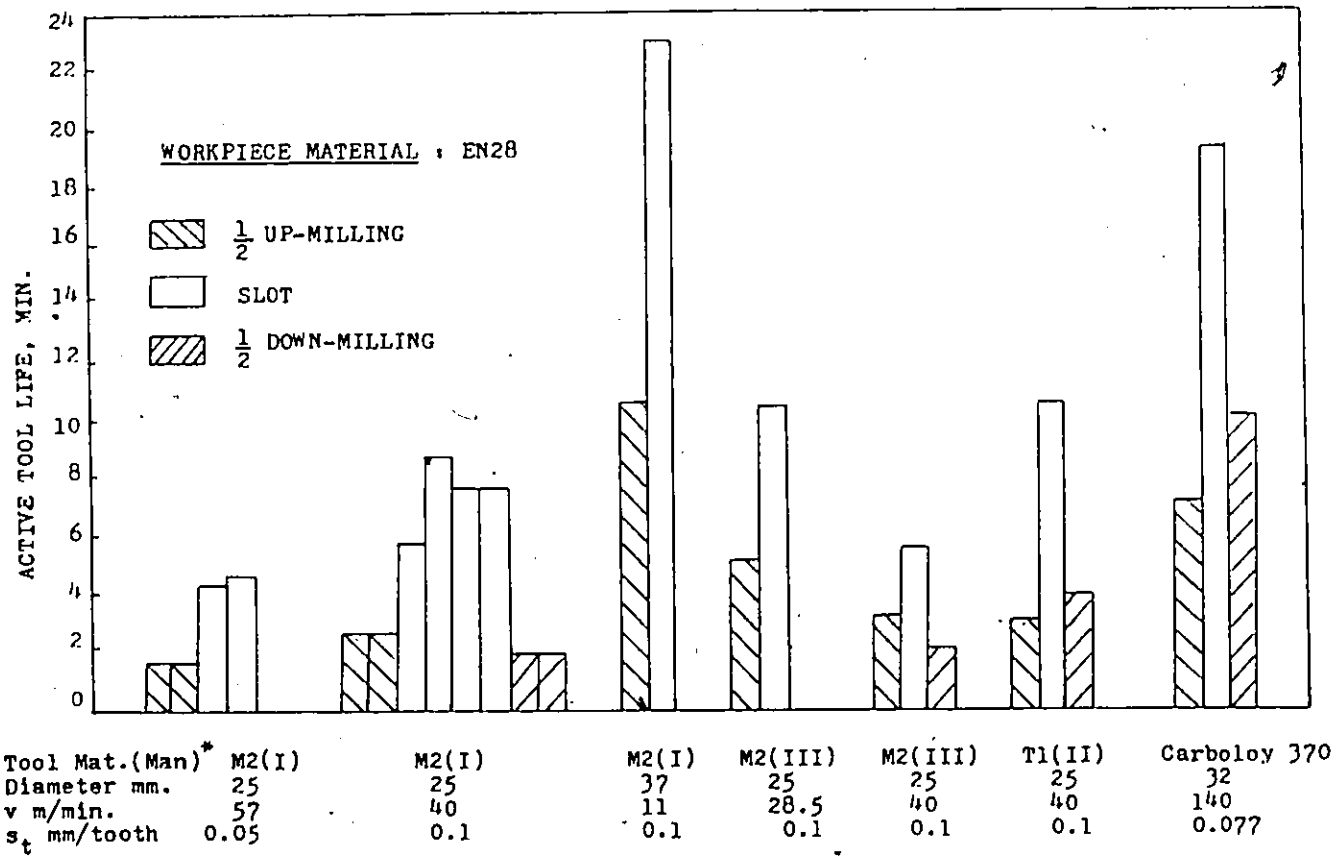

Fig. 7.1 Comparison of active tool life for half and full immersion.

* Mat.(Man.): Material (Manufacturer)

Continued Fig. 7.1

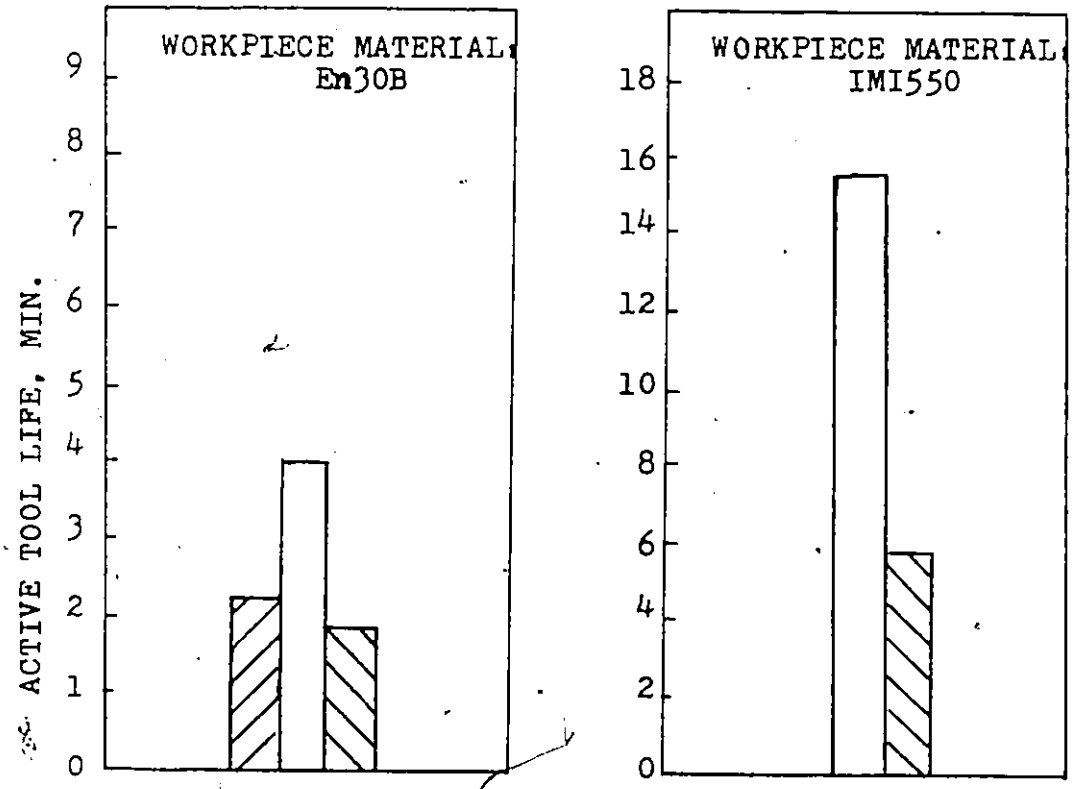

Tool Mat.(Man.)	M2(I)	Carboloy 883
Diameter mm.	25	32
v m/min.	18	50
s_t mm/tooth	0.125	0.09

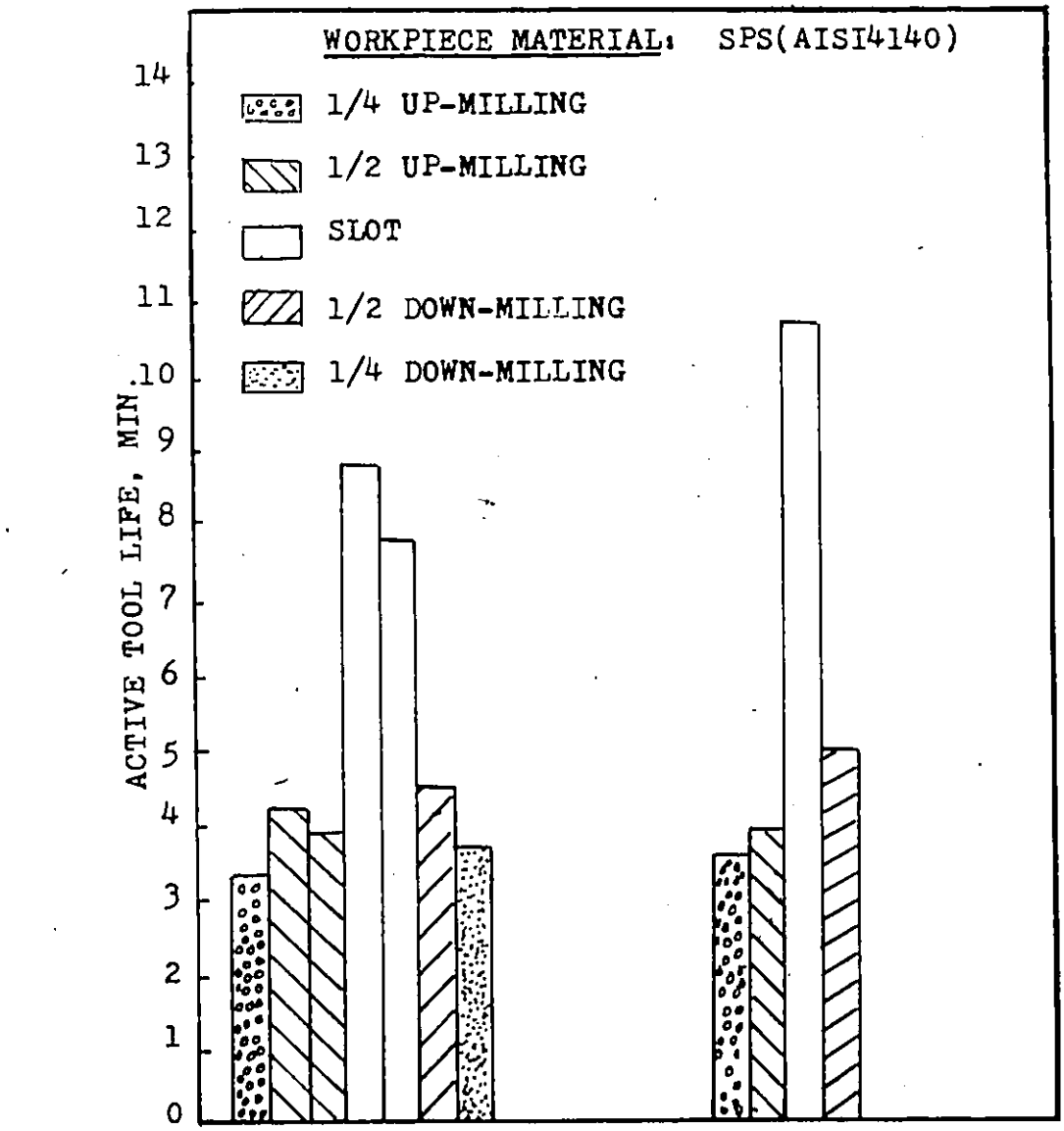

Fig. 7.2 Comparison of active tool life for quarter, half and full immersion.

removed per tool life, as in half immersion both up- and down-milling operations.

b) Another feature is that there is no substantial difference in tool life between up- and down-milling.

The substantial difference in tool life between half immersion and slotting could be attributed to either thermal or mechanical influences. The mechanical influence may be due to unfavourable entry and exit conditions in the cases of up- and down-milling, respectively, which is not in the case of slotting. Many authors have concentrated on tool chipping and breakage and found the exit conditions, i.e., up-milling, most detrimental[16]. Other investigators have concluded that machining of high strength materials with unfavourable initial contact at the entry of the tool to the workpiece, could lead to premature tool failure. This means that the tool in the down-milling cut could be faced with repeated mechanical impacts which would lead to the reduction of tool life[14,15]. However, in these experiments, the tool life was based on flank wear, and, in accordance with feature b) described above, there is no substantial difference in tool life in up- and down-milling tests.

Furthermore, in order to differentiate between the mechanical and thermal effect, Yellowley and Barrow[12] arranged for a special test in which the slotting cut was repeated using a "split bar". The test arrangement is shown in Fig. 7.3, in which a small gap of 1.8 mm in the middle is prearranged between two bars of steel. The small break in the cycle does not have any significant influence on the thermal stress cycling, but it ensures that the mechanical influences operate in the same way as they did in half immersion cuts. The cutter life

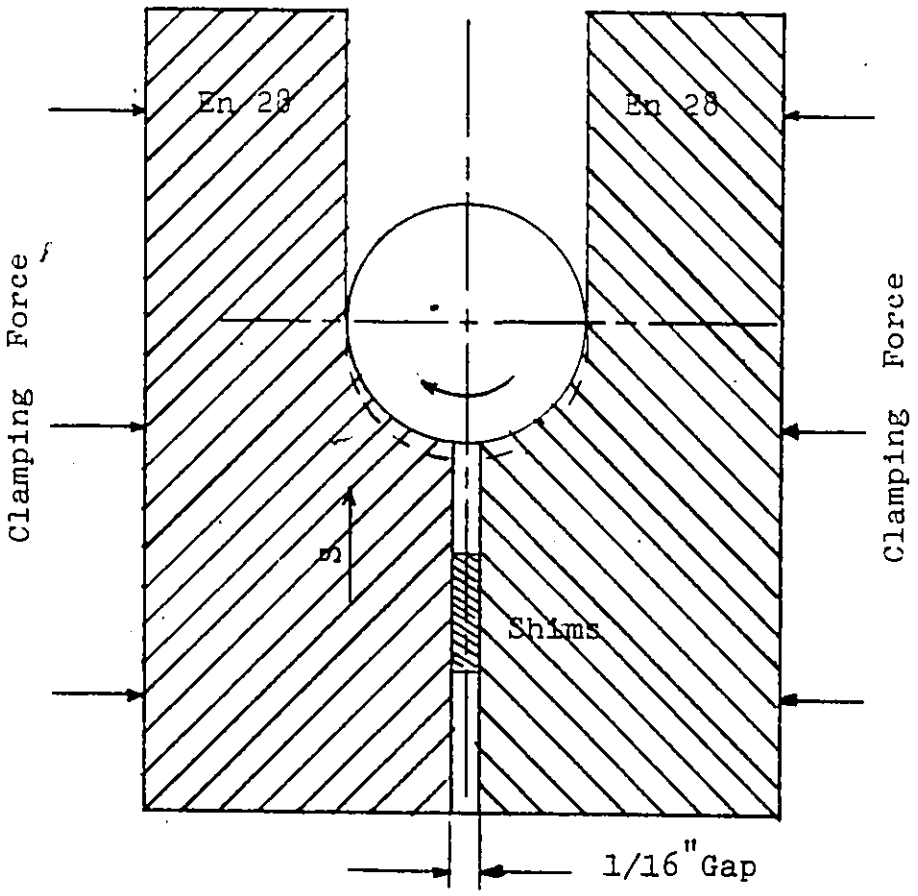

Fig. 7.3 Split bar test.(12)

resulting from this test was the same as that which occurred in the original slotting test. Therefore, it was concluded that the thermal influence is the one which should be analyzed in detail.

7.3 ANALYSIS OF THE EXPERIMENTAL RESULTS IN THE LIGHT OF THERMAL CYCLING COMPUTATIONS

The transient temperature distribution fields and the associated thermal stresses have been computed by applying the procedures explained in Chapter 5 and Chapter 6. The simulation of the thermal cycling was aimed at studying the influence of the cutting time ratio on the parameters which may affect the tool wear in milling. Thus, the thermal cycling has been computed for quarter, half and full immersion. The work material was low alloy steel AISI 4140 and the tool was 25 mm in diameter M2-H.S.S. end mill. The cutting conditions are given in Table 5.3.

The selected parameters which might influence the tool wear and tool life under these conditions are divided into two groups as follows:

(1) Temperature Parameters:

   (a) Peak temperature of the cutting edge which may affect the levels of stresses in both heating and cooling periods.

   (b) Temperature range which is proportional to strain range.

(2) Stress Parameters:

   (a) Tensile stresses on the tool flank which may lead to microcracks and promote wear.

   (b) Maximum shear stress.

(c) Maximum range of compressive stress in the vicinity of the cutting edge. It may produce plastic strain in the compressive mode which might be followed by high tensile stresses in the tensile or low compressive mode.

The effects of the cutting time ratio on the temperature and the stress parameters are summarized in Figs. 7.4 and 7.5, respectively. Figure 7.4 shows the effect of cutting time ratio on the peak temperature (graph a), and the temperature range (graph b) at the cutting edge. It is seen that there is very little difference between these very different cases in the two thermal parameters.

Figure 7.5 shows the effect of cutting time ratio on the maximum thermal tensile stress (graph a), the maximum thermal shear stress (graph b), and the maximum range of compressive stress (graph c) at the cutting edge. Again, almost no difference is observed among the various cases. It should also be appreciated that the maximum mechanical stresses are the same because the maximum cutting force is the same for half-immersion (up and down) and slotting.

Now, the main question is presented in Fig. 7.1 and in Fig. 7.2, and an explanation is sought for the experimental evidence of the ability of the tool (both H.S.S. and carbides) to remove twice as much metal in a slotting operation as in a half immersion operation (both up- and down-milling) for the same flank wear. In all of these cases, the flank wear develops uniformly and increases in proportion to cutting time.

The evidence summarized in Figs. 7.4 and 7.5 shows rather convincingly, that the lesser durability of the tools in operations with longer cooling periods is not due to a larger range of thermal stresses

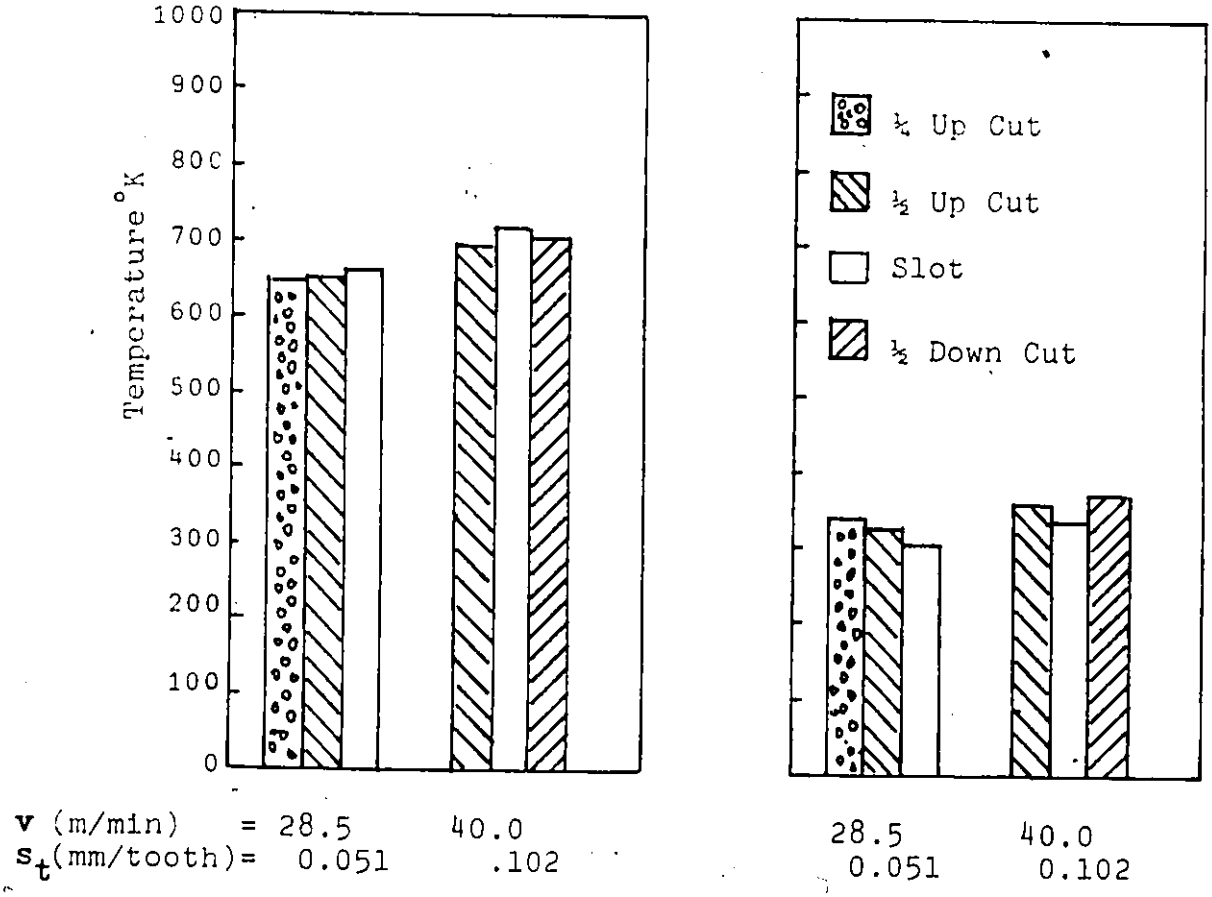

(a) Cutting Edge Peak temp. (b) Temperature Range

Fig. 7.4 Comparison of maximum temperature and temperature range for quarter, half and full immersion.

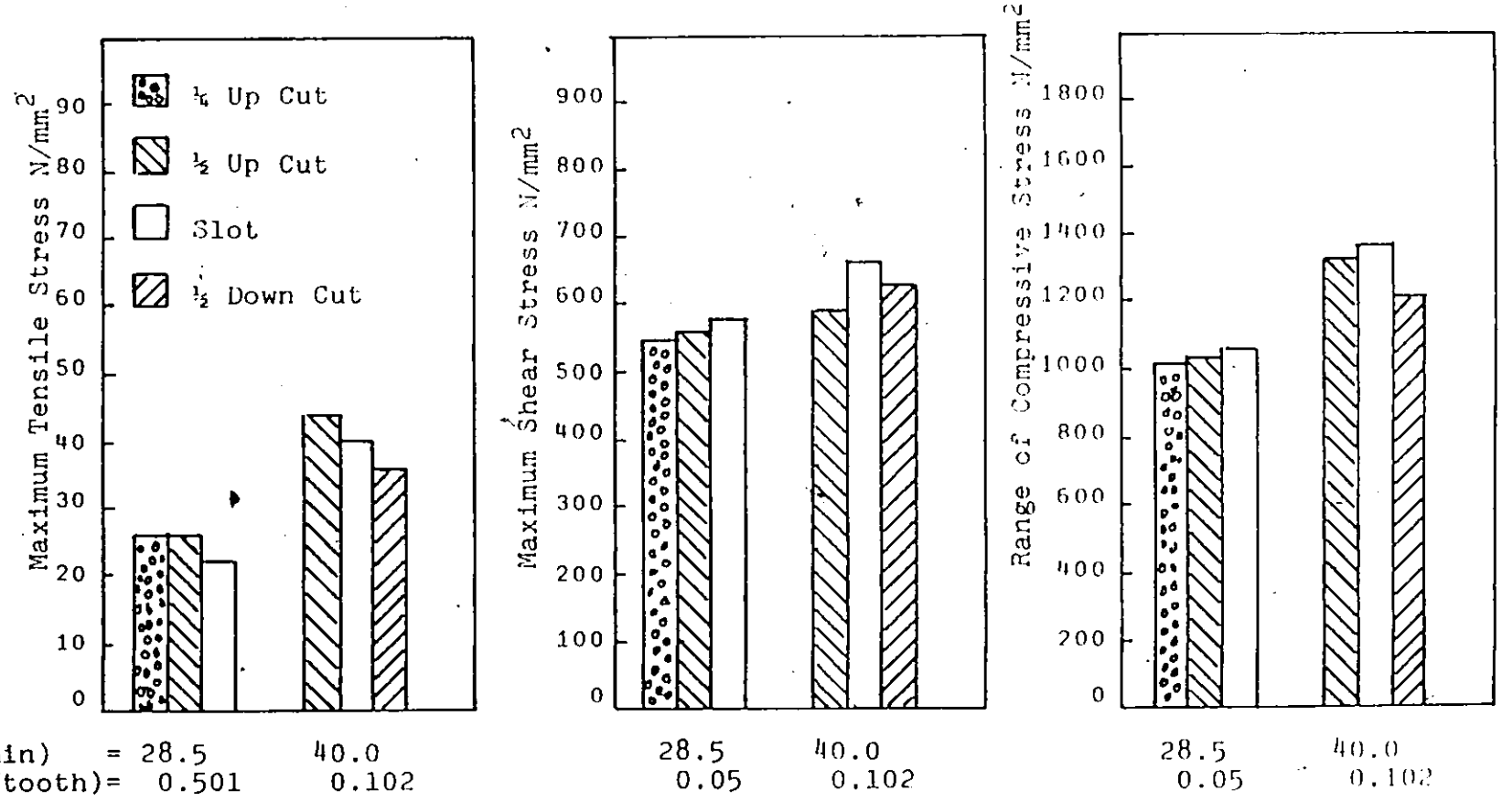

(a) Maximum tensile stress (b) Maximum shear stress (c) Maximum range of Compressive Stress.

Fig. 7.5 Comparison of maximum tensile, maximum shear and range of compressive stress for quarter, half and full immersion.

or any thermal parameters. This applies at least for H.S.S. tools and the corresponding cutting speed range for which these investigations were made.

Hence, the only basic parameter which offers itself as an answer to the above presented question is the number of thermal cycles, or similarly, of mechanical cycles. Therefore, the tool life test data shown in Fig. 7.1 and Fig. 7.2 are re-examined and the tool life has been defined in terms of the number of cycles and plotted as shown in Fig. 7.6 and Fig. 7.7. Comparing the tool life of half immersion with slotting, the tool life with the latter is slightly higher than with the former, and the mean ratio between tools' lives in 18 tests is about 1.13. Naturally, the slotting has removed twice as much metal by cutting through twice the radial depth of cut every cycle.

Next, we suggested that it is not the mechanical stress cycling to be involved in our explanation. First, if it was so then there would have to be substantial difference between up- and down-milling because of the significant difference in entry and exit conditions. Secondly, in the "slot bar" test conducted by Yellowley and Barrow, because of the small gap, the tool was subjected to the same number of thermal cycles but twice as many mechanical entries and exits without any effect on the tool life. Finally, it has been seen in the preceding Chapter that the cutting forces contributions on the overall stress is very small compared to the thermal stress. Thus, we believe that the thermal fatigue is responsible for the tool wear problem and a fatigue parameter should be developed based on the thermal stresses.

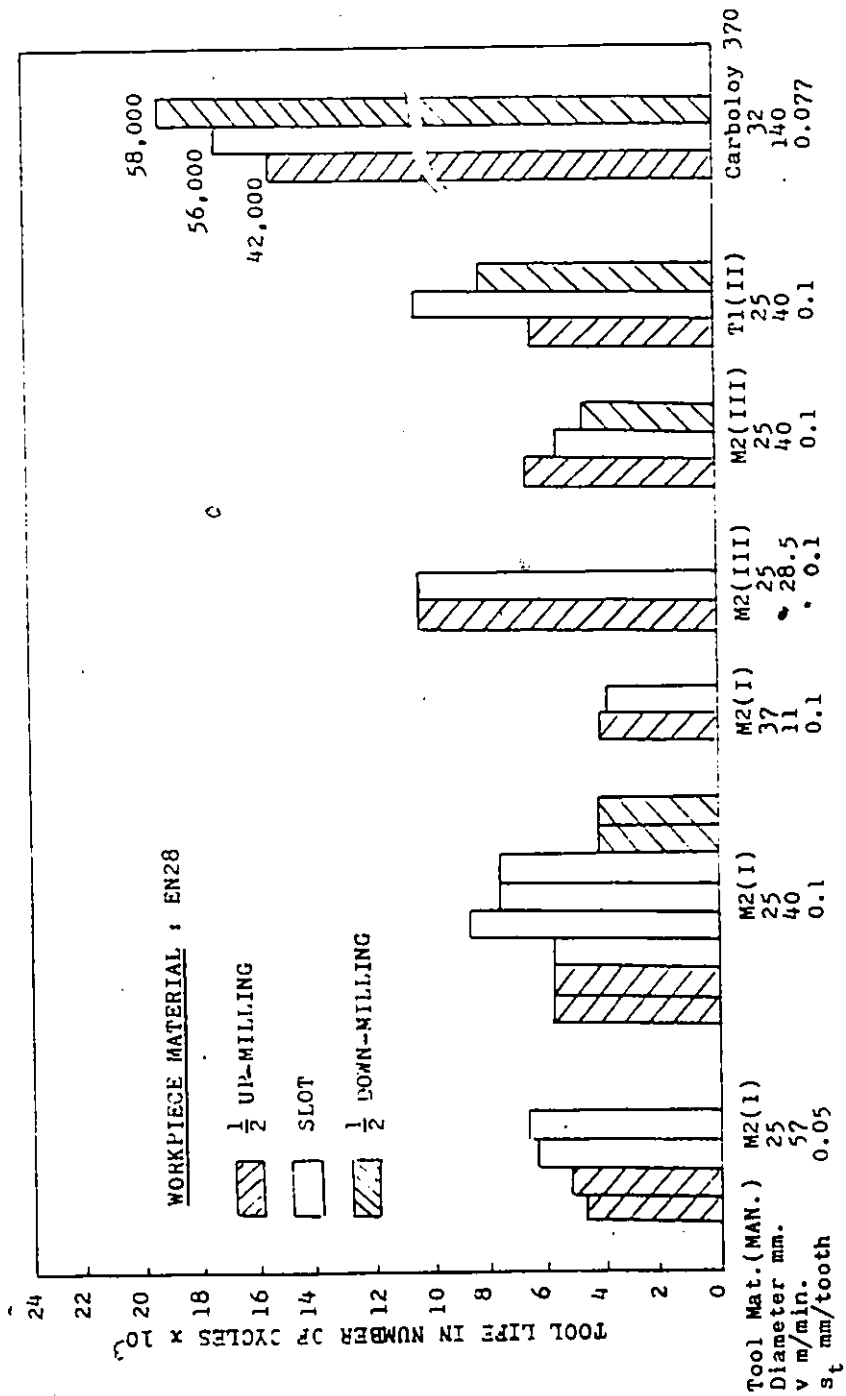

Fig. 7.6 Comparison of cyclic tool life for half and full immersion.

Continued Fig. 7.6

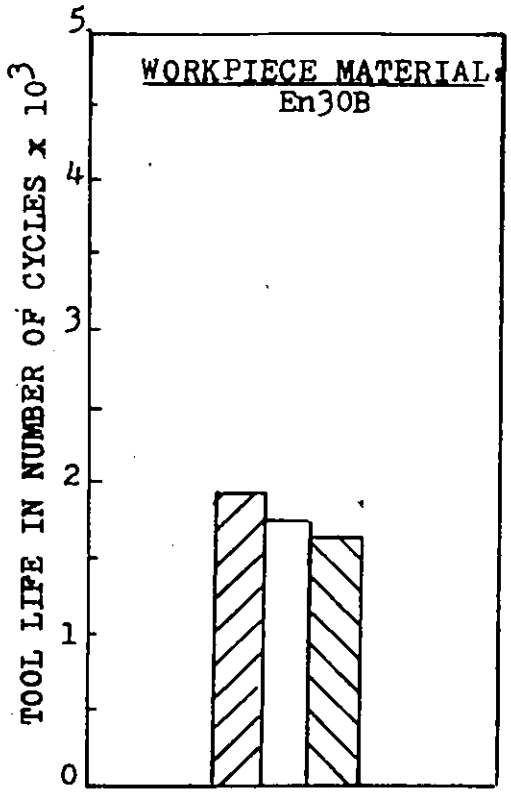

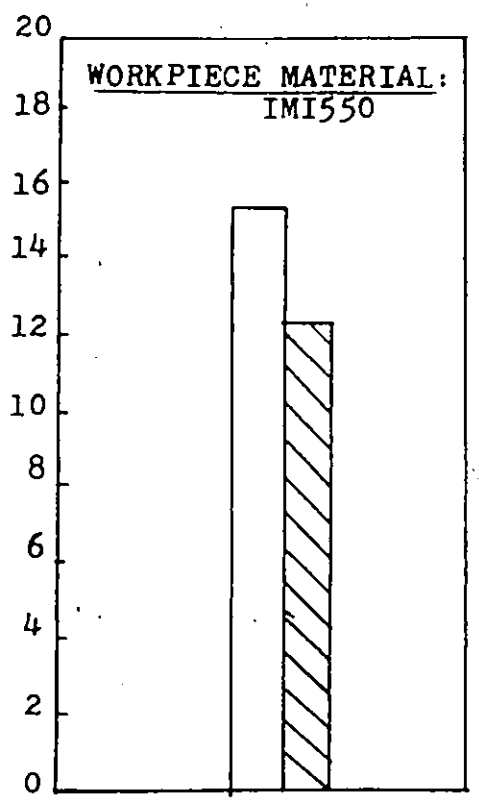

Tool Mat.(Man.)	M2(I)	Carboloy 883
Diameter mm.	25	32
v m/min.	18	50
s_t mm/tooth	0.125	0.09

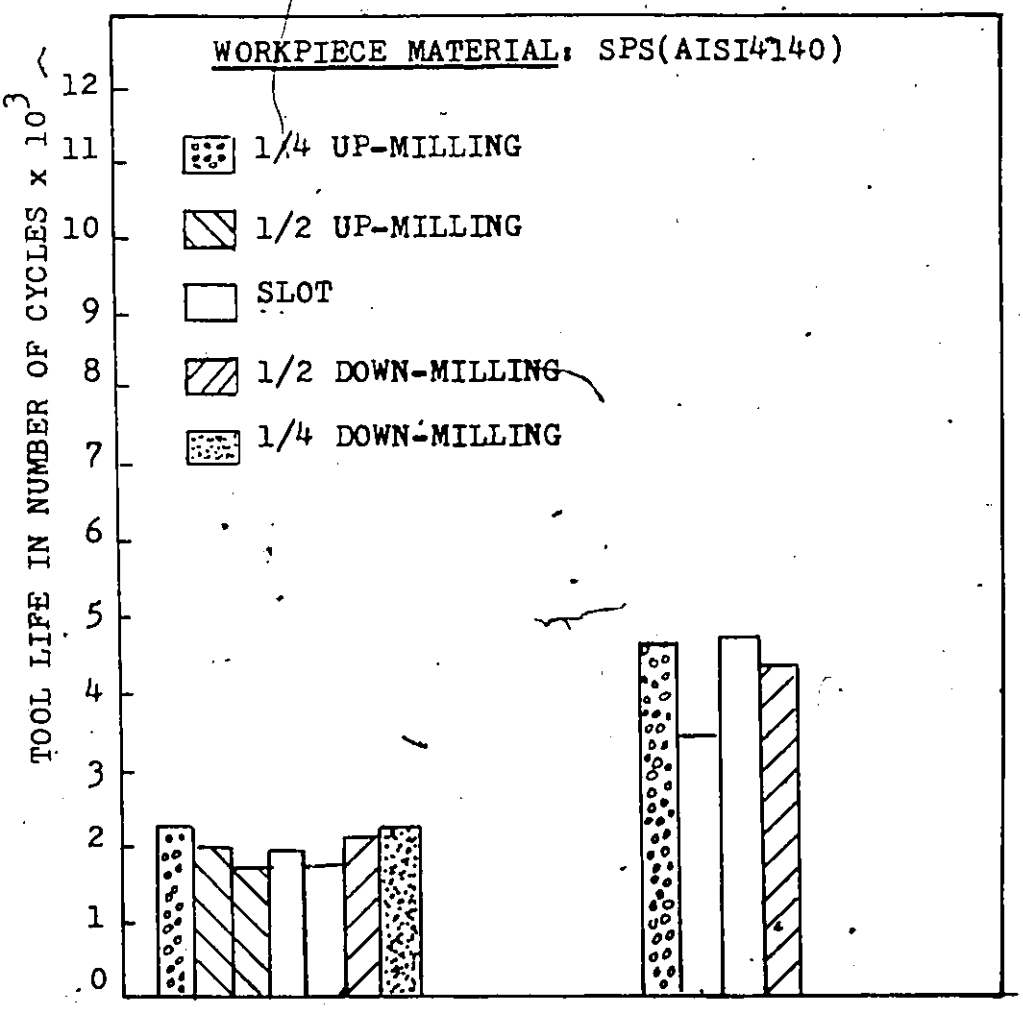

Tool Mat.(Man.)	M2(IV)	M2(IV)
Diameter mm.	127	63.5
v m/min.	45	45
s_t mm/tooth	0.113	0.113

Fig. 7.7 Comparison of cyclic tool life for quarter, half and full immersion.

7.3.1 Development of Fatigue Parameters

The stress in the vicinity of the cutting edge is not a simple static stress, but it is a three dimensional alternating stress. Figure 7.8 shows a stress spectrum at a point in the vicinity of the cutting edge. The three principle stresses are not alternating around zero mean stress and they are almost in phase.

Sines[68] developed a theory concerning the behaviour of metals under complex alternating stresses. The assumptions made were that, in the case of an isotropic material, the direction of the principle stresses is not important and only the magnitudes are significant. Also, each principle stress varied at the same frequency.

Based upon diverse experimental data, Sines[68] has developed a criterion of fatigue failure which includes the effect of different combinations of alternating stresses with static (mean) stresses. It is the simple statement that the permissible alternation of the octahedral shear stress is a linear function of the sum of the orthgonal normal static stresses. Or mathematically:

$$\frac{1}{3}\{(P_1 - P_2)^2 + (P_2 - P_3)^2 + (P_1 - P_3)^2\}^{1/2} < A - a\,(S_1 + S_2 + S_3)$$

where P_1, P_2, P_3 are the amplitude of alternating principle stresses and S_1, S_2 and S_3 are the orthogonal mean stresses (see Fig. 7.8). A is a constant for the material and is equal to $\sqrt{\frac{2}{3}}\, f_1$, where f_1 is the amplitude of the reversed axial stress which would cause failure at the desired cyclic lifetime and 'a' gives the variation of the permissible range of stress with static stress.

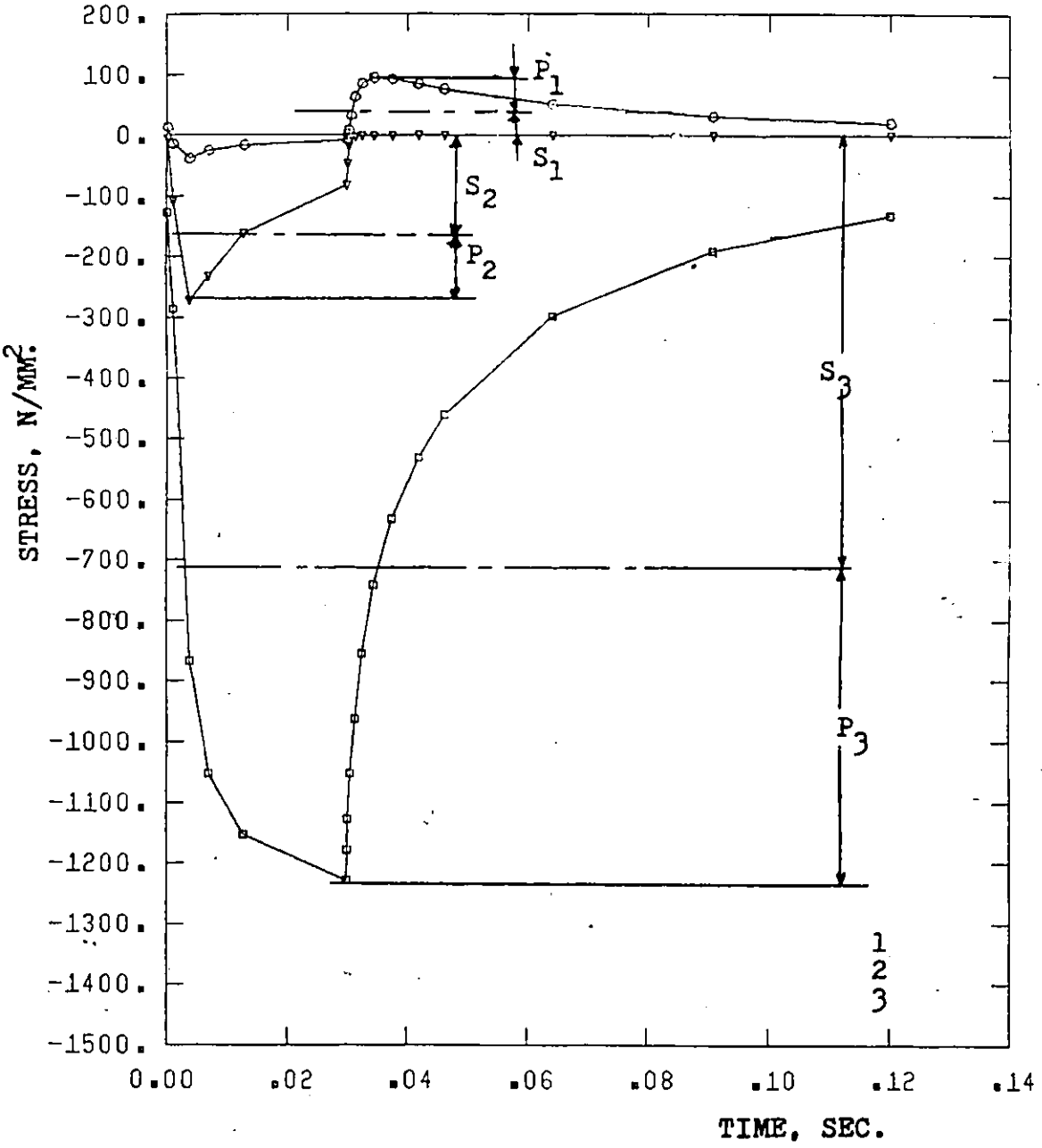

Fig. 7.8 Stress spectrum for a node in the vicinity of the cutting edge.

The above criterion could be separated into alternating stress σ_a and static mean stress σ_m which are defined as:

$$\sigma_a = \frac{1}{3}\{(P_1 - P_2)^2 + (P_2 - P_3)^2 + (P_3 - P_1)^2\}^{1/2}$$

and

$$\sigma_m = S_1 + S_2 + S_3$$

Examining the above criterion, it can be seen that the compressive (negative) mean stresses are beneficial.

For the purpose of analyzing the problem at hand, the alternating stress σ_a and the mean stress σ_m have been computed. The results are plotted in Fig. 7.9 for different cutting time ratios. Figure 7.9 shows that the alternating stress is almost constant and the mean stress, in case of full immersion, is more compressive than for half immersion, which means that the life in the case of full immersion will be longer than in half immersion. This may be explained with the help of the modified Goodman[69] diagram given in Fig. 7.10. Points a and b are representing two cases, where $(\sigma_{al})_a = (\sigma_{al})_b$ and $(\sigma_m)_a$ is more compressive than $(\sigma_m)_b$. The life of a is longer than that of b.

Note: comparing 1/4 immersion and half or full immersion is not recommended because the maximum mechanical stresses in both cases are different.

Finally, it could be concluded from the above analysis that the number of cycles of thermal stress is the decisive factor which determines the tool life in the two cases under consideration.

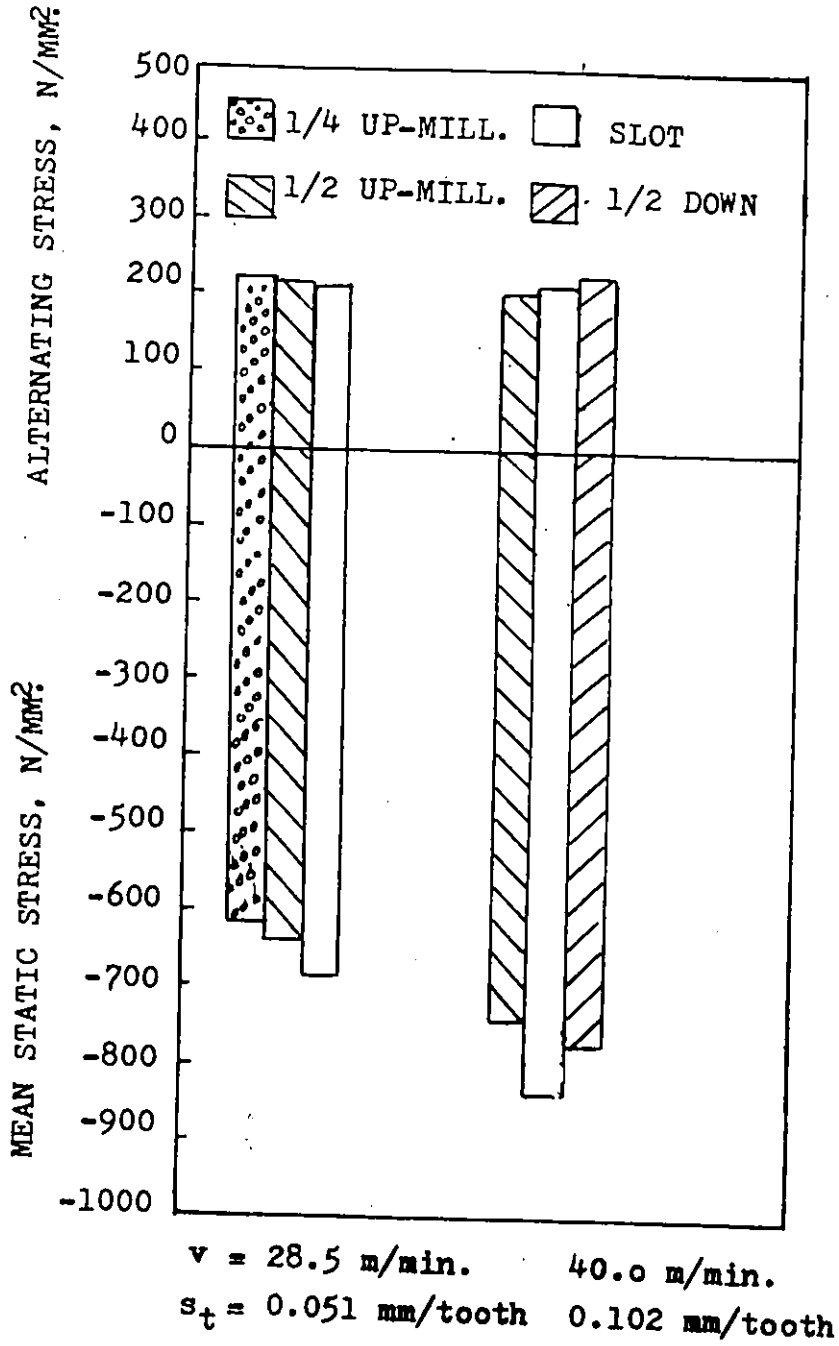

Fig. 7.9 Comparison of mean and alternating stress for slotting.

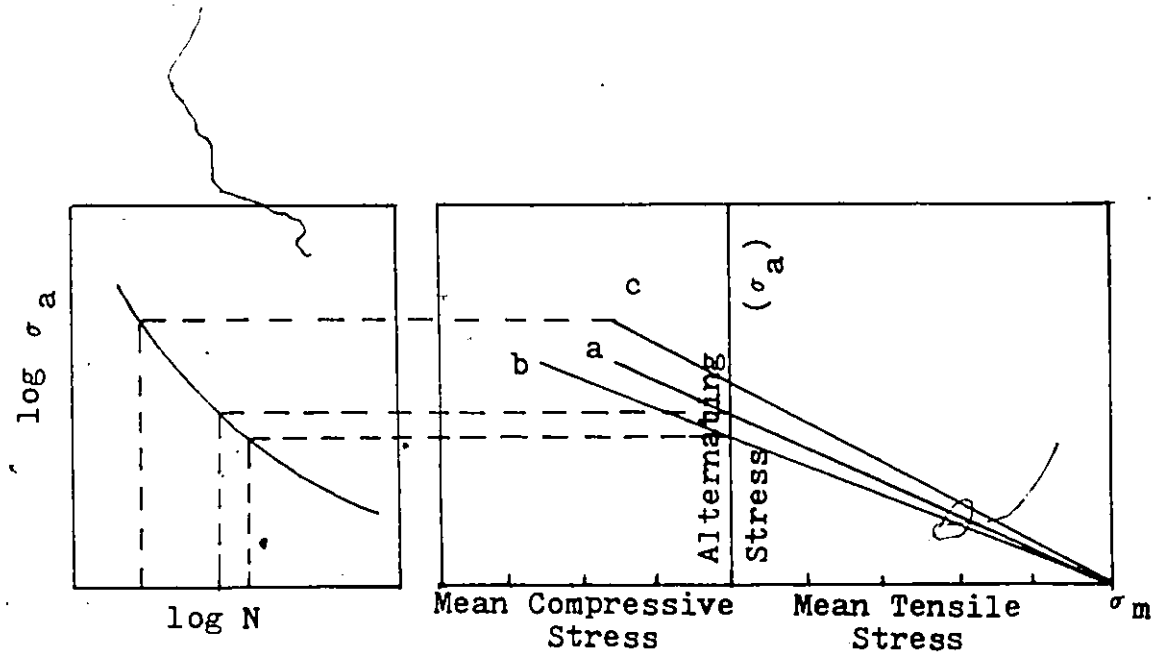

Fig. 7.10 Procedure for determining cyclic life in material subjected to alternating stress superimposed on a mean stress using Goodman's diagram.

CHAPTER 8

CONCLUSIONS AND RECOMMENDATIONS FOR FURTHER WORK

8.1 CONCLUSIONS

The aim of this thesis was to investigate the influence of thermal cycling on the tool life in intermittent cutting processes. The work has focussed on the peripheral milling process.

The tool life in peripheral milling, measured according to the flank wear criterion and evaluated in terms of active cutting time, is significantly influenced by the cutting time ratio. The most significant feature of the experimental results is that the tool life with full immersion (slotting) is more than doubled when compared with the tool life with half immersion. This means that milling tools (both H.S.S. and carbides) in slotting remove twice as much metal as in a half-immersion operation (both up- and down-milling) for the same tool wear. This phenomenon could be attributed to either mechanical or thermal influences. However, most of the experimental evidence in our work showed little difference in tool life between up- and down-milling. This indicates that the mechanical effect on the flank wear is negligible. This conclusion is also supported by a special test (split bar test) which was designed by Yellowley and Barrow[12]. Hence, it is concluded that the thermal cycling is the most significant factor which affects tool life and tool wear in peripheral milling.

According to the above conclusion our theoretical analysis concentrated on the analysis of the thermal cycling. A two-dimensional tool/chip model has been developed which considers the interaction between heat sources. The finite element method has been employed to compute the transient temperature distribution and the associated thermal stresses using the above model. The finite element formulation of the transient convective-transport problem has been presented. The finite element discretization results in a system of first order ordinary differential equations (ODEs). This system of ODEs is characterized as "stiff" system which necessitates using appropriate time-stepping scheme; a small time step at start which is increasing progressively. The recurrence schemes used are the two-point recurrence schemes for first order equations. In order to fulfill the above requirement, an automatic steplength control algorithm has been derived which can be used to determine the starting steplength and, automatically, the subsequent steplength. This algorithm has been successfully used with the developed heat transfer program. Another finite element program has been developed to compute the stresses. This program can be used to compute the transient thermal and mechanical stresses.

The transient temperature distribution and thermal stresses have been computed for end milling slotting, and for half and quarter immersion for several cutting conditions. The results of the computation are presented and discussed.

The significant parameters which might cause differences in tool life include:

a) Temperature parameters; peak temperature, and temperature range through a cycle,

b) Thermal stress parameters; maximum tensile stress, maximum shear stress and maximum range of compressive stress,

and

c) The number of cycles.

The temperature and stress parameters are evaluated at the cutting edge for slotting, half and quarter immersion for different cutting conditions. The results obtained in this study showed rather convincingly that the reduction of the tool life in an operation with longer cooling periods is not due to a larger range of thermal stresses or any other thermal parameters. This has been confirmed at least for the high speed steel tools and the cutting speed range investigated here. Therefore, we concluded that the most significant parameter which affects the tool life in peripheral milling is the number of thermal cycles.

Specifically, the thesis has provided the following contributions:

1) A finite element solution for the transient temperature distribution and the associated thermal stresses in intermittent cutting processes. For the first time, a two-dimensional tool/chip model and software system have been developed and used to solve this problem. This has required the following:

   i) Finite element formulation of the convective-transport and Fourier heat transfer equations.

   ii) Modelling of the intermittent cutting process.

iii) Implementation of the software programs (Heat Transfer Program and Stress Program).

iv) Derivation and implementation of an automatic steplength control algorithm. This has been done to achieve numerical stability of the two-point recurrence scheme and reduce the computational effort.

2) Study of the influence of thermal cycling on tool life in peripheral milling based on the two-dimensional tool/chip model which takes into account the interaction between the heat sources. The study involves, for the first time, the computation of complete temperature and stress fields. The computed results have been correlated with experimental data.

8.2 RECOMMENDATIONS FOR FURTHER WORK

1) This study shows that the flank wear is strongly affected by the thermal cycling and it progresses approximately in proportion to the number of cycles. The damage done to the flank wear by the thermal cycle is much larger than that due to the "rubbing" along the length of the actual cutting path of the tool. The stress levels obtained with the investigated cutting conditions are not high. Thus, it will be hypothesized that locally, along the grain boundaries of the tool material, the concentrated stress levels may be much higher. These stresses may lead to a loosening of the grains on the cutting edge which then may drag between the tool and workpiece and cause wear. The computation in

this thesis assumed a homogeneous tool material and could not, therefore, prove this hypothesis. It is suggested that in further work such an analysis be carried out which could look into the stresses in the microstructure of the cutting edge.

2) The wear rate during a cycle may be related to a physical phenomena such as oxidation. The temperature computation showed that there is no substantial difference between the maximum temperature obtained with full, half and quarter immersion. It may be hypothesized that when the tool leaves the cut a layer of oxides is formed on the tool surface. The oxidation rate is temperature dependent. Thus, the same layer may be formed in each cycle and when the tool enters the cut, the oxides may be removed by rubbing between tool and workpiece. It is suggested that further work may be carried out to investigate the formation of oxides on the tool.

3) The software system and model developed here can be used to investigate the crack formation in carbide and ceramic tools. Such an investigation should be based on a measurement of cutting forces and on observation of the cracks.

REFERENCES

1. Okushima, K. and Hoshi, T. "Thermal Crack in the Carbide Face Cutter-I", Bulletin of JSME, V5, n17, 1962, pp. 151-160.

2. Okushima, K. and Hoshi, T. "Thermal Crack in the Carbide Face Cutter-II", Bulletin of JSME, V6, n22, 1963, pp. 317-326.

3. Pekelharing, A.J. "A Story About the Cracking of Ceramic Tools When Cutting Steel", Ann. CIRP, V7, 1962, pp. 25-36.

4. Zorev, N.N. "Machining Steel with a Carbide Tipped Tool in Interrupted Heavy Cutting Condition", Russ. Eng. J., V43, n 2, 1963, pp. 43-47.

5. Okushima, K. and Hoshi, T. "Tool Fracture in Face Milling Operation", Bulletin of JSME, V15, 1967, pp. 309-324.

6. Braiden, P.M. and Dugdale, D.S. "Failure of Carbide Tool in Intermittent Cutting", Material for Metal Cutting, BISRA-ISA Conference, Scarborough, April 14-16, 1970, pp. 30-34.

7. Andreev, G.S. "Thermal State of Tool Cutting Edge in Intermittent Metal Cutting", Russ. Eng. J., V54, n8, 1974, pp. 56-58.

8. Bhatia, S.M. et al. "Thermal Cracking of Carbide Tools During Intermittent Cutting", Wear, V51, 1979, pp. 201-211.

9. Wu, H. and Mayer, Jr., J.E. "An Analysis of Thermal Cracking of Carbide Tools in Intermittent Cutting", ASME, Technical Paper No. 78-WA/Prod-22.

10. Yellowley, I. and Barrow, G. "The Influence of Thermal Cycling on Tool Life in Peripheral Milling", Int. J. Mach. Tool Des. Res., V16, n1, 1976, pp. 1-12.

11. Yellowley, I. and Barrow, G. "The Assessment of Tool Life in Peripheral Milling", Proc. of the 19th MTDR Conference, 1978, pp. 443-452.

12. Yellowley, I. and Barrow, G. "Tool Life in Milling with Specific Reference to Peripheral Milling Operation", Chapter 3 of Report on Prediction of Machinability, Division of Machine Tool Engineering, The University of Manchester, Institute of Science and Technology, Jan. 1975.

13. Tlusty, J. and Masood, Z. "Chipping and Breakage of Carbide Tools", ASME Trans., J. of Eng. for Ind., V100, n4, Nov. 1978, pp. 403-412.

14. Beckhaus, H. and Optiz, H. "Influence of Initial Contact on Tool Life When Face Milling High Strength Materials", SME, Material Removal Technical Paper, 1971.

15. Kronenberg, M. "Analysis of Initial Contact of Milling Cutter and Work in Relation to Tool Life", Trans. ASME, V68, 1946, pp. 217-228.

16. Pekelharing, A. "The Exit Failure in Interrupted Cutting", Annals of the CIRP, V27, n1, 1978, pp. 5-10.

17. Boston, O. and Gilbert, W. "Influence in Tool Life and Power of Nose Radius, Chamfer and Peripheral Cutting Edge Angle When Face Milling a 40,000 psi Cast Iron", Trans. ASME, V69, 1947, pp. 117-124.

18. Optiz, H. and Frohlich. "Neue Erkentrisse-uber den VerschleiB der Wertzeug beim Frasen von Baustall", Z.V.D.I., B6 96, 1954, p. 822.

19. Okushima, K. and Hoshi, T. "Measurement of Cyclic Temperature Change of Tool/Chip Interface in Carbide Fly Milling", Bulletin of JSME, V10, n37, 1967, pp. 206-215.

20. Okushima, K. and Hoshi, T. "Internal Temperature Distribution of Carbide Fly Cutting Tool", Bulletin of JSME, V10, n[redacted]67, pp. 566-573.

21. Braiden, P. "Thermal Condition in Metal Cutting", Material for Metal Cutting, BISRA-ISA Conference, Scarborough, April 14-16, 1970, pp. 35-37.

22. Tlusty, J. "Breakage of Cutting Tools", The Society of Carbide Engineers, 7th Carbide Cutting and Forming Seminar, McMaster University, Hamilton, June 10-12, 1975, pp. 179-191.

23. Carslaw, H.S. "An Introduction to Mathematical Theory of the Conduction of Heat in Solids", MacMillan & Co., published in London, 1921.

24. Blok, H. "Theoretical Study of Temperature Rise at Surface of Actual Contact Under Oiliness Lubricating Condition", Proc. General Discussion re: Lubricants, Inst. Mech. Eng., London, V2, 1937, p. 222.

25. Jeager, J.C. "Moving Sources of Heat and the Temperature at Sliding Contacts", Proc. Royal Society of New South Wales, V76, 1942, p. 203.

26. Rosenthal, D. "The Theory of Moving Sources of Heat and Its Application to Metal Treatments", Trans. ASME, V68, 1946, p. 849.

27. Schmidt, A.O. and Roubik, J.R. "Distribution of Heat Generated in Drilling", Trans. ASME, V7, 1949.

28. Hahn, R.S. "On the Temperature Development at the Shear Plane in Metal Cutting Process", Proc. U.S.A. National Congress in Applied Mechanics, 1951, pp. 661-666.

29. Leone, W.C. "Distribution of Shear Zone Heat in Metal Cutting", Trans. ASME, V76, 1954, pp. 121-125.

30. Trigger, K.J. and Chao, B.T. "Analytical Evaluation of Metal Cutting Temperature", Trans. ASME, V73, 1951, pp. 57-68.

31. Loewen, E.G. and Shaw, M.C. "On the Analysis of Cutting Tool Temperatures", Trans. ASME, V76, 1954, pp. 217-231.

32. Chao, B.T. and Trigger, K.J. "The Significance of Thermal Number in Metal Machining", Trans. ASME, V75, 1953, pp. 109-120.

33. Trigger, K.J. and Chao, B.T. "Temperature Distribution at the Tool/Chip Interface in Metal Machining", Trans. ASME, V77, 1955, pp. 1107-21.

34. Weiner, J.H. "Shear Plane Temperature Distribution in Orthogonal Machining", Trans. ASME, V77, 1955, pp. 1331-41.

35. Rapier, A.C. "A Theoretical Investigation of the Temperature Distribution in the Metal Process", Brit. J. Appl. Phys., No. 5, 1954, pp. 400-405.

36. Boothroyd, G. "Temperature in Orthogonal Metal Cutting", Proc. Instr. of Mech. Eng., V177, 1963, pp. 789-810.

37. Tay, A.O., Stevenson, M.G., and Davis, G. "Using the Finite Element Method to Determine Temperature Distribution in Orthogonal Machining", Proc. Instr. Mech. Engrs., V188, 1974, pp. 628-638.

38. Tay, A.O., et al. "A Numerical Method for Calculating Temperature Distribution in Machining from Force and Shear Angle Measurement", Int. J. Mach. Tool Des. Res., V16, 1976, pp. 335-349.

39. Barrow, G., "A Review of Experimental and Theoretical Techniques for Assessing Cutting Temperatures", Annals of the CIRP, V22/2, 1973, pp. 203-11.

40. Nakayama, K. "Temperature Rise of Workpiece During Metal Cutting", Bull. Fac. Eng., Yokohama National University, V5, 1956.

41. Arndt, G. and Brown, R.H. "On the Temperature Distribution in Orthogonal Machining", Int. J. Mach. Tool Des. Res., 1967, V7, pp. 39-53.

42. Qureshi, A.H. and Koenigsberger, F. "An Investigation into the Problem of Measuring the Temperature Distribution on the Rake Face of Cutting Tool", Annals of CIRP, V14, 1966, pp.

43. Boothroyd, G. "Photographic Techniques for Determination of Metal Cutting Temperatures", Brit. J. Appl. Phys, V12, 1961.

44. McFeron, D.E. and Chao, B.T. "Transient Interface Temperature in Plain Peripheral Milling", Trans. ASME, V80, 1958, pp. 321-329.

45. Wang, K.K., Wu, S.M., and Iwata, K. "Temperature Responses and Experimental Error for Multitooth Milling Cutter", Trans. ASME, J. of Eng. for Ind., V90, n2, 1968, pp. 353-59.

46. Wang, K.K., et al. "Investigation of Face-Milling Tool Temperatures by Simulation Techniques", Trans. ASME, J. of Eng. for Ind., V91, n3, 1969, pp. 772-780.

47. Huebner, K. "The Finite Element Methods for Engineers", Wiley-Interscience, 1976.

48. Desai, C.S. and Abel, J.F., "Introduction to Finite Element Method", Van Nostrand Reinhold, 1972.

49. Zienkiewicz, O.C. "The Finite Element Method", Third Edition, McGraw-Hill, 1977.

50. Zienkiewicz, O.C. and Parekh, C.J. "Transient Field Problem; Two-Dimensional and Three-Dimensional Analysis by Isoparametric Finite Elements", Int. J. Num. Meth. Eng., V2, 1970, pp. 61-71.

51. Zlatev, Z. and Thomsen, P.G. "Application of Backward Differentiation Methods to the Finite Element Solution of Time Dependent Problems", Int. J. Num. Meth. Eng., V14, 1979, pp. 1051-1061.

52. Zienkiewicz, O.C. and Lewis, R.W., "An Analysis of Various Time-Stepping Schemes for Initial Value Problems", Earthquake Engineering and Structural Dynamics, V1, 1973, pp. 407-408.

53. Lambert, J.D. "Computational Methods in Ordinary Differential Equations", John Wiley & Sons, 1973.

54. Chua, L.O. and Lin, P.M. "Computer-Aided Analysis of Electronic Circuits", Englewood Cliffs, New Jersey, Chapters 11, 12 and 13.

55. Irons, B.M. "Applications of a Theorem on Eigenvalues to Finite Element Problems", Univ. of Wales, Dept. of Civil Eng., Swansea, 1970 (CR/132/70).

56. Zlámal, M. "The Finite Element Methods in Heat Conduction Problems", pp. 85-104, "The Mathematics of Finite Element and Application II', ed. Whiteman, J., Academic Press.

57. Heinrich, P.S., Huyakorn, P.S., and Zienkiewicz, O.C. "An 'Upwind' Finite Element Scheme for Two Dimensional Convective Transport Equation", Int. J. Num. Meth. Eng., V11, 1977, pp. 131-143.

58. Christie, I., Griffiths, D.F., Mitchell, A.R., and Zienkiewicz, O.C. "Finite Element Methods for Second Order Differential Equations with Significant First Derivatives", Int. J. Num. Meth. Eng., V10, 1976, pp. 1389-1396.

59. Ben-Sabar and Rasnell, R. "A Stable Finite Element Simulation of Convective-Transport Problems", Int. J. Num. Meth. Eng., V14, 1979, pp. 545-565.

60. Palmer, W.B. and Oxley, P.L. "Mechanics of Orthogonal Machining", Proc. Inst. Mech. Engrs., V173, 1959, p. 623.

61. Bitans, K. and Brown, R.H. "An Investigation of the Deformation in Orthogonal Cutting", Int. J. Mach. Tool Des. Res., V5, 1965, p. 155.

62. Armarego, E.J. and Brown, R.H. "The Machining of Metals", Prentice-Hall, Inc., 1969.

63. Nakayama, K. "Studies on the Mechanism of Metal Cutting", Bull. Fac. Eng., Nat. Univ. Yokohama, V7, 1958, 1.

64. Boothroyd, G. "Effect of Surface Slope on Shear Angle in Metal Cutting", Trans. ASME, J. of Eng. for Ind., V92, Feb. 1970, pp. 115-118.

65. Tlusty, J. and Koenigsberger, F. "Specifications and Tests of Metals Cutting Machine Tools", UMIST Manchester, April 1970.

66. Sabberwal, A. "Chip Section and Cutting Force During the Milling Operation", Annals of CIRP, 1960, pp. 197-203.

67. Arpaci, V.S. "Conduction Heat Transfer", Addison-Weseley Publishing Company, 1966.

68. Sines, G. "Behaviour of Metal Under Complex Static and Alternating Stresses", Metal Fatigue, Edited by Sines, G. and Waisman, J.L., McGraw-Hill, 1959.

69. Manson, S.S. "Thermal Stress and Low Cycle Fatigue", McGraw-Hill, 1966.

70. Loladze, T.N. "Requirements of Tool Materials", Proc. of the 9th MTDR Conf., Pergamon Press, Manchester, England, 1968.

APPENDIX A

FINITE ELEMENT EQUATIONS FOR THERMAL TRIANGULAR ELEMENT AND CONSTANT STRAIN ELEMENT

A.1 ELEMENT EQUATIONS FOR LINEAR THERMAL TRIANGULAR ELEMENT:

In Chapter 4, the general element equation has been deduced and written in a matrix form as follows

$$([K_c]^e + [K_t]^e + [K_v]^e)\{T\}^e + [K_h]^e\{\dot{T}\}^e - \{Q\}^e + \{q\}^e - \{C_v\}^e = 0 \qquad (A.1.1)$$

where $[K_c]^e$ is the conduction matrix, and is defined by the coefficients

$$k_{c_{ij}} = \int_{A^e} (k_x \frac{\partial N_i}{\partial x} \cdot \frac{\partial N_j}{\partial x} + ky \frac{\partial N_i}{\partial y} \cdot \frac{\partial N_j}{\partial y}) \, dxdy \qquad (A.1.2)$$

$[K_t]^e$ is the heat transport equation, and is defined by

$$k_{t_{ij}} = \int_{A^e} \rho \, C \, N_i (u \frac{\partial N_i}{\partial x} + v \frac{\partial N_j}{\partial y}) \, dxdy \qquad (A.1.3)$$

$[K_h]^e$ is the heat capacitance matrix, and is defined by

$$k_{h_{ij}} = \int_{A^e} \rho \, C \, N_i N_j \, dxdy \qquad (A.1.4)$$

$\{Q\}^e$ is the matrix representing the heat generated inside the element, and is defined by

$$Q_i = \int_{A^e} \bar{Q} \, N_i \, dxdy \qquad (A.1.5)$$

$\{q\}^e$ is the boundary conduction matrix, and is defined by

$$q_i = \int_{\Gamma_2^e} q\, N_i \, d\Gamma^e \qquad (A.1.6)$$

and

$[K_v]^e$ and $\{C_v\}^e$ are the convection matrices, and are defined by

$$k_{v_{ij}} = \int_{\Gamma_2^e} \bar{h}\, N_i N_j \, d\Gamma^e \qquad (A.1.7)$$

$$C_{v_i} = \int_{\Gamma_2^e} \bar{h}\, T_\infty \, N_i \, d\Gamma^e \qquad (A.1.8)$$

The above equations will be evaluated for the triangular element. The triangular element, shown in Fig. A.1, is defined by the nodes 1-2-3 in counterclockwise. Assume that the temperature (T), at any instant in time t, varies linearly within the element, then the interpolation function can be written as

$$T^e(x,y,t) = \sum_{i=1}^{3} N_i(x,y)\, T_i(t) \qquad (A.1.9)$$

where N_i are the natural coordinates for the triangular element given by

$$N_i(x,y) = \frac{1}{2\Delta}(a_i + b_i x + c_i y) \quad , \quad i = 1,2,3 \qquad (A.1.10)$$

in which

Δ = the area of the triangular element, and

$$a_1 = x_2y_3 - x_3y_2 \qquad b_1 = y_2 - y_3 \qquad c_1 = x_2 - x_3$$

Other coefficients a_2, a_3, b_2, b_3, c_2 and c_3 are obtained by cyclically permuting the subscripts. The partial derivatives of N_i with respect to x and y are

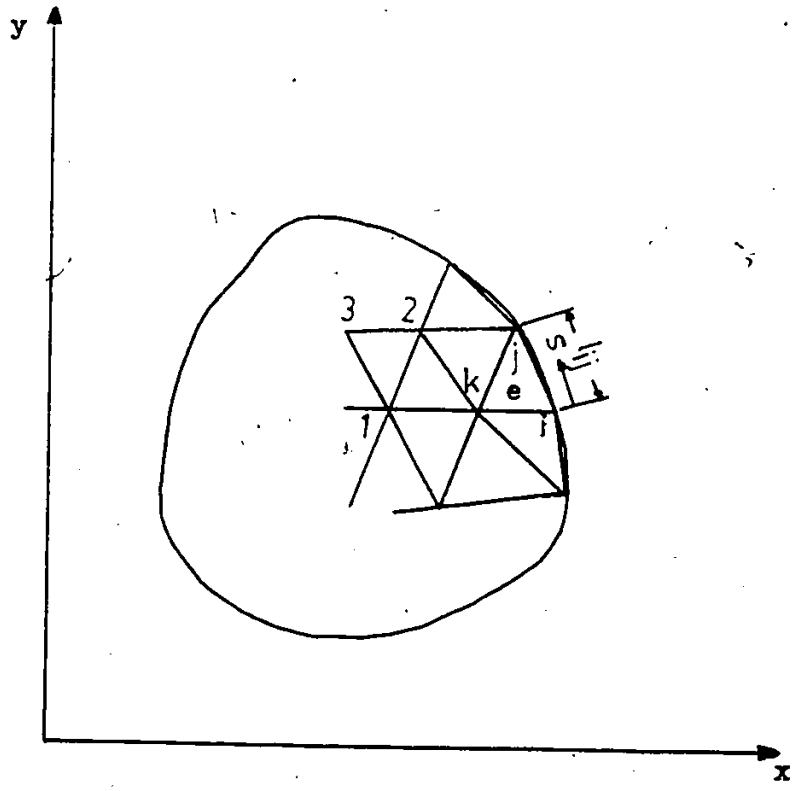

Fig. A.1 Boundary elements where convection or conduction are specified.

$$\frac{\partial N_i}{\partial x} = \frac{b_i}{2\Delta} \quad \text{and} \quad \frac{\partial N_i}{\partial y} = \frac{c_i}{2\Delta} \tag{A.1.11}$$

Now, we may refer to Equations (A.1.2) through (A.1.8) to write the element matrices.

(a) Conduction matrix:

Substituting Equation (A.1.11) in Equation (A.1.2), the coefficients of the element matrix $[K_c]^e$ are

$$k_{c_{ij}} = \int_{A^e} \left(k_x \frac{b_i}{2\Delta} \cdot \frac{b_j}{2\Delta} + k_y \frac{c_i}{2\Delta} \cdot \frac{c_j}{2\Delta}\right) t \, dxdy \quad ,$$

$$i = 1,2,3 \quad , \quad j = 1,2,3 \tag{A.1.12}$$

where t is the thickness of the element and usually taken as unity.

If k_x and k_y can be assigned constant average values within the element, the evaluation of the integral is

$$k_{c_{ij}} = \frac{t}{4\Delta} \left(k_x \, b_i b_j + k_y \, c_i c_j\right) \tag{A.1.13}$$

(b) Heat transport matrix:

Following the same procedure used with the conduction matrix, Equation (A.1.3) can be evaluated for the triangular element as follows:

$$k_{t_{ij}} = t \int_{A^e} \rho \, C \, N_i \left(u \frac{b_i}{2\Delta} + v \frac{c_i}{2\Delta}\right) dxdy \tag{A.1.14}$$

Again, if ρ, c, u and v are treated similar to k_x and k_y, the above integral can be evaluated using the formula for integrating area coordinates over the area of the triangular element, which is

$$\int_{A^e} N_1^\alpha \, N_2^\beta \, N_3^\nu \, dA^e = \frac{\alpha!\beta!\nu!}{(\alpha+\beta+\nu+2)!} \cdot 2\Delta \tag{A.1.15}$$

Integrating Equation (A.1.14), the coefficients of the elemental matrix

can be written as

$$k_{t_{ij}} = \frac{t\rho C}{6} (u\, b_i + v\, c_j) \qquad (A.1.16)$$

(c) Heat capacitance matrix:

Similarly, Equation (A.1.4) can be written as follows

$$k_{h_{ij}} = t\, \rho\, C \int_{A^e} N_i N_j \, dxdy \qquad (A.1.17)$$

Using the integration formula (A.1.15), the coefficient of the heat capacitance matrix for the triangular element is

$$[K_h]^e = \frac{t\rho C}{12} \begin{bmatrix} 2 & 1 & 1 \\ 1 & 2 & 1 \\ 1 & 1 & 2 \end{bmatrix} \qquad (A.1.18)$$

(d) Internal heat generation matrix:

For elements where heat is generated, the load vector $\{Q\}^e$ is evaluated from Equation (A.1.5), we have for node i

$$Q_i = t \int_{A^e} \bar{Q}\, N_i \, dxdy \qquad (A.1.19)$$

Assuming that $\bar{Q}$ is constant within the element, and using the integration formula (A.1.15), the coefficients of the load vector become

$$\{Q\}^e = \frac{\bar{Q} t \Delta}{3} \begin{Bmatrix} 1 \\ 1 \\ 1 \end{Bmatrix} \qquad (A.1.20)$$

(e) The boundary matrices:

If the element e forms a part of the boundary curve, where conduction or convection is specified, the boundary integrals (Equations A.1.6 and A.1.7 and A.1.8) should be evaluated.

Let element (e) lie on the boundary segment Γ_2 with nodes i→j as shown in Fig. A.1. For simplicity, assume that $\bar{h}$ and T_∞ are constant

over the boundary segment of length ℓ_{ij}, and that q may be linearly interpolated in terms of the nodal values as:

$$q = \tilde{q}_i N_i + \tilde{q}_j N_j \qquad (A.1.21)$$

Thus, the coefficients of the boundary matrices can be written as:

$$q_i = t \int_{i\to j} (\tilde{q}_i N_i + \tilde{q}_j N_j) N_i \, ds \qquad (A.1.22)$$

$$K_{v_{ij}} = t\bar{h} \int_{i\to j} N_i N_j \, ds \qquad (A.1.23)$$

and

$$C_{v_i} = t\bar{h} T_\infty \int_{i\to j} N_i \, ds \qquad (A.1.24)$$

The line integral for typical terms in the above matrices can be evaluated as follows:

$$\int_{i\to j} N_i \, ds = \int_o^{\ell_{ij}} \left(1 - \frac{s}{\ell_{ij}}\right) ds = \frac{\ell_{ij}}{2} \qquad (A.1.25a)$$

$$\int_{i\to j} N_i N_j \, ds = \int_o^{\ell_{ij}} \left(1 - \frac{s}{\ell_{ij}}\right) \frac{s}{\ell_{ij}} \, ds = \frac{\ell_{ij}}{6} \qquad (A.1.25b)$$

$$\int_{i\to j} N_i^2 \, ds = \int_o^{\ell_{ij}} \left(1 - \frac{s}{\ell_{ij}}\right)^2 ds = \frac{\ell_{ij}}{3} \qquad (A.1.25c)$$

Thus, the conduction load vector $\{q\}^e$ can be evaluated,

$$\{q\}^e = \frac{t\ell_{ij}}{6} \begin{Bmatrix} 2\tilde{q}_i + \tilde{q}_j \\ \tilde{q}_i + 2\tilde{q}_j \\ 0 \end{Bmatrix} \qquad (A.1.26)$$

Since N_K is zero on the boundary i-j; the boundary convection matrix $[K_v]$ can be evaluated using the integral formulea (A.1.25) and written as

$$[K_v]^e = \frac{t\ell_{ij}}{6}\begin{bmatrix} 2 & 1 & 0 \\ 1 & 2 & 0 \\ 0 & 0 & 0 \end{bmatrix} \qquad \text{(A.1.27)}$$

For the remaining matrix $\{C_v\}^e$, the coefficient at node i is

$$C_{v_i} = t\bar{h}\, T_\infty \int_{\ell_{ij}} N_i \, ds = t\bar{h}\, T_\infty \, \ell_{ij}/2$$

and similarly for node j. Thus

$$\{C_v\}^e = \frac{t\bar{h}\, T_\infty}{2}\begin{Bmatrix} 1 \\ 1 \\ 0 \end{Bmatrix} \qquad \text{(A.1.28)}$$

A.2 FINITE ELEMENT EQUATION FOR PLANE ELASTICITY TRIANGULAR ELEMENT:

In the development of the finite element equation for the triangular element, we closely followed the procedure of Ziawkiewicz[49]. The triangular element (shown in Fig. A.2) has the following characteristics:

(a) Displacement function:

The displacement of a node has two components, u and v such that

$$a_i = \begin{Bmatrix} u \\ v \end{Bmatrix} \qquad \text{(A.2.1)}$$

and the six components of element displacement are expressed in a vector as:

$$\{a\}^e = \begin{Bmatrix} a_i \\ a_j \\ a_k \end{Bmatrix} \qquad \text{(A.2.2)}$$

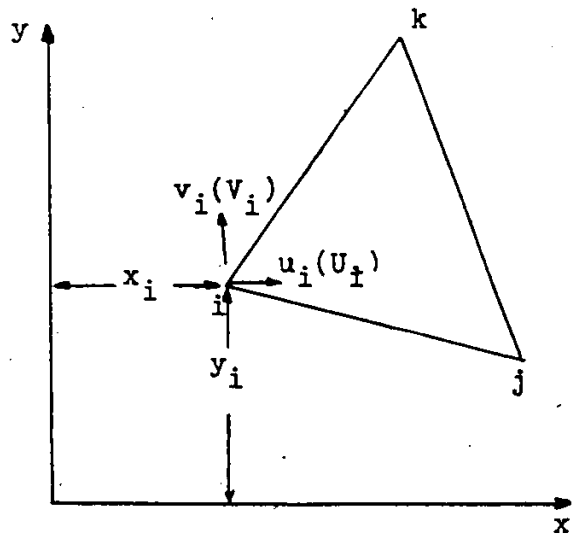

Fig. A.2 An element of a continuum in plane stress or plane strain.

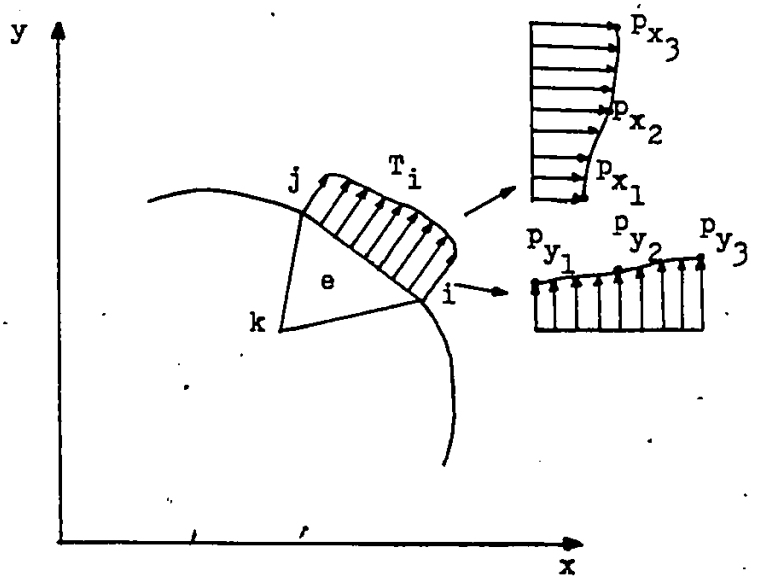

Fig. A.3 Distribution of boundary forces.

Assuming that the displacements are linearly distributed over the element, which means a constant strain element, then the interpolation function can be written as:

$$\{u\} = \sum_{i=1}^{3} N_i(x,y)\, a_i = [I\ N_i,\ I\ N_j,\ I\ N_K]\begin{Bmatrix} a_i \\ a_j \\ a_K \end{Bmatrix} \qquad (A.2.3)$$

where N_i are the natural co-ordinates of the triangular defined in Equation (A.1.10), and

$$I = \begin{bmatrix} 1 & 0 \\ 0 & 1 \end{bmatrix}$$

(b) Strain:

The total strain at any point within the element is defined by:

$$\{\varepsilon\} = \begin{Bmatrix} \varepsilon_x \\ \varepsilon_y \\ \varepsilon_{xy} \end{Bmatrix} = \begin{bmatrix} \frac{\partial}{\partial x} & 0 \\ 0 & \frac{\partial}{\partial y} \\ \frac{\partial}{\partial y} & \frac{\partial}{\partial x} \end{bmatrix} \begin{Bmatrix} u \\ v \end{Bmatrix} = [L]\{u\} \qquad (A.2.4)$$

Substituting Equation (A.2.3) in Equation (A.2.4) yields

$$\{\varepsilon\} = [B]\{a\}^e = [[B_i],[B_j],[B_k]]\begin{Bmatrix} a_i \\ a_j \\ a_k \end{Bmatrix} \qquad (A.2.5)$$

with typical $[B_i]$ matrix given by

$$[B_i] = [L][I]N_i = \begin{bmatrix} \frac{\partial N_i}{\partial x} & 0 \\ 0 & \frac{\partial N_i}{\partial y} \\ \frac{\partial N_i}{\partial y} & \frac{\partial N_i}{\partial x} \end{bmatrix} = \frac{1}{2\Delta}\begin{bmatrix} b_i & 0 \\ 0 & c_i \\ c_i & b_i \end{bmatrix} \qquad (A.2.6)$$

(c) Initial strain:

The initial strain vector due to temperature changes is defined as

$$\{\varepsilon_o\} = \begin{Bmatrix} \varepsilon_{xo} \\ \varepsilon_{yo} \\ \varepsilon_{xyo} \end{Bmatrix} \qquad (A.2.7)$$

Although this initial strain may, in general, depend upon the position within the element, it will usually be defined by the average, constant, values. This is consistent with the constant strain condition imposed by the prescribed displacement function. Thus, for the case of plane stress and an isotropic material in an element subjected to temperature rise θ^e, the initial strain components are defined as:

$$\{\varepsilon_o\} = \begin{Bmatrix} \alpha \ \theta^e \\ \alpha \ \theta^e \\ 0 \end{Bmatrix} \qquad (A.2.8a)$$

where

θ^e is the average temperature of the element, and

α is the linear coefficient of thermal expansion.

In the case of plane strain, the initial strain components are defined by

$$\{\varepsilon_o\} = (1 + \nu) \begin{Bmatrix} \alpha \ \theta^e \\ \alpha \ \theta^e \\ 0 \end{Bmatrix} \qquad (A.2.8b)$$

where ν is the Poisson's ratio.

(d) Stress in the element:

The stress in the element is given by:

$$\{\sigma\} = [D] (\{\varepsilon\} - \{\varepsilon_o\}) \qquad (A.2.9)$$

where [D] is the elasticity matrix which, for plane stress in an isotropic material, is given by

$$[D] = \frac{E}{1-\nu^2}\begin{bmatrix} 1 & \nu & 0 \\ \nu & 1 & 0 \\ 0 & 0 & (1-\nu)/2 \end{bmatrix} \qquad (A.2.10)$$

and for plane strain, [D] is given by

$$[D] = \frac{E(1-\nu)}{(1+\nu)(1-2\nu)}\begin{bmatrix} 1 & \nu/1-\nu & 0 \\ \nu/1-\nu & 1 & \\ 0 & 0 & (1-2\nu)/2(1-\nu) \end{bmatrix} \qquad (A.2.11)$$

(e) Nodal forces due to initial strain (ε_o):

The nodal forces are obtained from

$$\{f\}^{(e)} = [B]^T [D] \{\varepsilon_o\} t\Delta \qquad (A.2.12)$$

where t is the element thickness.

(f) Nodal forces due to external loads:

Consider the boundary elements shown in Fig. A.3. Nodes i and j lie on the boundary segment where normal (P_x) and tangential (P_y) stress are specified. Further, suppose that the normal and tangential stress vary along the edge i-j, and can be approximated by a parabolic expression. The load vector can be derived, and it takes the following form:

$$\{F_T\}^e = \frac{t\,\ell_{ij}}{6}\begin{Bmatrix} P_{x_1} + 2P_{x_2} \\ P_{y_1} + 2P_{y_2} \\ 2P_{x_2} + P_{x_3} \\ 2P_{y_2} + P_{y_3} \\ 0 \\ 0 \end{Bmatrix} \qquad (A.2.13)$$

(g) Stiffness matrix:

The stiffness matrix of the element is defined by

$$[K]^e = \int_{V^e} [B]^T[D][B] \, dvol \qquad (A.2.14)$$

and its coefficients are defined as

$$k_{ij} = t \int_{A^e} [B_i]^T[D][B_j] \, dxdy \qquad (A.2.15)$$

Since neither of the matrices contains x or y, then

$$k_{ij} = [B_i]^T[D][B_j] \; t \cdot \Delta \qquad (A.2.16)$$

The overall nodal forces and stiffness matrices of the whole system, {F} and [K], are obtained by assembling the above elemental force and stiffness matrices to give

$$[K]\{a\} = \{F\} \qquad (A.2.17)$$

Equation (A.2.17) is to be solved to obtain the deformation in a given elastic continuum.

APPENDIX B

SOFTWARE DEVELOPED

B.1 FINITE ELEMENT COMPUTER PROGRAMS:

The following two finite element computer programs have been developed:

a) Heat Transfer Program

b) Stress Analysis Program

B.1.1 Heat Transfer Program:

The heat transfer program was developed based on the finite element formulation presented in Chapter 4. The element equations are deduced for a linear triangular element and presented in Appendix A.1. The block diagram given in Fig. B.1 shows the basic steps of temperature computation procedure implemented in this program. The program can be used to compute the numerical solution for the steady-state and transient temperature distribution in a two-dimensional structure. The solution can be obtained for both the convective-transport and the Fourier heat transfer equations with boundary conditions, in the following situations:

a) All boundary conditions are time dependent.

b) All boundary conditions are time independent.

c) Only the specified temperature in the boundary is time dependent.

d) Only the convective or conductive boundary conditions are time dependent.

HEAT TRANSFER PROGRAM

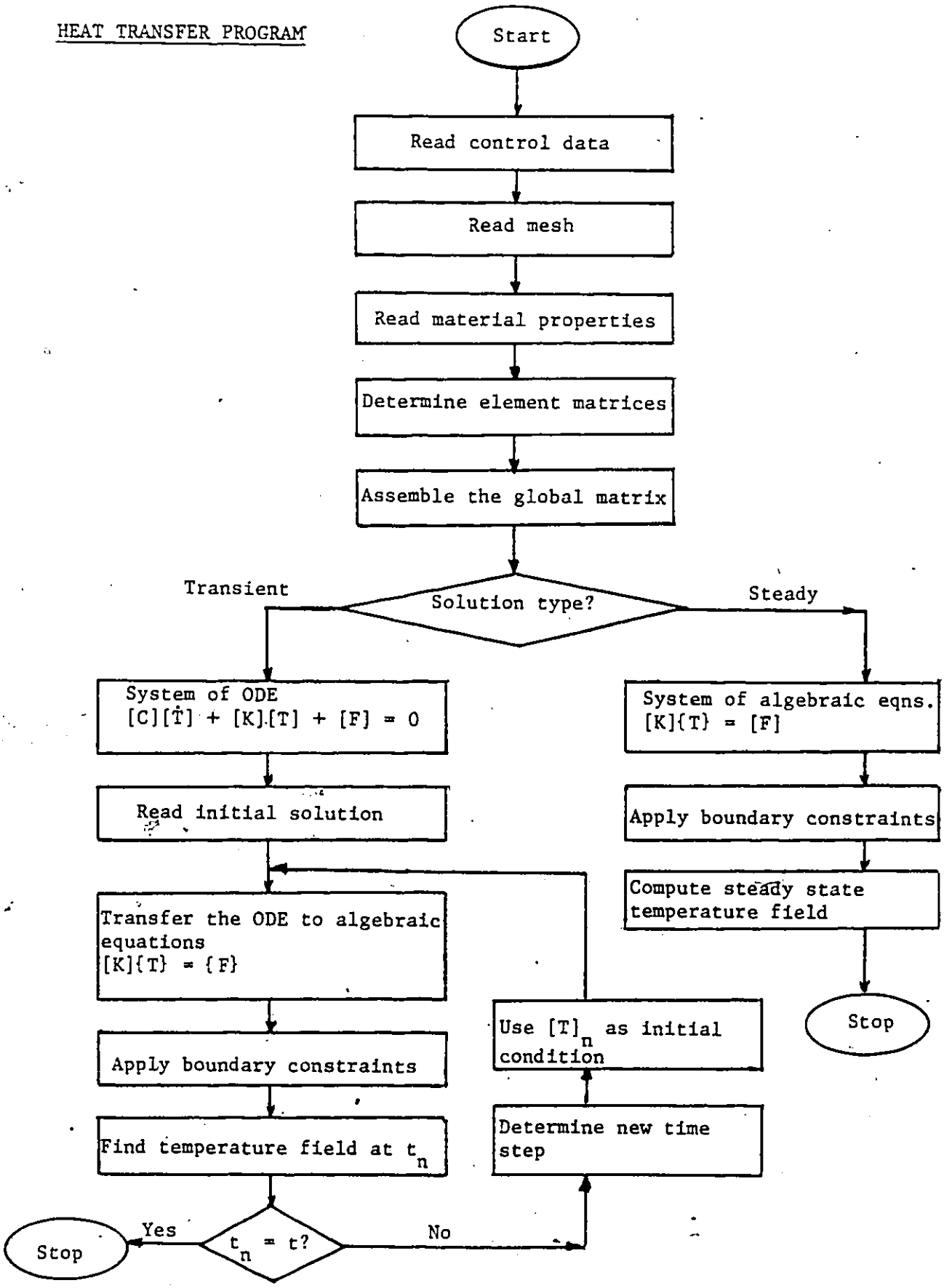

Fig. B.1 Flow Diagram for the Heat Transfer Program.

The program uses the θ-recurrence scheme to solve the system of first order ordinary differential equations, which is the result of the finite element discretization. It can determine the optimal starting and subsequent time steps automatically using the automatic step control algorithm derived for θ-scheme and presented in Chapter 4.

The program has been developed to compute the transient temperature field for both the cutting period and the non-cutting period in sequence for a specified number of cycles. It also writes a temperature file to be used with the "Stress Analysis Program" to compute the thermal stresses. The steady state solution of the convective transport and Laplace heat transfer equation can be obtained using the same program.

B.1.2 Stress Analysis Program

This program was developed based on the finite element theory for elastic continuum. It can be used to compute the solution for plane stress and plane strain linear elasticity problems.. The program is written for constant strain triangular element for which characteristic equations are given in Appendix A.2.

The block diagram in Fig. B.2 shows the basic steps of stress computation. The program reads the temperature files (transient temperature distribution files previously written by the Heat Transfer Program) to compute the thermal deformation and thermal stresses. Also, it can compute the mechanical stresses only, or the combined mechanical and thermal stresses.

STRESS PROGRAM

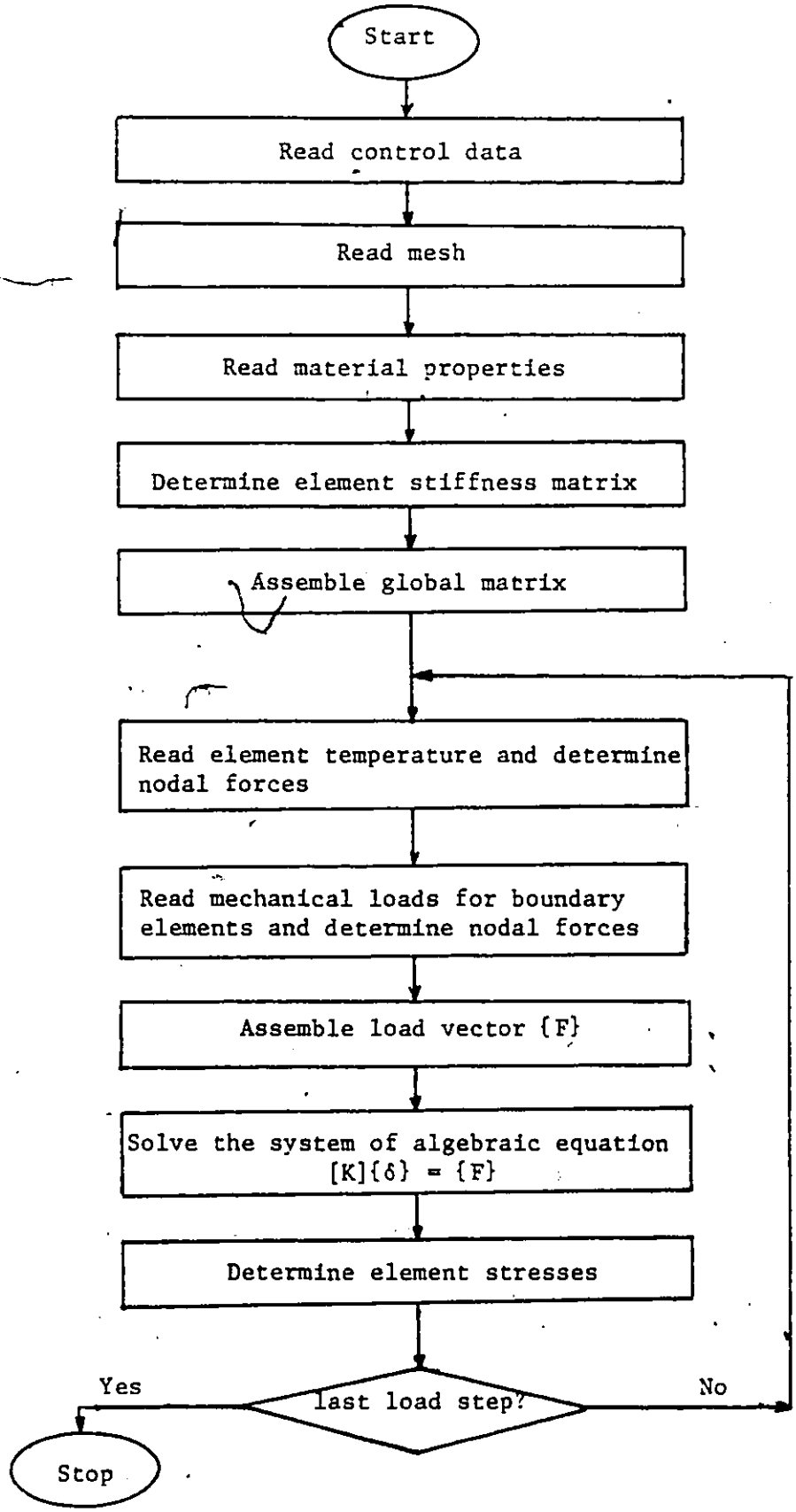

Fig. B.2 Flow Diagram for the Stress Analysis Program.

B.2 AUTOMATIC GRID GENERATOR:

An automatic grid generator has been developed to generate the grid with minimum input data. The input data include, tool and chip dimensions, contact length, shear angle, rake and clearance angles, number of elements in the contact area and number of elements outside the contact area. The program can generate a mesh with fine elements inside the contact area, and the size of the elements increases gradually with the distance outside the contact area. The program can generate a grid for the chip only, the tool only, or the tool and the chip combined. Figure B.1 and Fig. B.4 are typical grids for the tool/chip and the tool finite element models, respectively.

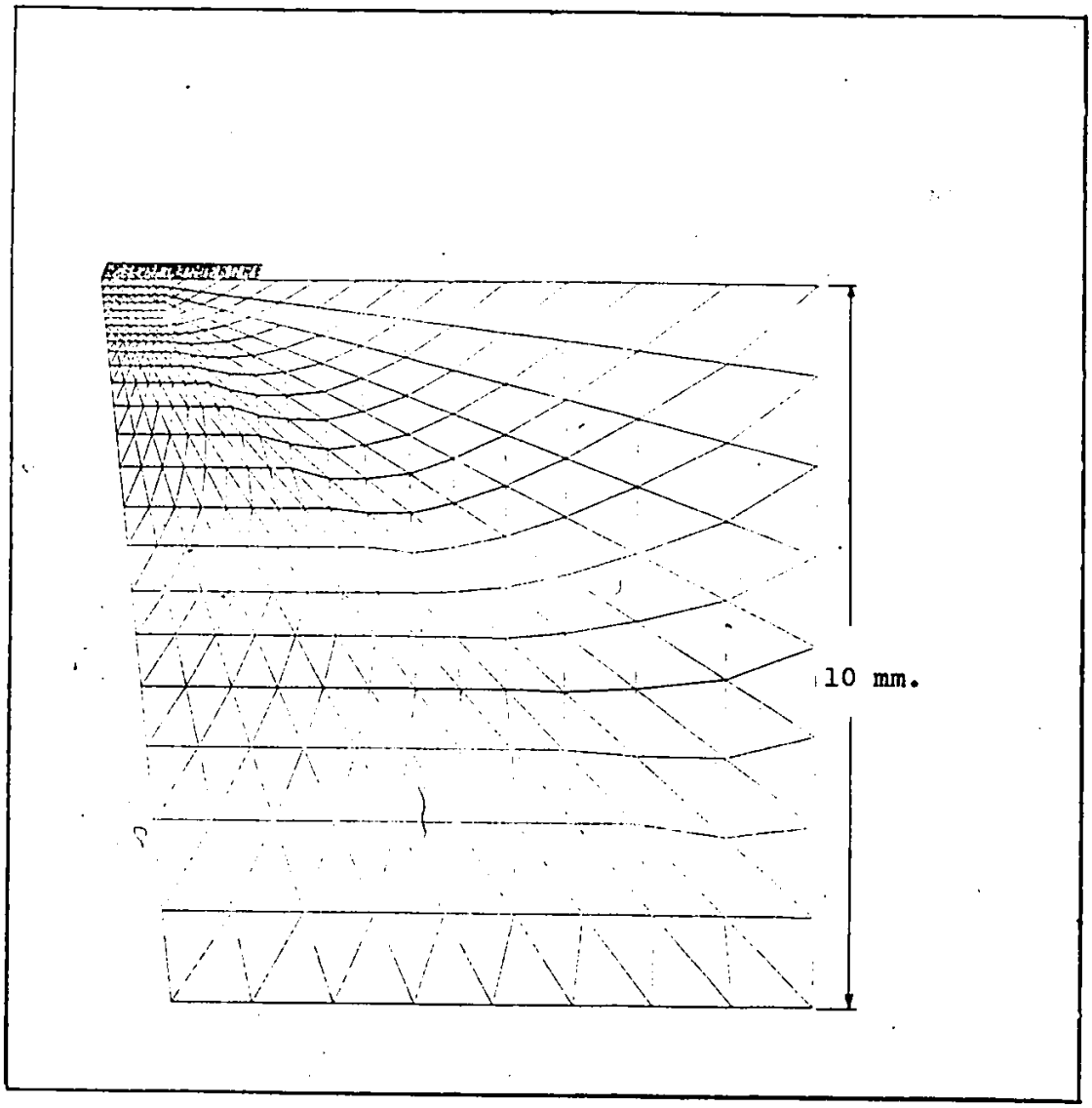

Fig. B.3 Tool/chip model finite element mesh.

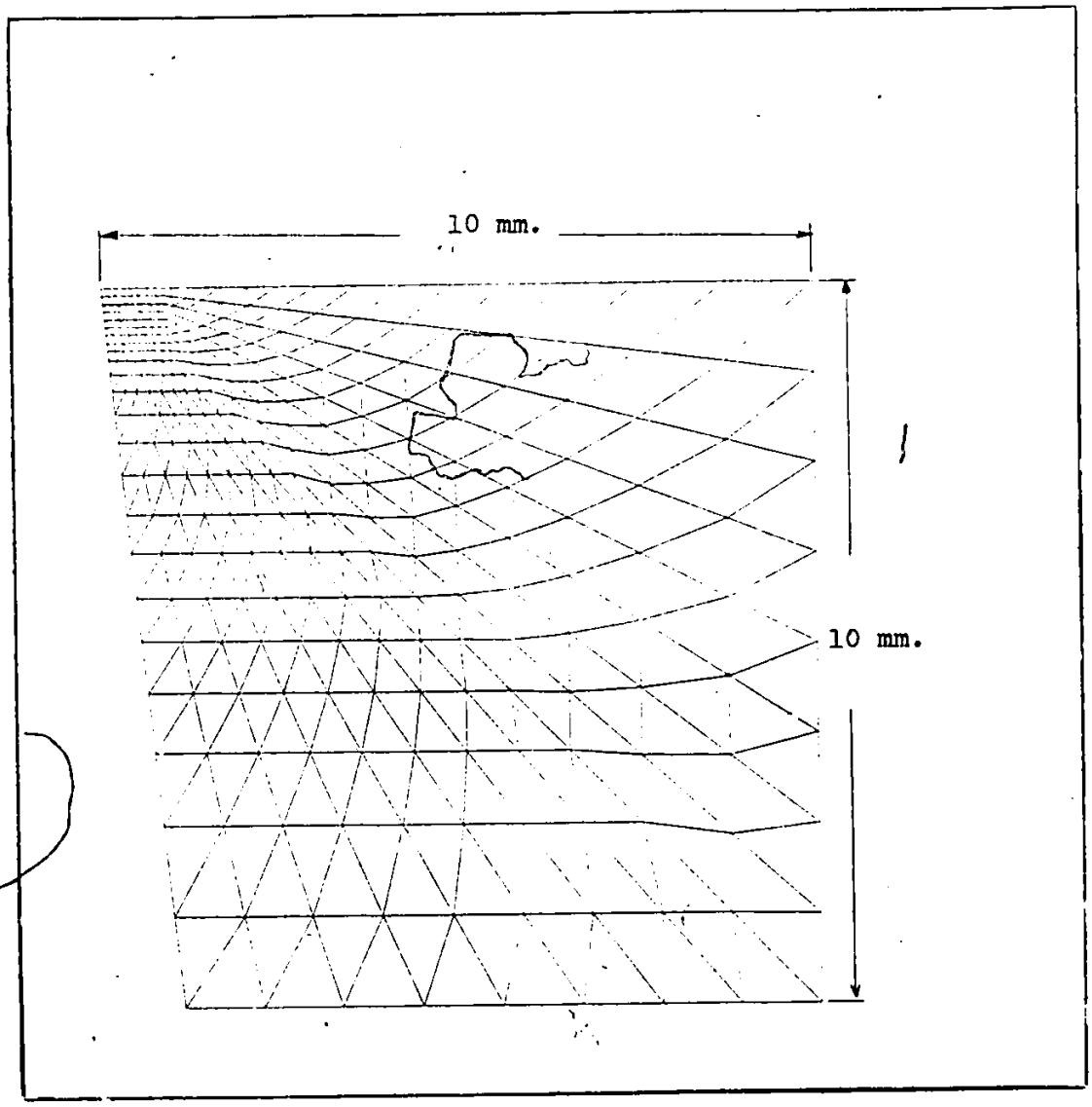

Fig. B.4 Tool model finite element mesh.

APPENDIX C

TESTING THE AUTOMATIC STEPLENGTH CONTROL ALGORITHM

The steplength control algorithm has been tested numerically when used with the finite element program to solve the transient convective-transport equation (Equation (4.5)) on the chip domain. The chip domain, together with the thermal boundaries, are shown in Fig. C.1. The shear plane temperature (T_s) is taken as the average temperature of the shear plane heat source, and considered as the prescribed temperature boundary. The tool/chip interface zone is assumed to be a plane heat source with uniform strength ($\bar{q}$), i.e., a conductive boundary. At a distance far from the heat generation zone, the chip temperature becomes uniform. Thus, no heat is conducted and the boundary is considered insulated, i.e., $\frac{\partial T}{\partial n} = 0$. Similarly, for the remaining boundaries, the convection and radiation to air are neglected, and therefore, the chip is considered insulated. The boundary data and the properties of the chip material are given in Table C.1.

The transient temperature distribution in the chip was obtained for three different values of θ (θ = 2/3, 7/8 and 1), and time span of 4 msec. The truncation error is assumed to be bounded with E = .001. The transient temperature at time points for selected nodes (marked in Fig. C.1 are given in Tables C.2, C.3 and C.4 for θ = 2/3, 7/8 and 1, respectively. These results were plotted in Fig. C.2 for node 37 and node 60. It is seen that the instantaneous nodal temperatures obtained with the three values of θ coincide, and no oscillation has been detected. The time step is very small at the start and increases as the solution

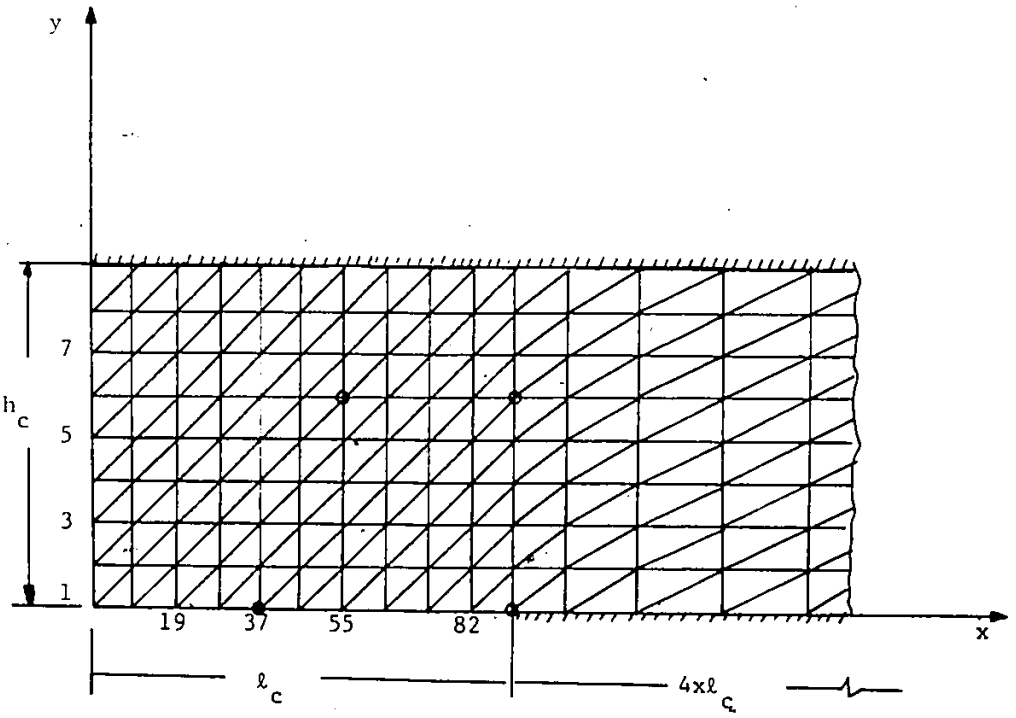

Boundary conditions

$$K\left(\frac{\partial T(x,0)}{\partial x} + \frac{\partial T(x,0)}{\partial y}\right) = q_f \qquad 0 < x < \ell_c$$

$$T(0,y) = T_s \qquad x = 0, \quad 0 < y < h_c$$

$$\frac{\partial T(x,y,t)}{\partial n} = 0 \qquad \ell_c < x < 5\ell_c, \quad y = 0$$
$$\text{and} \quad 0 < x < 5\ell_c, \quad y = h_c$$

Initial condition

$y(x,y,0) = 293\ ^\circ K$

where

q_f = friction heat

T_s = average shearplane temperature

//// insulated boundaries

Fig. C.1 Thermal boundaries and initial condition for the chip problem

progresses. The number of time steps to reach a span of 4 msec is 26, 17 and 22 for θ = 2/3, 7/8 and 1, respectively. This indicates that θ = 7/8 is optimal since it requires the least computational effort.

The steady state solution of the above problem, based on the finite element formulation for the steady convective-transport energy equation, has been obtained. The results obtained were, then, compared to the steady state conditions for the three values of θ. Table C.5 shows the steady state temperatures for selected nodes on the chip domain. The nodal temperature obtained with the four solutions are exactly the same. Hence, we may conclude that the steplength control algorithm is successfully working and θ = 7/8 is optimal.

Table C.1

Boundary Data and Properties of the Chip Material

Boundary Data	
Shear plane temperature (T_s)	703.91 °K
Friction heat source strength (q_f)	42.94 W/mm^2
Heat transfer coefficient (h)	.00248 W/mm^2 °K
Properties of Carbon Steel Grade 1035	
Thermal conductivity	.052338 W/mm °K
Volumetric specific heat	.0034757 J/mm^3 °K

Table C.2

The Nodal Temperatures as Obtained Using $\theta = 2/3$

Time in sec	Node 37	Node 91	Node 60	Node 96
.5509E-4	315.28	305.7804	292.997	293.003
.80137E-4	320.1861	310.4317	292.9964	293.0012
.10518E-3	324.4926	314.4924	293.0194	293.0035
.14465E-3	336.7415	320.2001	292.9538	293.0179
.18412E-3	357.9025	325.359	293.0268	293.0618
.22348E-3	387.514	330.1106	294.1314	293.1571
.28554E-3	444.7741	336.9068	301.6815	293.4675
.3475E-3	505.6174	343.1328	318.6905	294.0284
.40946E-3	562.8427	349.0856	345.9192	295.0422
.49698E-3	629.7828	358.5316	397.9862	298.5841
.5845E-3	679.8421	371.6945	456.9404	306.7187
.672E-3	715.0239	391.4619	514.4629	322.0395
.75955E-3	738.7205	419.5601	565.0633	346.1447
.8858E-3	758.8962	474.0761	620.723	395.8679
.10121E-2	764.4827	537.6844	658.1899	455.9598
.11384E-2	774.8639	601.6635	681.53	517.6972
.12647E-2	777.5366	658.9083	695.2585	573.7126
.1391E-2	778.841	705.5778	702.9789	619.8014
.1578E-2	779.6369	753.3247	708.3698	667.2394
.1765E-2	779.9032	781.6145	710.4694	695.4179
.19519E-2	779.9905	796.8544	711.2488	710.5696
.21389E-2	780.0188	804.4602	711.5276	718.09
.2329E-2	780.0278	808.0268	711.6244	721.5871
.31723E-2	780.0319	810.7141	711.6732	724.1724
.3454E-2	780.0319	810.7451	711.6733	724.2002
.4000E-2	780.0319	810.7529	711.6734	724.207

Table C.3

The Nodal Temperatures as Obtained With $\theta = 7/8$

Time in secs	Node 37	Node 91	Node 60	Node 96
.2736E-4	308.1716	301.2038	293.002	293
.41E-4	313.2825	304.3885	292.993	293.0001
.547E-4	316.83	307.1566	292.989	293.0001
.7426E-4	320.413	310.6412	293.0059	293.0011
.11E-3	328.54	316.1882	293.0053	293.0096
.139E-3	338.6288	320.2997	293.0055	293.0278
.168E-3	353.1024	324.1232	295.1947	293.0654
.226E-3	394.32	331.1135	295.619	293.2301
.27E-3	433.14	335.890	301.59	293.4731
.3578E-3	514.8431	344.728	327.2018	294.4264
.44E-3	581.9754	353.595	368.3614	297.2901
.761E-2	732.7344	426.1884	559.8989	352.7778
.11885E-2	774.3024	620.9604	681.657	536.9472
.1755E-2	779.7076	771.8485	709.204	685.6981
.2553E-2	780.0256	808.3466	711.609	721.8721
.3688E-2	780.0319	810.7195	711.673	724.1759
.4000E-2	780.0319	810.7535	711.6734	724.2074

Table C.4

The Nodal Temperatures as Obtained with $\theta = 1$

Time in sec	Node 37	Node 91	Node 60	Node 96
.2484E-4	307.5591	300.924	293.001	293.
.3727E-4	312.3409	303.858	292.995	293.001
.4969E-4	315.8593	306.4356	292.992	293.003
.6212E-4	318.5207	308.7744	292.997	293.007
.80712E-4	321.874	311.9354	293.01	293.0019
.11E-3	329.036	316.3965	292.9943	293.0103
.1354E-3	338.	319.9923	292.9953	293.0275
.1609E-3	350.236	323.3658	293.1555	293.06
.1864E-3	365.7238	326.5563	293.706	293.1131
.2118E-3	384.09	329.59	294.927	293.1915
.2493E-3	415.4805	333.7756	299.047	293.3734
.2868E-3	449.318	337.733	306.14	293.6408
.324E-3	483.899	341.526	316.56	294.0306
.3617E-3	517.8668	345.244	330.33	294.6094
.44E-3	579.883	354.12	370.168	297.8625
.6019E-3	678.168	380.088	468.204	314.1017
.93083E-3	757.399	501.533	624.7869	422.4999
.133E-2	776.78	673.56	693.59	588.5543
.1905E-2	779.81	784.0182	710.054	697.7832
.264E-2	780.0245	808.4177	711.6022	721.9351
.3646E-2	780.031	810.6774	711.67	724.1356
.4000E-2	780.0319	810.7533	711.6734	724.2073

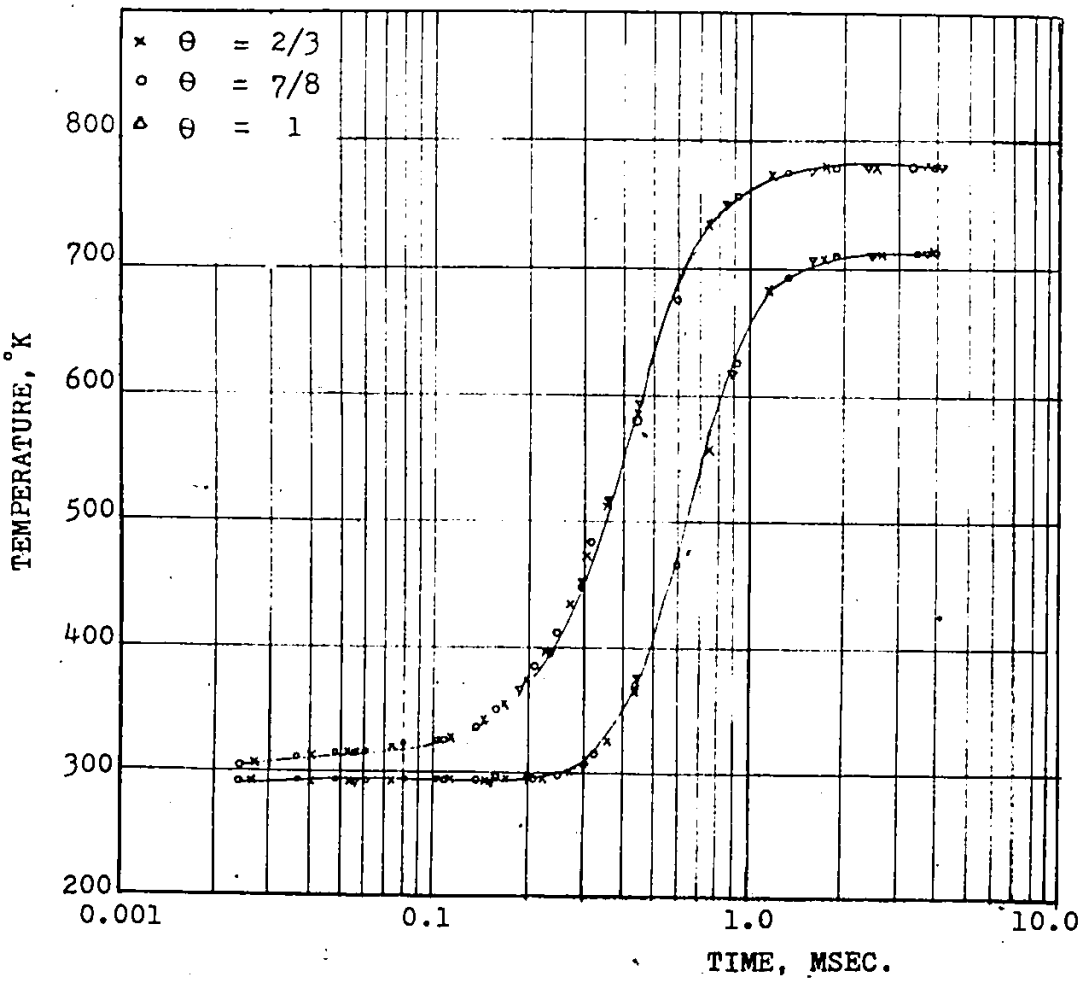

Fig. C.2 Nodal temperature variations.

Table C.5

Steady State Nodal Temperatures

Node	Steady State Formulation	$\theta = 1$	$\theta = 7/8$	$\theta = 2/3$
10	737.58859	737.5886	737.5886	737.5886
37	780.03191	780.0319	780.0319	780.0319
50	714.23343	714.2334	714.2334	713.2334
56	766.89163	766.8916	766.8916	766.8916
67	733.48651	733.4865	733.4865	733.4865
80	709.41445	709.4144	709.4145	709.4145
85	744.05193	744.0519	744.0519	744.0519
82	820.39600	820.3959	820.3960	820.3960
91	810.75347	810.7533	810.7535	810.7535
96	724.20741	724.2073	724.2074	724.2074
120	762.53476	762.5316	762.5347	762.5347
130	751.96970	751.9620	751.9696	751.9695
135	724.60535	724.5985	724.6053	724.6051
137	761.52496	761.5038	761.5244	761.5246
146	758.34968	758.3017	758.3485	758.3480
150	738.98989	738.9454	738.9890	738.9878
152	731.62899	731.5868	731.6284	731.6265
157	749.07478	748.0438	749.0680	749.0744
160	736.46429	736.3306	736.4571	736.4646
166	748.26782	748.0204	748.2559	748.2629
177	741.8936	741.1884	741.8364	741.9227
180	736.54605	736.8256	737.4881	737.5823